2019

Climate Change And Land Use/cover Change Impacts On Watershed Hydrology, Nutrient Dynamics – A Case Study In Missisquoi River Watershed

Linyuan Shang
University of Vermont

CLIMATE CHANGE AND LAND USE/COVER CHANGE IMPACTS ON WATERSHED HYDROLOGY, NUTRIENT DYNAMICS – A CASE STUDY IN MISSISQUOI RIVER WATERSHED

A Dissertation Presented

by

Linyuan Shang

to

The Faculty of the Graduate College

of

The University of Vermont

In Partial Fulfillment of the Requirements
for the Degree of Doctor of Philosophy
Specializing in Natural Resources

January, 2019

Defense Date: Oct 29, 2018
Dissertation Examination Committee:

Carol Adair, Ph.D., Advisor
Arne Bomblies, Ph.D., Chairperson
Asim Zia, Ph.D.
William (Breck) Bowden, Ph.D.
Cynthia J. Forehand, Ph.D., Dean of the Graduate College

ABSTRACT

Watershed regulation of water, carbon and nutrient dynamics support food, drinking water and human development. Projected climate changes and land use/cover change (LUCC) have been identified as drivers of watershed nutrient and hydrological processes and are likely to happen jointly in the future decades. Studying climate change and LUCC impacts on watersheds' streamflow and nutrients dynamics is therefore essential for future watershed management.

This research aimed to unveil how climate change and LUCC affect water and nutrient dynamics in the Missisquoi River watershed, Vermont. We used 12 scenarios of future climate data (2021 – 2050) generated by three GCMs (ccsm4, mri-cgcm3, and gfdl-esm2m) under four Representative Concentration Pathways (RCPs). For LUCC, we used three different scenarios generated by the Interactive Land Use Transition Agent-Based Model (ILUTABM). The three LUCC scenarios were Business As Usual (BAU), Prefer Forest (proForest), and Prefer Agriculture (proAg). New land use maps were generated every 10 years for the period of 2021 – 2050. Combining each climate change and LUCC scenario resulted in 36 scenarios that were used to drive Regional Hydro-Ecologic Simulation System (RHESSys) ecohydrological model.

In chapter 3, we used RHESSys to study streamflow. We found climate was the main driver for streamflow because climate change directly controlled the system water input. For streamflow, climate change scenarios had larger impacts than LUCC, different LUCCs under the same climate change scenario had similar annual flow patterns.

In chapter 4, we used RHESSys to study streamflow NO_3-N and NH_4-N load. Because fertilizer application is the major source for nitrogen export, LUCC had larger impacts; watersheds with more agricultural land had larger nitrogen loads.

In chapter 5, we developed RHESSys-P by coupling the DayCent phosphorus module with RHESSys to study climate change and LUCC impacts on Dissolved Phosphorus (DP) load. RHESSys-P was calibrated with observed DP data for 2002 – 2004 and validated with data for 2009 - 2010. In both calibration and validation periods, simulated DP basically captured patterns of observed DP. In the validation period, the R^2 of simulated vs observed DP was 0.788. Future projection results indicated BAU and proForest annual loads were around 4.0×10^4 kg under all climate change scenarios; proAg annual loads increased from around 4.0×10^4 kg in 2021 to 1.6×10^5 kg in 2050 under all climate change scenarios. The results showed LUCC was the dominant factor for dissolved phosphorus loading.

Overall, our results suggest that, while climate drives streamflow, N and P fluxes are largely driven by land use and management decisions. To balance human development and environmental quality, BAU is a feasible future development strategy.

ACKNOWLEDGEMENTS

I would like to express my gratitude to those who helped and supported me through my study, including my family, advisors, committee, colleagues, friends, Rubenstein School and Vermont EPSCoR.

I would like to thank my advisor Carol Adair and co-advisor Asim Zia, my committee Arne Bomblies and William (Breck) Bowden for their guidance and support. I would like to thank professors working in EPSCoR, Donna Rizzo, Beverley Wemple, Andrew Schroth. I would like to specially thank Xiaoli Chen and Janet Choate from UC Santa Barbara, I remember those days you spent your weekends discussing RHESSys code bugs with me. I would like to thank Patrick Clemens, Scott Turnbull, Morgan Rodgers for their computer technical expertise. I would like to thank Carol's lab mates: Tyler Goeschel, Ali Kosiba, Erin Seybold, Stephanie Juice, Bar Barbieri, Adam Noel, Brittany Lancellotti, Kyle Dittmer. I miss those lab meetings in Rubenstein School. I would like to thank my colleagues in EPSCoR: Yu-Shiou Tsai, Yaoyang Xu, Ibrahim Mohammed, DongJoo Joung, Justin Guilbert, Jody Stryker, Gabriela Bucini, Sarah Coleman, Steve Exler, Scott Hamshaw, Peter Isles. I would like to thank EPSCoR center and Rubenstein School for the opportunity and financial support to finish my study.

Finally, I would like to thank my wife Guolin Yao. She always accompanied with me, encouraged me.

TABLE OF CONTENTS

Page

LIST OF TABLES

LIST OF FIGURES

CHAPTER 1: DISSERTATION FRAMEWORK

Anthropogenic activities have dramatically changed our world and are still changing our world. Two urgent issues are climate change and Land Use/Cover Change (LUCC).

According to the Intergovernmental Panel on Climate Change (IPCC)'s Fifth Assessment Report (AR5) (Pachauri et al., 2014), the global average surface temperature showed a warming trend of 0.85 ℃ from 1880 to 2012. Global temperatures are projected to rise by 2-4 °C by 2100 if greenhouse gas emissions can't be mitigated in the future. The impacts of climate change are huge, including altered global energy patterns, ecosystems, global economic.

At the same time, dramatic changes in global land use/cover change (LUCC), including conversion (i.e. complete replacement of one type by another type) and modification (i.e. small changes in one type without overall change) (Coppin et al., 2004), have occurred over the past two centuries (Meiyappan & Jain, 2012). LUCC converts natural ecosystems to human use systems, including agriculture, pasture land, and urban areas (Foley et al., 2005). In the year of 2000, cropland covered 12% of the Earth's ice-free land surface and pasture covered 22% (Ramankutty et al., 2008). Land use/cover change also has large impacts, including the potential to alter earth surface processes, such as energy and water exchange with the atmosphere, soil erosion, and hydrology (Ban et al., 2015).

Either climate change or LUCC can have dramatic impacts on many aspects of global and ecosystem functions and properties. The combined impacts of climate change and LUCC will likely be even more dramatic and complex. Although impacts will range from local to global in scale, my dissertation will focus on the intermediate scale of the watershed. At this scale, I will be able to investigate climate change and LUCC impacts on important watershed dynamics, including hydrology and biogeochemistry. This study will examine these impacts on the Missisquoi River watershed in Vermont, US.

The research tools used in the study include General Circulation Models (GCMs) for generating future climate data under different Representative Concentration Pathways (RCPs), an agent-based land transition model – Interactive Land Use Transition Agent-Based Model (ILUTABM) (Y. Tsai et al., 2015), and an Eco-hydrologic model – Regional-Hydro-Ecologic Simulation System (RHESSys) (Band et al., 1993; Band et al., 2000; C. L. Tague & Band, 2004).

The dissertation organization is as follows:

Chapter 1 is the dissertation introduction.

Chapter 2 is a comprehensive literature review covering the topics on climate change and LUCC impacts on watershed hydrology and water quality.

Chapter 3 is the study of how climate change and LUCC impact streamflow in Missisquoi River watershed with RHESSys in the period of 2021 - 2050.

Chapter 4 is the study of how climate change and LUCC impact streamflow nitrogen (NO_3-N and NH_4-N) in Missisquoi River watershed with RHESSys in the period of 2021 - 2050.

Chapter 5 is RHESSys-P model development, which added dissolved phosphorus module into current RHESSys model, which does not include phosphorus module. After calibration and validation in Missisquoi River watershed , we used RHESSys-P to study climate change and LUCC impacts on streamflow dissolved phosphorus patterns in the period of 2021 – 2050.

Chapter 6 concludes the whole dissertation work and suggests some future work.

CHAPTER 2: LITERATURE REVIEW

2.1. Brief history of watershed research development

A watershed (basin or catchment) is the area where precipitation or snow falls and, through overland flow or groundwater flow, finally flows to the same outlet (Sauer et al., 2008). Watersheds support social systems, economics, manufacturing, food production, and drinking water. Therefore, healthy watersheds are critical to sustainable development. However, several factors can combine to result in diminished watershed health: flooding (Alderman et al., 2012; Hunter et al., 2007), soil erosion (Garcia-Ruiz et al., 2015; Patil et al., 2015), excess nutrient export, and water quality degradation (Bouwman et al., 2013). These environmental issues drive people to understand and predict complex watershed processes such as water and nutrient transport.

Why choose the watershed scale for research? A watershed usually has a clear natural geography boundary, making it a relatively closed and independent system in the hydrologic cycle (Cai et al., 2001). Watersheds processes are complex, involving the atmosphere, hydrosphere, biosphere and pedosphere. Research on understanding watershed processes dates back to watershed hydrology, which stemmed from hydrology(Singh & Woolhiser, 2002). Key watershed hydrology processes, which were established between 1910 and 1960 (Singh & Woolhiser, 2002), include infiltration (Heber Green & Ampt, 1911), overland flow (Horton, 1939), evapotranspiration (Penman, 1948), and groundwater hydrology (Theis, 1935). After 1960, many watershed models sprang up and have developed in the past decades, such as Stanford Watershed Model-SWM (Crawford & Linsley, 1966), Agricultural Non-Point Source Model

(AGNPS) (Young et al., 1989), Distributed Hydrology Soil Vegetation Model (DHSVM) (Wigmosta et al., 1994), Soil Water Assessment Tool (SWAT) (Arnold et al., 1998; Srinivasan et al., 1998), Regional-Hydro-Ecologic Simulation System (RHESSys) (Band et al., 2000; C. L. Tague & Band, 2004) and a global scale model—Global Nutrient Export from Watersheds (NEWs) (S. P. Seitzinger et al., 2005). Generally, current watershed models are developing in the direction of physical process-based, distributed system and are also integrating anthropogenic activities. Another important development is that watershed models are moving to simulate both ecological and hydrologic processes rather than only hydrologic processes (Kemanian et al., 2011; C. L. Tague & Band, 2004).

Along with watershed model development, more and more data is available for model use: Remote sensing and GIS technologies provide Digital Elevation Models (DEMs) and land cover and land use information; meteorological stations provide long term temperature and precipitation data; soil texture data is available from Food and Agriculture Organization (FAO); and in the US, the United States Geological Survey (USGS) stream gauges provide long-term stream flow data across the nation. This huge data inventory can function as input data, to calibrate and validate watershed models. Watershed models are maturing and are being effectively used for research and watershed management.

2.2. Current watershed research focuses and research questions

The development of watershed models, growing data availability, and growth of computing power have made watershed models a significant tool for tackling new, challenging questions in watershed research (Dunn et al., 2014; Ficklin et al., 2013; Yadav et al., 2009): How will global climate change and land use and land cover change affect watershed processes (Christensen et al., 2004; D'Agostino et al., 2010; Elsner et al., 2010; Fan & Shibata, 2015; Luo et al., 2013)? What adaptive strategies should we take to mitigate the effects of these changes (Park et al., 2014)? In this study, I will use a hydro-ecological model (RHESSys) to investigate concurrent climate change and land use/land cover change impacts on watershed ecological and hydrological processes.

2.2.1. Climate change impacts on watershed hydrology

According to the Intergovernmental Panel on Climate Change (IPCC)'s Fifth Assessment Report (AR5) (Pachauri et al., 2014), the global average surface temperature showed a warming trend of 0.85 degree Celsius from 1880 to 2012. Based on different Green House Gas (GHG) emission levels, IPCC released four Representative Concentration Pathways (RCPs) for the 21st century: RCP2.6, RCP4.5, RCP6.0 and RCP8.5. The number after each RCP refers to radiative forcing values in year 2100 relative to pre-industrial values (+2.6, +4.5, +6.0 and +8.5 W/m^2). In these scenarios, RCP2.6 represents the least emissions and RCP8.5 represents the most emissions. Global mean surface temperature is projected to increase 1.0 degree under RCP2.6, and 3.7 degrees under RCP8.5 by 2100. Under all RCPs scenarios, globally, the area encompassed by monsoon systems will increase and precipitation is likely to intensify.

Generally, the strategy for determining how climate change may affect watershed processes in most studies is to obtain temperature and precipitation data from future climate projections based on the GHG emission scenarios using General Circulation Models (GCMs), and then use the future climate projection data as input for watershed hydrological models to project future stream flow, and nutrient load (Christensen et al., 2004; Elsner et al., 2010; Zhang et al., 2015).

Climate change is projected to affect future hydrological regimes directly and indirectly (Elsner et al., 2010; Luo et al., 2013; Viola et al., 2015; Zhang et al., 2015). Direct impacts of climate change on hydrology include changing precipitation and temperature. Projected precipitation changes (temporal pattern and total precipitation change) will directly alter the water input for watersheds and further alters streamflow. In an agricultural watershed study of southern Quebec (Canada), annual precipitation increases of 7 to 12% resulted in streamflow increases of 11 to 21% (Gombault et al., 2015) . Increasing temperature is projected to increase evapotranspiration (Masood et al., 2015) and brings earlier snow melt which leads to shifts in the timing of spring streamflow in snowmelt dominant area (Elsner et al., 2010). Indirect impacts on hydrological regimes due to climate change include increasing CO_2 concentration and growing season length change. High CO_2 concentration reduces leaf stomatal conductance and affects plant transpiration, which further alters watershed hydrological processes. Luo et al. (2013) integrated CO_2 effects on plants in SWAT model and showed doubling CO_2 reduced evapotranspiration (ET) by 10.6% for agricultural land, 5.7% for deciduous forest, and 4.2% for rangeland. Growing season length expansion also

increased plant ET, resulting in reduced streamflow and more water from the watershed entering into the atmosphere (Band et al., 1996).

One potentially important indirect effect of climate change is the lengthening the growing season, which may result in phenological changes in vegetation. Phenological change resulting from climate change has been documented in the mid-high latitudes of the northern hemisphere since the 1960s (Jeong et al., 2011; Kolarova et al., 2014; Menzel & Fabian, 1999; Piao et al., 2007). The average growing season length extended 10.8 days from 1960s to 1990s in Europe (Menzel & Fabian, 1999). In the US, the average growing season length increased about 9.4 days from 1982 to 2008 (Jeong et al., 2011). Growing season length extension affects ecosystem functions. Piao et al. (2007) showed growing season length increased by 0.30 days yr^{-1} in the northern hemisphere during 1980-2002, and one day growing season length extension could increase annual gross primary productivity (GPP) by 0.6%. Carbon dynamics are closely coupled with water cycle (Luo et al., 2013), so the longer growing season length could also potentially impact the watershed water cycle through water uptake and ET.

Although much research has studied the direct impacts of climate change (i.e. temperature and precipitation change) on watershed hydrological regimes, the impacts of changes in growing season length on watershed hydrology were rarely studied. Band et al. (1996) used a model to study changes in growing season length, however, the growing season length change was implemented by increasing plants LAI in the growing season instead of simulating growing season length directly. In other research,

Christiansen et al. (2011) studied climate change impacts on the growing season length, defined as the period between the last spring frost and the first hard frost in the fall, in 14 basins in United States. The future climate and the projected growing season length then were used as input for a hydrological model Precipitation-Runoff Modeling System (PRMS) to project the watershed response in the 21st century. However, in Christiansen's model, the growing season length definition could not directly reflect the earlier leaf onset and later leaf fall. Additionally, no control experiment was implemented, so the results could not identify how changes in growing season length impacted watershed hydrology. Thus, the impacts of growing season length extension on watershed hydrology have lacked quantitative assessment.

2.2.2. Land use/cover change (LUCC) impacts on watershed hydrology

Global land use/cover change (LUCC), including conversion (i.e. complete replacement of one type by another type) and modification (i.e. small changes in one type without overall change) (Coppin et al., 2004), has been dramatic over the past two centuries (Meiyappan & Jain, 2012). LUCC converts natural ecosystem to human use systems, including agriculture, pasture land, and urban areas (Foley et al., 2005). In the year of 2000, cropland covered 12% of the Earth's ice-free land surface and pasture covered 22% (Ramankutty et al., 2008).

Land use/cover change has the potential to alter earth surface processes, such as energy and water exchange with the atmosphere, soil erosion, and hydrology (Ban et al., 2015). The dramatic LUCC in the past and possible future trends has drawn researchers

to study LUCC impacts on watershed hydrology (Dong et al., 2015; Ling et al., 2015; van Roosmalen et al., 2009; Yang et al., 2012). To study LUCC impacts on hydrology, two important aspects must be considered, The first is what method is used to represent LUCC; and the second is what method is used to reflect hydrology response to LUCC. Currently, hydrological models are mostly used for reflecting hydrology responses, so the key question is how to represent LUCC.

Generally, the methods used to represent LUCC have three categories: The first assumes some LUCC scenarios based on land use demand (Viola et al., 2014; Yuan et al., 2015); the second uses two (Gessesse et al., 2015; Zhi Li et al., 2009) or several (Yang et al., 2012) satellite images in different years for the same study area; and the third uses a land use transition model to simulate land use (Fan & Shibata, 2015; Ling et al., 2015; Wu et al., 2015). For the first two methods, a base land use/cover (earlier year) and a changed land use/cover (later year) are usually retrieved. The base and changed land use/cover are used separately as input for a hydrological model and the model responses for different land use/cover are used to reflect the LUCC impacts on hydrology. The drawback is that the land use/cover is assumed to be unchanged during a period of time, which is dynamically changing in reality. In contrast, the land use transition models can provide LUCC dynamics over a period of time, which provides the potential for hydrological models to reflect the dynamic LUCC processes. Additionally, land use transition models can project possible future land use scenarios, which could combine projected climate data to study the joint impacts of LUCC and climate change on hydrology (Fan & Shibata, 2015). Because LUCC and climate change are likely to

occur jointly in the future, studying combined LUCC and climate change impacts on hydrological processes is essential and meaningful for future land use planning (Fan & Shibata, 2015; Tong et al., 2012).

Several statistical land use transition models have been used for hydrology studies, such as the Conversion of Land Use and its Effects (CLUE) model (Fan & Shibata, 2015), and Dynamic Conversion of Land-Use and its Effects (Dyna-CLUE) (Ling et al., 2015), Dynamic Land Use System (DLS) model (Wu et al., 2015). These statistical models are based on biophysical characteristics, such as soil type, elevation, slope, and aspect (Fan & Shibata, 2015). However, these models don't explicitly simulate landowner behavior, which is a key factor in determining land use. Fan and Shibata (2015) suggested agent-based model including decision-making behavior would be an improvement for predicting agricultural land use transition. Therefore, I use an agent-based land transition model – Interactive Land Use Transition Agent-Based Model (ILUTABM) (Y. Tsai et al., 2015) – to study LUCC change impacts on hydrology. In addition, I will combine LUCC scenarios with future climate change scenarios to study the joint impacts of LUCC and climate change on hydrological processes.

2.2.3. Watershed nutrient dynamics

Riverine nutrient fluxes (carbon, nitrogen and phosphorus) play an important role in linking terrestrial with aquatic systems. Excess nutrients in water can degrade water quality and cause environmental problems, such as eutrophication. Nutrient transport from land to water is highly reliant on hydrological processes. Therefore, nutrients

dynamics in watersheds are best studied using models that combine watershed ecological and hydrological processes.

Dissolved organic carbon (DOC) export has been extensively studied due to its roles in carbon cycle and water quality (Jennings et al., 2010). Traditionally, water sampling on a regular basis with water flow data is used to quantify the DOC fluxes from a watershed (Veum et al., 2009). Recently, high frequency measurements have been applied in DOC monitoring, which can capture hourly variation and provide more precise fluxes estimates (Strohmeier et al., 2013). In a review for 550 worldwide watersheds, DOC contributed to 73 ±21% of total organic carbon (TOC) export (Alvarez-Cobelas et al., 2012) . Generally, freshwater ecosystems are not considered important in global or regional carbon cycles, but Cole et al. (2007) found that freshwater's role in the global carbon budget cannot be ignored. Several studies have integrated aquatic carbon fluxes into watershed carbon budgets. Shibata et al. (2005) showed the carbon export was very small (~ 2%) compared with net ecosystem exchange (NEE) in a forested watershed in Japan. Jonsson et al. (2007) found carbon export in a boreal watershed was around 6% of NEE. Other studies found the carbon export could be over 10% of NEE in peatland watersheds (Dinsmore et al., 2010; Juutinen et al., 2013). Therefore, integrating carbon export, especially DOC, in carbon dynamics in watersheds is essential.

Nitrogen and phosphorus export is another important topic in watershed research because of their key roles in freshwater eutrophication (Conley et al., 2009). Non-point source pollution, especially non-point agricultural sources, are considered major

contributors to excess nitrogen and phosphorus loads (Zhernwei Li et al., 2015; Ongley et al., 2010; Ulen et al., 2007) and best management practices have been implemented in farmlands to mitigate nutrient load (Smith et al., 2015).

Because of the complexity of nitrogen and phosphorus dynamics processes in watersheds, hydrological models have been the main tools for nutrient study. To better integrate terrestrial nutrient sources and changes in land uses or land use management, some hydrological models have incorporated nitrogen and phosphorus processes. For example, SWAT, which integrates fertilizer application, management practices, and nutrient transport, has been used to quantify watershed nutrient export (Sen et al., 2012) and nutrient hot spots at the watershed level (Jacobson et al., 2011). Climate change is projected to affect future hydrological regimes (Christensen & Lettenmaier, 2007), which could further affect nutrient transport and export (Jeppesen et al., 2011). Fan and Shibata (2015) used SWAT to study the impacts of climate change on water quality in the Teshio River watershed of Japan, assuming land cover and land management practices did not change. Their results showed the impacts on water quality varied with seasons: Snowmelt shifted from April to March increased monthly N yield in March; N yield decreased in May due to the enhanced plant uptake and less water yield.

2.2.4. Extreme events

According to IPCC's Fifth Assessment Report, extreme weather and the number of heavy precipitation events have increased since 1950 (Pachauri et al., 2014). Although the occurrence of extreme events is relatively rare, the environmental impacts are huge.

For example, 10 extreme events in 205 erosion events contributed 83.8% of the total suspended sediment load in a small agricultural watershed in the Three Gorges Area of China (Fang et al., 2013). Extreme storms can dramatically increase carbon, nitrogen and phosphorus load (Y. Gao et al., 2014), deteriorating water quality. Therefore, understanding extreme events is essential to watershed management.

Climate change and land use/cover change (LUCC) are considered the two most important factors contributing to the increased frequency of extreme events (Poelmans et al., 2011; Tavakoli et al., 2014). Extreme weather induced by climate change can directly alter precipitation quantity and intensity; LUCC can alter water flow path ways or generate more runoff in some land use/cover types (e.g. urban) and lead to extreme flows. Because climate change and LUCC are very likely to occur in the future, understanding how climate change and LUCC could influence future extreme events (e.g. extreme event frequency) is essential for future management. Tavakoli et al. (2014) studied how extreme flows in a watershed in Belgium responded to climate change and urban growth. They found that extreme low flows were decreased by climate change and extreme peak flows were predicted to increase due to climate change and urban expansion.

Currently, only a few studies focused on the climate change and LUCC impacts on extreme events. Among those studies, most focused on water flow rather than nutrient export. It is urgent to study the impacts of extreme events on water flow and nutrient export for future management.

2.3. Regional-Hydro-Ecologic Simulation System (RHESSys)

This dissertation used RHESSys as a tool to study watershed hydrology and nutrient dynamics, and also developed a new model with a dissolved phosphorus module. The reason why we chose RHESSys is that RHESSys is a process-based hydro-ecological model, and RHESSys is also easy to customize its application. For example, RHESSys can be easily integrate dynamic land use change on the model run. Compared with RHESSys, although SWAT is a powerful and widely used hydrological model, integrating dynamic land use change in SWAT is complex. This section will cover RHESSys model and its development.

2.3.1. RHESSys development history

RHESSys is a Geographical Information System (GIS)-based hydro-ecological model that simulates watershed water, carbon and nutrient (nitrogen) dynamics (Band et al., 1993; Band et al., 2000; C. L. Tague & Band, 2004). Detailed model information can be found on the RHESSys website (http://fiesta.bren.ucsb.edu/~rhessys/).

RHESSys was developed in 1990s and thus belongs to a later generation of watershed models. Importantly, RHESSys coupled ecosystem processes with hydrology. Thus, RHESSys can simulate the water cycle in ecosystems using process-based modules, such as rain interception and evapotranspiration. Band et al. (1993) developed the first version of RHESSys by coupling the biogeochemistry model FOREST-BGC (S. W. Running & Coughlan, 1988) and the hydrological model TOPMODEL (Beven & Kirkby, 1979). The first version only partitioned a watershed into different hillslopes and

water routing on the land was implicit. Later, an explicit routing method modified from DHSVM (Wigmosta et al., 1994) was introduced into RHESSys (C. L. Tague & Band, 2001). Now, the user can choose either routing method. In 2000, a more detailed land hierarchy structure was developed (Band et al., 2000), which further divided hillslopes into climate zones, patches and canopy strata. In 2001, the nitrogen module in RHESSys was further improved by integrating BIOME-BGC (Steven W Running & Hunt, 1993) and Century-NGAS (Parton et al., 1996), to include decomposition, nitrification, denitrification, plant uptake, and nitrogen export processes. These key developments form the main framework of current RHESSys structure, although new features are still being added to the model.

2.3.2. Structure and application of RHESSys model

RHESSys uses a hierarchical structure to represent landscapes, which includes basins, hillslopes, zones, patches and canopy strata (Figure 2.1). RHESSys provides a tool, GRASS2WORLD in GRASS (Geographic Resources Analysis Support System) GIS environment, that partitions the landscape into different structure levels using a Digital Elevation Model (DEM), land cover map, and soil texture, and then generates a text file called worldfile, which represents the landscape structure. This worldfile is used as input file to RHESSys.

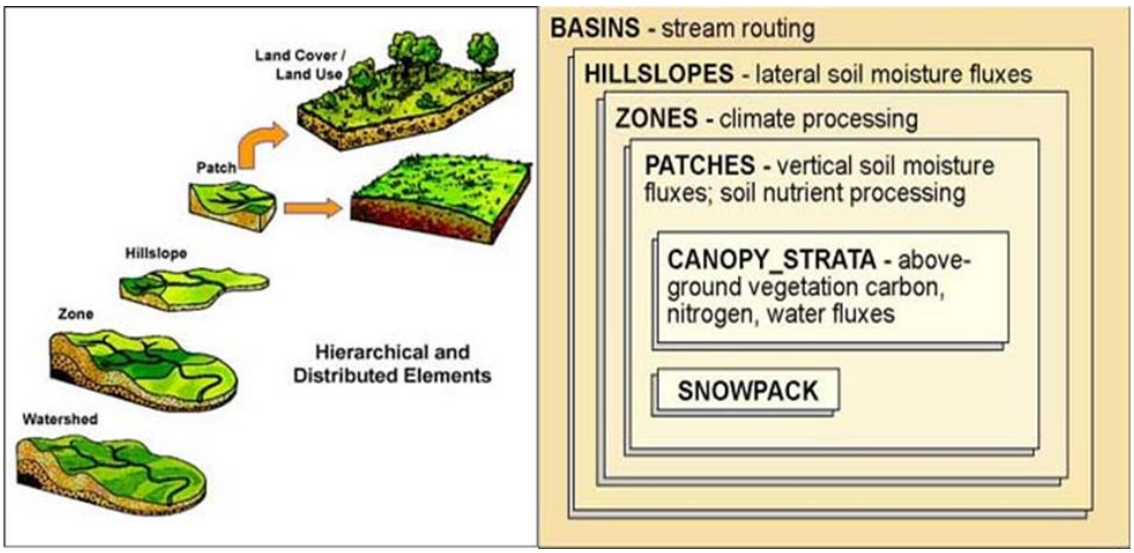

Figure 2.1: RHESSys hierarchical structure and corresponding functions (From RHESSys website, http://fiesta.bren.ucsb.edu/~rhessys/data/data.html)

More specifically, the RHESSys model's hierarchical structure contains the following elements:

- **Basin:** a closed drainage area equivalent to a whole watershed area.
- **Hillslope:** the area draining into one side of a stream reach. In RHESSys, deep ground water processes are processed at the hillslope level. Deep ground water is simulated with a linear reservoir model. On a daily basis, a portion of the deep ground water enters its connected stream reach as base flow. Explicit water routing between patches is also processed at the hillslope level.
- **Zone:** areas with similar climate. Meteorological data is processed at the zone level. Each zone is linked with one base station, which provides the meteorological data such as daily max temperature, daily min temperature, and daily precipitation. In version 5.19, RHESSys can process hourly precipitation input and process the

precipitation on an hourly step. The MT-CLIM model (S. W. Running et al., 1987) was integrated in RHESSys to process climate data. The model uses one climate base station that a zone links, along with the topography, slope and aspects etc. to estimate each zone's meteorological data, is integrated at the zone level.

- **Patch:** the smallest spatial unit and the basic modeling unit in RHESSys. Patches represent homogeneous soil and land cover characteristics. Vertical water movement is simulated at the patch level, including infiltration into the root zone (for vegetated patch) and unsaturated zone, and recharge to the saturated zone. Soil nutrient fluxes are also simulated at the patch level, such as plant uptake, leaching, decomposition, nitrification and denitrification. Some farmland management practices are implemented at the patch level by linking the patch to a base station, including irrigation and fertilizer application. The linked base station provides a spatial time series of land management information for each patch. Users can specify irrigation and fertilizer application amounts and dates in the patch linked base station.
- **Canopy strata:** these have the same spatial unit as patches but represent the vertical aboveground layers. All layers are sorted into different groups by layer height. For vegetation canopy strata, precipitation falls through layers from highest to lowest. At each layer height, a portion of the precipitation is intercepted. When the precipitation penetrates all layers, it becomes throughfall to the litter layer. The litter layer intercepts some water, and the remaining throughfall infiltrates into the soil, which is processed at the patch level. The canopy strata also simulates plant growth, including radiation interception and photosynthesis by the Farquhar model

(Farquhar & von Caemmerer, 1982), respiration, phenology (controlling leaf out and leaf fall date), and evapotranspiration using the Penman-Monteigh equation (Monteith, 1965).

RHESSys has been applied to study water (Godsey et al., 2014; C. L. Tague & Band, 2001), carbon (Hwang et al., 2008; Vicente-Serrano et al., 2015) and nitrogen (Band et al., 2001) fluxes. The model has been confirmed as a suitable tool for simulating climate change impacts on hydrology (Zierl et al., 2007) and has been used for projecting hydrological regime changes under different climate change scenarios (Lopez-Moreno et al., 2014; Meyers et al., 2010). However, one problem with using the RHESSys model for a long-term climate change study is that the current model version (5.19) uses a static CO_2 concentration rather than dynamic. The Mauna Loa CO_2 record (www.esrl.noaa.gov/gmd/ccgg/trends/) indicates that CO_2 increased from around 320 ppm in 1960 to around 400 ppm in 2015. Atmospheric CO_2 levels can affect photosynthesis, plant water use efficiency and ET (Luo et al., 2013; C. Tague et al., 2009), thereby further affecting carbon and water cycles. Thus, future long term studies using RHESSys should consider integrating a dynamic CO_2 data module.

2.4. Study area

The Missisquoi River watershed is located along the border of US and Canada. The predominant land cover is forested (~ 70%) with ~14% pasture/hay land cover and ~5% crop land cover (Table 2.1). The Missisquoi River drains into Missisquoi Bay, which is in the northern part of Lake Chaplain (Figure 2.2). In the past decades, the

Missisquoi Bay has experienced eutrophication due to excess nitrogen and phosphorus load from non-point source pollution, especially from agriculture (Isles et al., 2015; Schroth et al., 2015). Efforts have been made to protect the lake. The Long-Term Water Quality and Biological Monitoring Project for Lake Champlain started in 1992, providing lake monitoring data and assessing the lake health. A recent study showed 20% of the Missisquoi river watershed area contributed 74% of the watershed total phosphorus load (Winchell et al., 2015), another study showed total phosphorus increased by 72% in Missisquoi Bay during 1979 – 2009 (Smeltzer et al., 2012). So identification of nutrient critical source area is important for cost-effective nutrient load management.

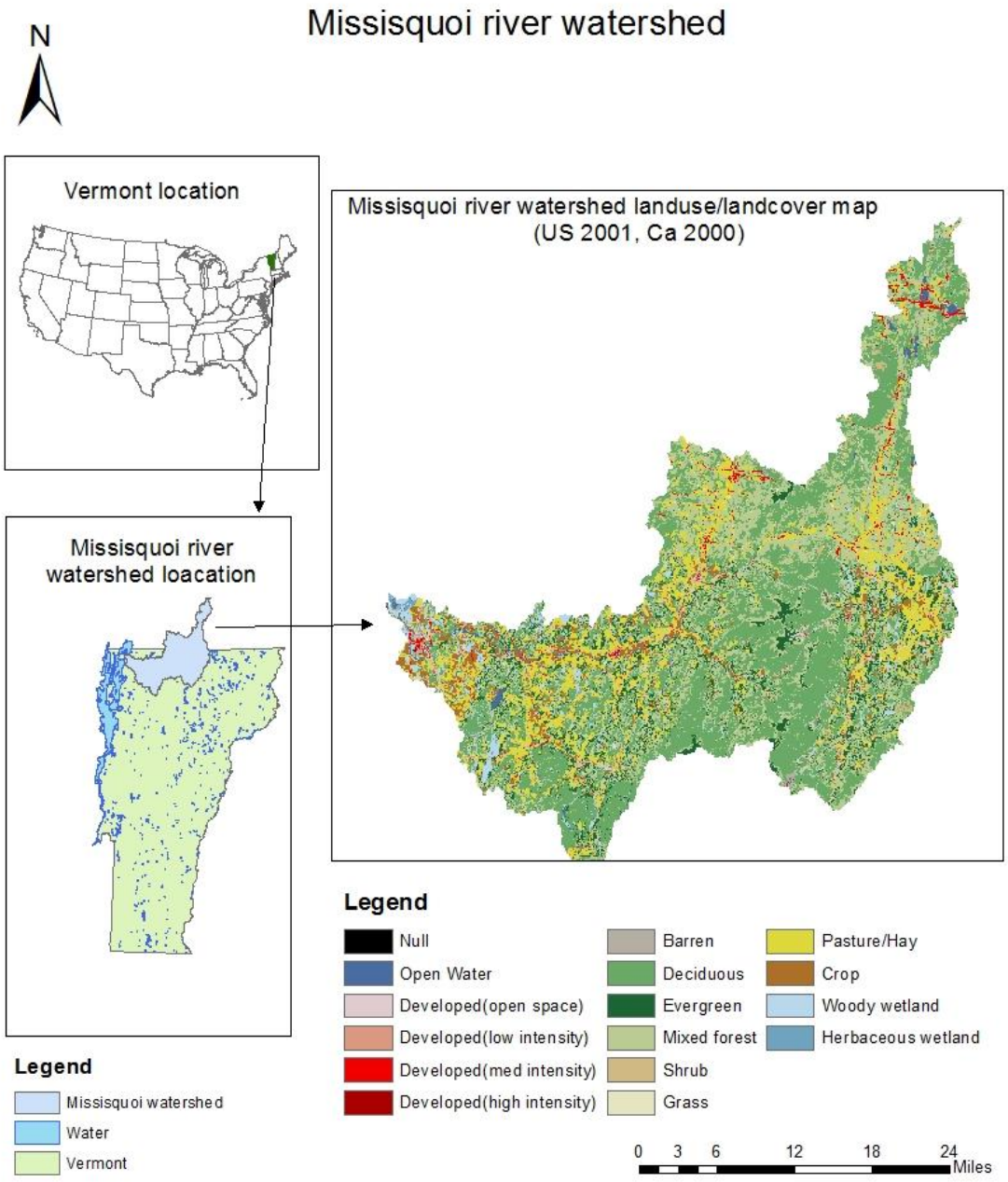

Figure 2.2 Missisquoi river watershed location and its landuse/landcover map, US landcover portion is from the year of 2001, and Canadian portion is from 2000.

Table 2.1: Landuse/Landcover area and percentage in Missisquoi river watershed

Landuse/Landcover	Area (ha)	Percentage (%)
Deciduous Forest	83953.26	37.8
Mixed Forest	54545.85	24.5
Pasture/Hay	31370.13	14.1
Evergreen Forest	17489.52	7.9
Crop	10283.4	4.6
Woody Wetland	7660.98	3.4
Developed, Open Space	4462.92	2.0
Developed, Med Intensity	2723.13	1.2
Developed, Low Intensity	2313.45	1.0
Shrub	2197.98	1.0
Open Water	1628.1	0.7
Herbaceous Wetland	1345.41	0.6
Grass	1126.98	0.5
Barren	965.07	0.4
Developed, High Intensity	129.69	0.1
Total	222195.87	100

2.5 Summary

Climate change and LUCC have been identified as the two main drivers for watershed hydrology. Many studies have been conducted on how climate change and LUCC impact on watershed hydrology separately. However, few studies investigate the joint impacts of climate change and LUCC. Furthermore, LUCC dynamics are rarely integrated into model simulations. Instead, LUCC is assumed to be constant for future scenario simulations. The reason is that current hydrologic models don't have a customized LUCC configuration interface, making the integration of dynamic LUCC hard for hydrologic model users. Yet, LUCC is not a constant, but changes over time and likely also changes in response to a changing climate.

Therefore, in my dissertation, I address this gap by developing a frame to incorporate climate change and LUCC dynamics for watershed simulation using RHESSys. I used agent-based land transition model ILUTABM to generate future LUCC dynamics and then developed a LUCC fusion module for RHESSys to take a series of LUCC to reflect LUCC in the simulation process. This work will answer the joint impacts of climate change and LUCC on watershed hydrology and nutrient loads.

CHAPTER 3: CLIMATE CHANGE AND LAND USE/COVER CHANGES IMPACTS ON STREAMFLOW IN MISSISQUOI RIVER WATERSHED

3.1. Introduction

Climate change has been occurring over the past 30 years and is projected to continue into the 21 century (Pachauri et al., 2014). Rising atmospheric CO_2 and climate change, including warming temperatures and altered precipitation, could impose significant impacts on hydrological processes and lead to floods, drought and water resource management problems (Luo et al., 2013; Zhang et al., 2015). Projected precipitation changes in temporal patterns and total precipitation will directly alter water inputs. In an agricultural watershed study in southern Quebec (Canada), annual precipitation increases of 7 to 12% resulted in streamflow increases of 11 to 21% (Gombault et al., 2015). Increasing temperature will also impact watershed hydrology. Increasing temperatures are projected to increase evapotranspiration (Masood et al., 2015) and bring earlier snow melt, which leads to shifts in spring streamflow timing in snowmelt dominant areas (Elsner et al., 2010).

At the same time, human activities have changed global land cover greatly. In the year 2000, cropland covered 12% of the Earth's ice-free land surface and pasture covered 22% (Ramankutty et al., 2008). Such Land Use/Cover Change (LUCC) can greatly impact hydrological process (Wu et al., 2015) by altering canopy interception, infiltration, and evapotranspiration processes, consequently leading to streamflow variation (Fan & Shibata, 2015; Gessesse et al., 2015; Yang et al., 2012). Generally, conversion of natural vegetation to cultivated or impervious land cover increases runoff

generation (Gessesse et al., 2015). However, the complexity (configuration) of land use/cover patterns mean that simple conclusions can't be drawn according to land use/cover change rates alone (Yang et al., 2012). Instead, it is critical to use spatially explicit models to understand LUCC impacts on watershed hydrology and inform land management.

Many publications have studied the separate impacts of LUCC (Sajikumar & Remya, 2015; Wu et al., 2015; Yang et al., 2012) or climate change (Al-Mukhtar et al., 2014; Andersen et al., 2006; Viola et al., 2015) on watershed hydrology. However, in the future, climate change and LUCC are likely to occur jointly (Ling et al., 2015). Thus, coupling of climate change and LUCC is important for watershed hydrology simulation (Fan and Shibata (2015), but hydrological models do not fully couple land use and climate change. Instead, the same land use scenario is typically used for the entire simulation period. Ling et al. (2015) noticed this gap and coupled Dyna-CLUE land use model with climate change scenarios to study the joint impacts on Heihe River Basin, China. The study provided a framework of coupling land use and climate change; however, Dyna-CLUE model is non-spatial, and does not simulate landowner's behavior.

Therefore, in this study, we coupled LUCC from an agent-based land transition model – Interactive Land Use Transition Agent-Based Model (ILUTABM) (Y. Tsai et al., 2015) and climate change to study their joint impacts on Missisquoi river watershed streamflow using the RHESSys model (C. Tague et al., 2004). We expected that climate change, especially precipitation change, would have larger impacts on streamflow than

LUCC. Using a spatially explicit model to understand climate change and LUCC impacts on watershed hydrology will improve our understanding of how these complex processes impact hydrology and support will stakeholder decisions around land management and policy making. The novelty of this study is coupling the climate change with dynamic LUCC process, and our experiment design can investigate the relative importance of LUCC, climate change due to RCPs and GCMs.

3.2. Data and methods

3.2.1. Study area

The Missisquoi River watershed is located along the border of the US and Canada and covers 2,200 km^2 (Figure 3.1). The altitude in this area ranges from 17 to 1172m. In 2001, the predominant land cover was forested (~ 70%). Pasture/hay land cover was ~14% and crop land cover was ~5%. The Missisquoi River drains into Missisquoi Bay, which is in the northern part of Lake Chaplain.

A USGS streamflow gauge (#04294000) is located at 44°55'00" N and 73°07'44" W (North American Datum 1927) near the Missisquoi river outlet. The gauge has recorded daily streamflow from March 1st, 1990 until now. The Lake Champlain Long-term Monitoring program also set up a sampling point at the streamflow gauge and recorded nutrient data from 1992 – Now (https://anrweb.vermont.gov/dec/_dec/LongTermMonitoringLakes.aspx).

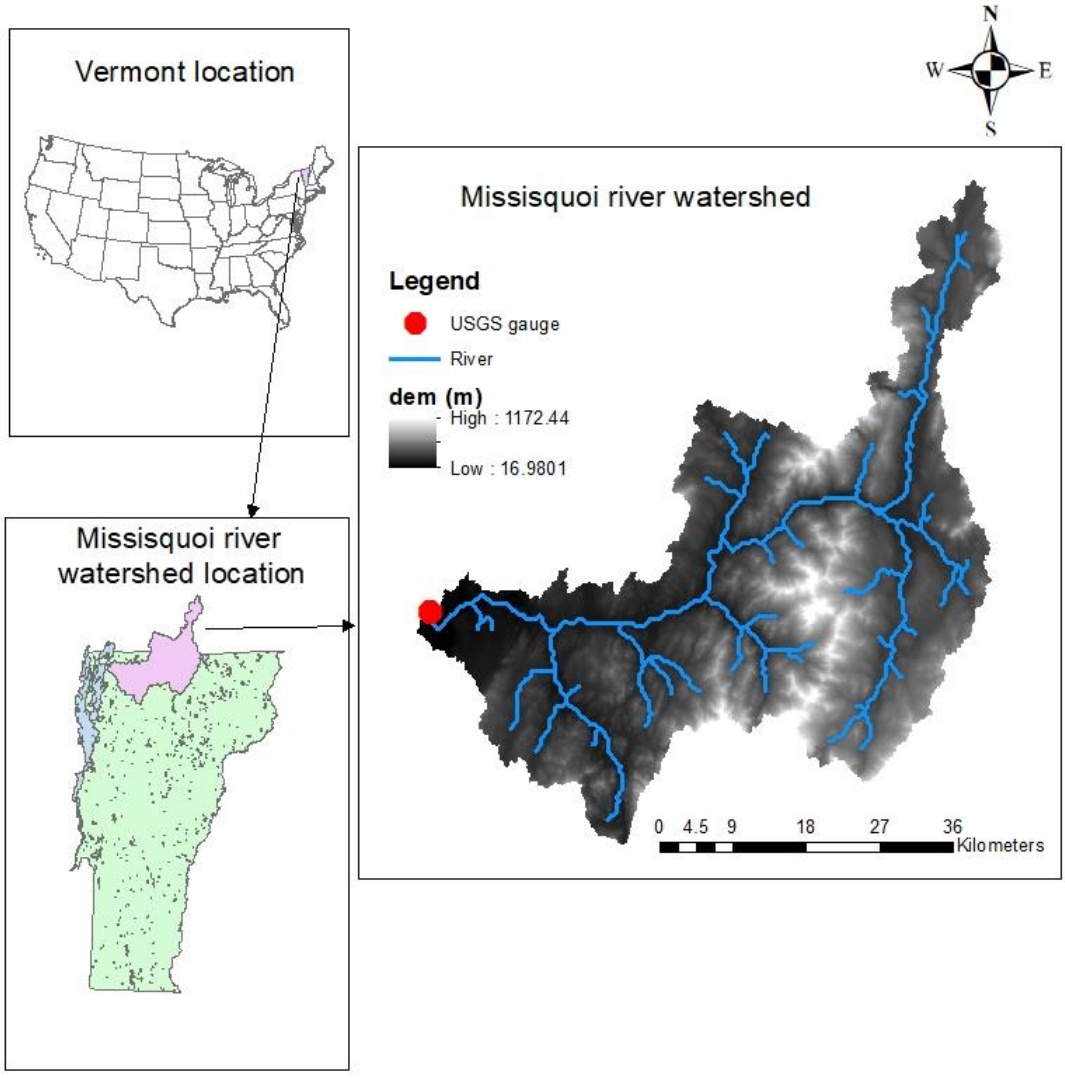

Figure 3.1 Missisquoi river watershed location, USGS gauge #04294000 is located at the outlet of Missisquoi river

3.2.2. RHESSys model description

We used the Regional Hydro-Ecologic Simulation System (RHESSys) (C. L. Tague & Band, 2004), version 5.20 for this study. RHESSys is a Geographical Information System (GIS)-based hydro-ecological model, simulating watershed water,

carbon and nutrient dynamics. RHESSys adopts a hierarchical structure to represent landscapes, which includes basins, hillslopes, zones, patches and canopy strata.

The basin is the whole watershed area. Stream and nutrient routing processes occur at this level, and the routing process iteratively occurs from the highest patch to the lowest patch. The hillslope is the area draining into one side of a stream reach. Groundwater lateral flow is processed at the hillslope level. Deep ground water is simulated as a linear reservoir model. On a daily basis, a fraction of the deep ground water enters its connected stream reach as base flow. Zones are areas with a similar climate. Meteorological data is processed at the zone level by linking the zone with a base station, which provides climate data. The MT-CLIM model (S. W. Running et al., 1987), which uses one climate base station linked to a zone, the topography, slope and aspects etc. to estimate each zone's meteorological data, is integrated at the zone level. The patch is the smallest spatial unit and the basic modeling unit in RHESSys. Patches represent homogeneous soil and land cover characteristics. Vertical water movement is simulated at the patch level, including infiltration in the root zone (for vegetated patches) and unsaturated zone, and recharge to the saturated zone. Soil nutrient fluxes are also simulated at the patch level, such as plant uptake, leaching, decomposition, nitrification and denitrification. Canopy strata have the same spatial area as patches but represent the vertical aboveground vegetation layers. BIOME-BGC (Steven W Running & Hunt, 1993) is integrated at the canopy strata level to simulate plant growth and element fluxes.

RHESSys provides a tool, GRASS2WORLD in GRASS (Geographic Resources Analysis Support System) GIS environment, that partitions the landscape into different structure levels using a Digital Elevation Model (DEM), land cover map, and soil texture, and then generates a text file called worldfile, which represents the landscape structure. This worldfile is used as an input file to RHESSys.

3.2.3. Data

3.2.3.1 Climate data

RHESSys requires at least daily minimum temperature (Tmin), daily maximum temperature (Tmax) and daily precipitation as climate data input. Historical climate data are from Daymet version 3 (Thornton et al., 2017), which provides 1-km grid daily data from 1980 to 2016 for North America. Because future projected downscaled climate data from general circulation models (GCM) have much courser spatial resolution (1/8 degree), Daymet data were resampled at 1/8 degree to be consistent with projected climate data (Figure 3.2).

Three GCM models were chosen based on the model credibility for Northeast United States (Thibeault & Seth, 2015): ccsm4, mri-cgcm3, and gfdl-esm2m. Each GCM has four projected climate datasets from 2020 – 2050 based on the four Representative Concentration Pathways (RCPs): RCP2.6, RCP4.5, RCP6.0 and RCP8.5. All climate data were downscaled to 1/8-degree bias correction with constructed analogs dataset (Zia et al., 2016). Thus, in total, 12 climate scenarios were used for future climate data.

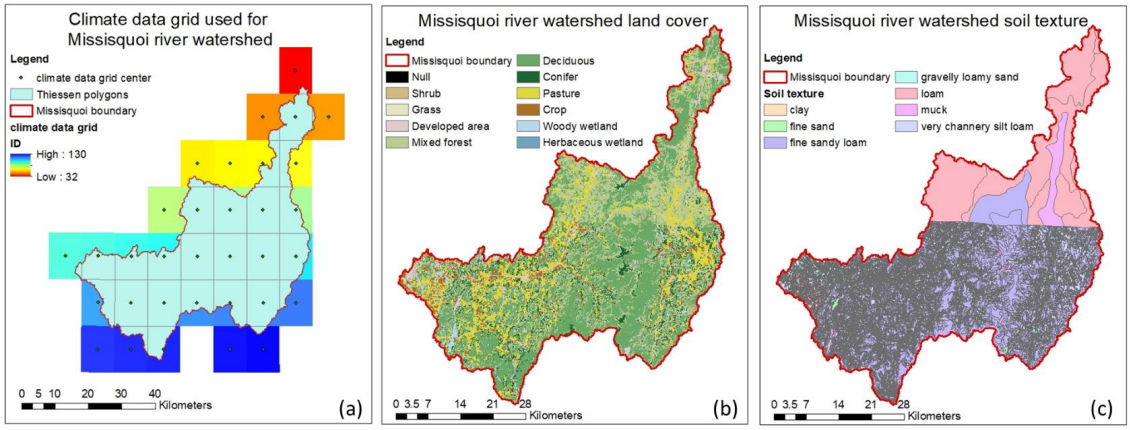

Figure 3.2: RHESSys input data. (a). 1/8 degree grid data used, the grid center points were used to generate Thiessen polygons for spatial climate data input. (b). Missisquoi river watershed land cover, U.S. side is from the year 2001, and Canada side is from the year 2000. (c). Missisquoi river watershed surface soil texture map.

3.2.3.2 Land use/cover data

The land use/cover map combined the US portion (National Land Cover Database, 2001) and Canadian portions (circa 2000, http://www.geobase.ca/) of the Missisquoi River watershed. This land use/cover map was used for RHESSys calibration with historical climate data and gauge data (Figure 3.2).

For the future period (2020 – 2050), we used the ILUTABM model (Y. S. Tsai et al., 2015) to generate three different land use scenario maps (Figure 3.3): Business As Usual (BAU), Prefer Forest (proForest) and Prefer Agriculture (proAg). The ILUTABM model can output land use map every year, but for this study, we outputted one land use map every 10 years. Thus, for each land use scenario, there were three land use maps for the period of 2020 to 2050 (Figure 3.3). Prior to model input, all land use/cover data were reclassified as RHESSys land use/cover types.

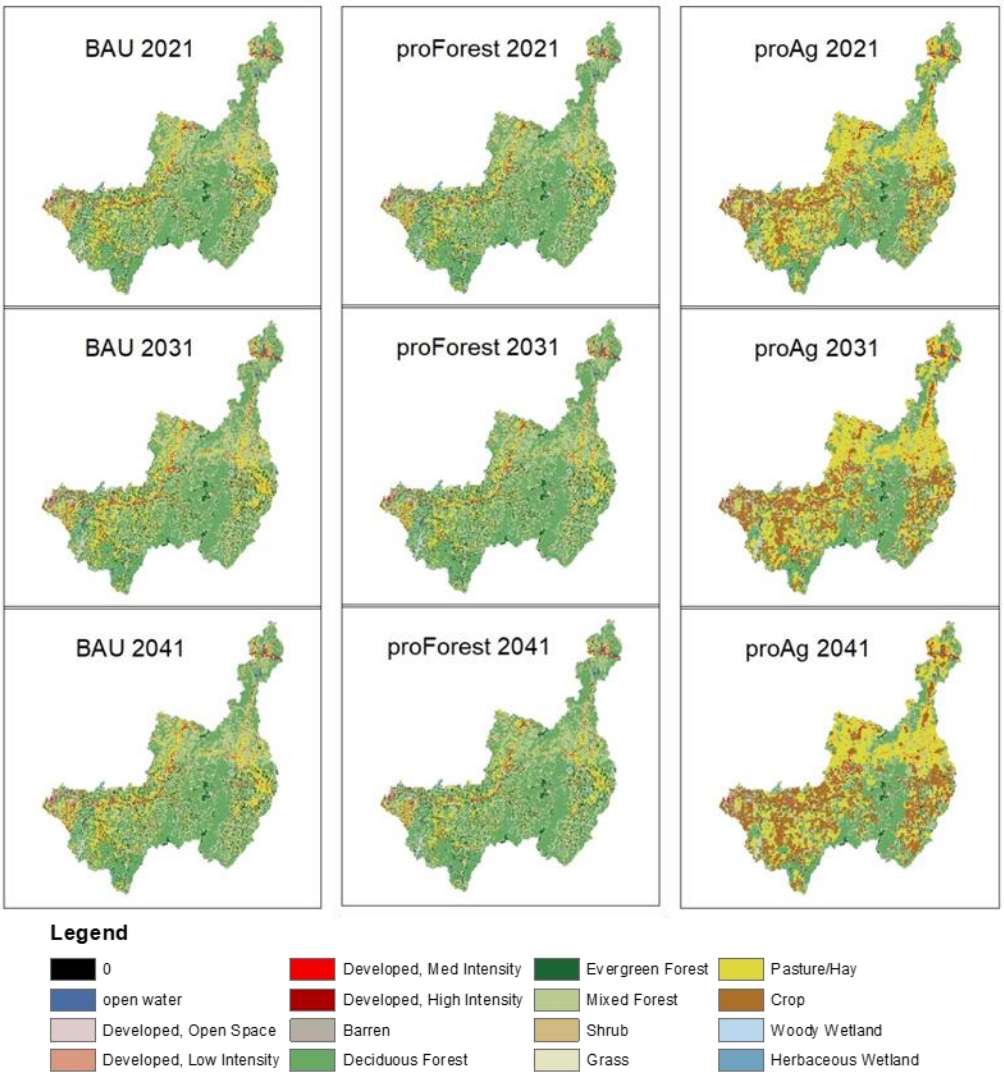

Figure 3.3: Projected land use of the year 2021, 2031 and 2041 for the three land use scenarios: Business As Usual, prefer forest and prefer agriculture.

3.2.3.3 Other input data

For the Missisquoi watershed, a Digital Elevation Model (DEM) of 1 arc-second (approximate 30 meters) from the American National Elevation Dataset was used (Figure 3.1). The DEM was used to generate slope, aspect, west and east horizon grid data. Surface soil texture data were from Vermont Center for Geographic Information (http://vcgi.vermont.gov/) and Soil Landscapes of Canada

(http://sis.agr.gc.ca/cansis/nsdb/slc/index.html). Agricultural land management practice data (fertilizer/manure application, harvest date) were from surveys (Department of Plant and Soil Science, the University of Vermont). Due to lack of spatial agricultural land management practice data, we assumed all agricultural land had the same management practices. Atmospheric nitrogen deposition data was from National Atmospheric Deposition Program (http://nadp.slh.wisc.edu/). The total nitrogen deposition for Missisquoi river watershed was 1g N/m^2/year.

3.2.4. Experiment design for climate change and LUCC impacts assessment

I spun-up the RHESSys model for about 1500 years to let plants and soil carbon and nitrogen pools reach equilibrium states. Then, the spun-up model was calibrated for streamflow at the outlet of Missisquoi river watershed. Finally, with the calibrated parameter set, the model was run with the different climate and LUCC scenarios. In this study, 12 climate scenarios (three GCMs with four RCPs for each GCM) and 3 LUCC scenarios were used, for a total of 36 total climate-LUCC scenarios.

3.2.4.1 Calibration and validation

Four parameters were used to calibrate RHESSys: *m*, *K*, *gw1* and *gw2*. *m* is the decay of hydraulic conductivity with depth (dimensionless); *K* is the surface lateral hydraulic conductivity (*m*/*day*); *gw1* is the proportion of net inflow water moving to the deep ground water store (dimensionless); and *gw2* is the proportion of water from deep

ground water store moving to the stream. The four parameter ranges used in this study were *m* (0 – 0.2), *K* (0 – 300), *gw1* (0 – 0.9) and *gw2* (0 – 0.9) (Saksa et al., 2017).

Monte Carlo simulations were used to calibrate RHESSys. A total of 5040 parameter sets were generated using the Latin-Hypercube sampling technique with even distribution for each parameter over the parameter range. The 5040 parameter sets were used to drive RHESSys model on NCAR Cheyenne cluster (Laboratory, 2017). The Nash-Sutcliff coefficient (NSE) was used to assess parameter set performance.

Streamflow was calibrated from 1992.1.1 to 1994.12.31 and validated from 1992.1.1 to 1994.12.31 (Table 3.1). Model fit during the calibration and validation periods was assessed using the Nash-Sutcliffe efficiency value (NSE) and RMSE. NSE is in the range of $-\infty$ to 1, NSE = 1 means perfect match and NSE = 0 means the model performance is equivalent to the average of observed data, and NSE < 0 means model performance is worse than the average of observed data. A threshold value of 0.6 for daily streamflow NSE is considered good fit (Guilbert, 2016). RMSE measures the average differences of simulated and observed data. The smaller the better.

Table 3.1: Calibration and validation period

	Calibration	Validation
runoff	1992.1.1 - 1994.12.31	1995.1.1 - 1999.12.31

3.2.4.2 Future projection under different climate and LUCC scenarios

Once the best parameter set was determined, it was used to drive RHESSys for all projected scenarios. For all scenarios, the historical land use (US 2000, and Canada 2001) was used to run 2011.1.1 to 2020.12.31 for model warm up. From 2021.1.1, projected land use of 2021 was used to run RHESSys until 2050.12.31. The land use map was updated every 10 years. The same processes were applied to other land use transition years.

In RHESSys, the worldfile is used to describe basin states. Land use change can affect 3 items in the worldfile: the base station a patch attached to, patch land use type, and patch vegetation type. The base station controls agricultural land management practices, such as fertilizer application. Land use type controls common land management configurations and vegetation type controls vegetation physiology characteristics. Changing these 3 items reflects the LUCC in the RHESSys model.

At the land use transition year, a new worldfile with a new land use map was used to compare with old worldfile (with old land use map). If any of the 3 items were different for the same landscape unit, the item value from new worldfile was used to replace the corresponding value in the old worldfile. In this way, land use change was integrated into model configuration.

3.2.4.3 Future projection results analysis

We used boxplots to show multiple temporal streamflow distribution characteristics under all climate change and LUCC scenarios. To test our hypothesis, we used annual streamflow standard deviations of RCPs, GCMs and LUCCs to study which factor was the dominant impacting factor on streamflow. This analysis further factored climate into RCPs and GCMs and would provide insights on climate change impacts on streamflow.

3.3. Results

3.3.1. Calibration and validation

Monte Carlo simulation was used to calibrate RHESSys with 5040 parameter sets. Model fit was examined using the streamflow Nash-Sutcliffe efficiency value (NSE) relationship with each parameter (Figure 3.4). Parameter *m* ranged from 0 to 20 and NSE increased with *m* in this range (Figure 3.4 a). Parameter *K* had no uniform relationship with NSE and most NSE values were above zero (Figure 3.4 b). Parameter *gw1* had a parabola relationship with NSE, with the NSE peak is in the range between 0.3 and 0.6 (Figure 3.4 c). Like parameter *m*, the NSE increased with parameter *gw2* (Figure 3.4 d).

Based on the NSE values of all parameter sets, one parameter set with the best performance for streamflow was chosen, and this parameter set was used for calibration, validation and future projections. The best parameter set had values of 19.2 for *m*, 206.08 for *K*, 0.299 for *gw1* and 0.888 for *gw2*.

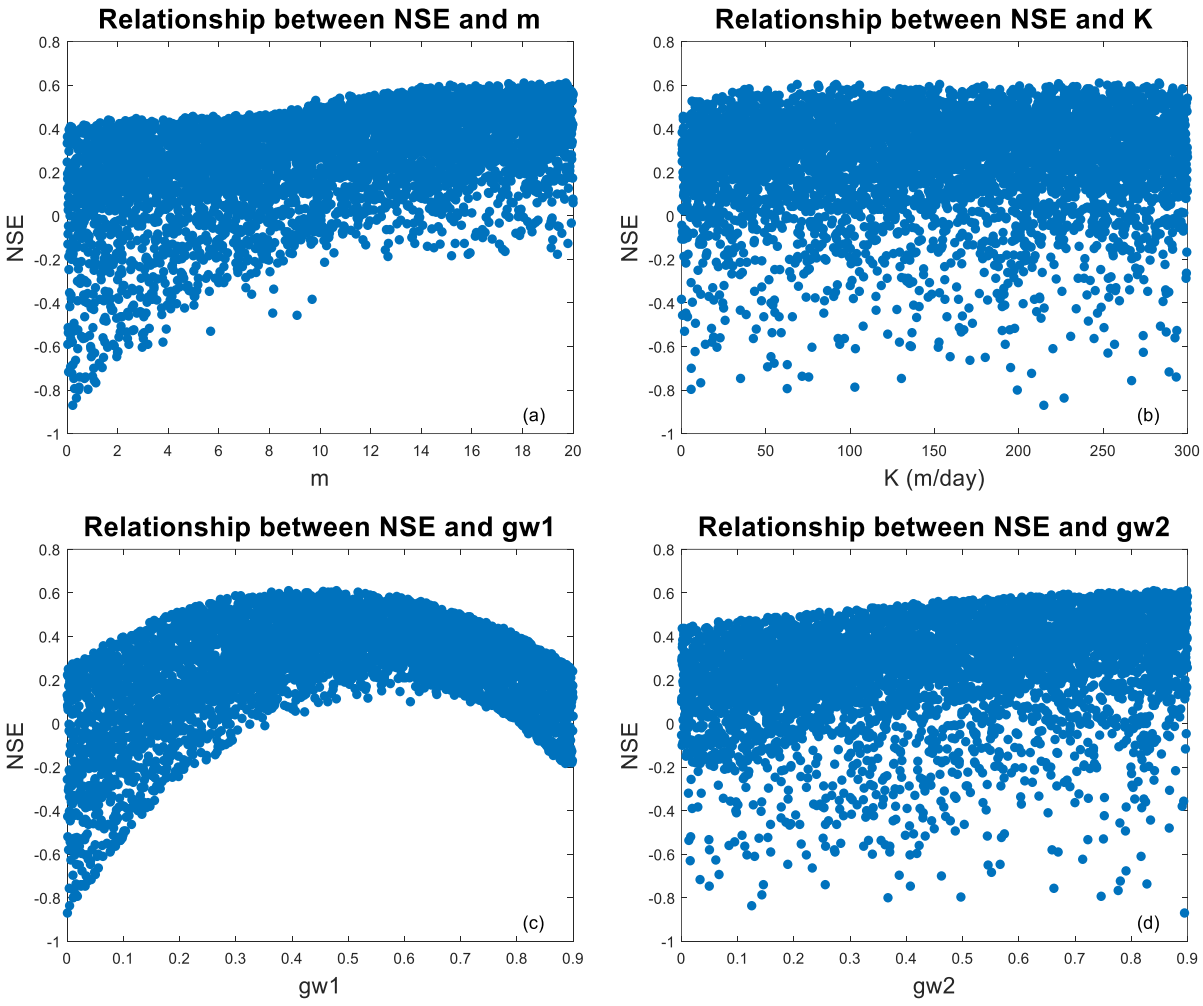

Figure 3.4: Daily streamflow NSE relationship with the 5040 calibrated parameter sets (m, K, gw1, and gw2) in the calibration period (1992.1.1 – 1994.12.31). (a) Parameter m. (b) Parameter K. (c) Parameter gw1. (d) Parameter gw2.

In the streamflow calibration period (01/01/1992 –12/31/1994), NSE was 0.59, RMSE was 1.5054 mm. In the validation period (1/1/1995 – 12/31/1998), NSE was 0.52 (Figure 3.5), RMSE was 2.1031 mm and the R^2 is 0.526 (Figure 3.6). Streamflow NSE and RMSE for each individual calendar year in the calibration and validation period was calculated (Table 3.2). In the calibration period, year 1994 reached the highest NSE

(0.77) and lowest RMSE (1.1873 mm) and year 1993 achieved the lowest NSE (0.41) and highest RMSE (1.8737 mm). In the validation period, the lowest NSE (0.41) occurred at the year 1996, and the highest NSE (0.61) was in the year 1998. The highest RMSE (2.5737 mm) occurred at the year of 1996, which was consistent with the lowest NSE; the lowest RMSE (1.4655) occurred at the year of 1995, which was different with the highest NSE year (1998).

Table 3.2: Streamflow NSE value for each individual year for the calibration and validation years.

Calendar year	1992	1993	1994	1995	1996	1997	1998
NSE	0.58	0.41	0.77	0.52	0.41	0.48	0.61
RMSE(mm)	1.3710	1.8737	1.1873	1.4655	2.5737	1.7771	2.3993

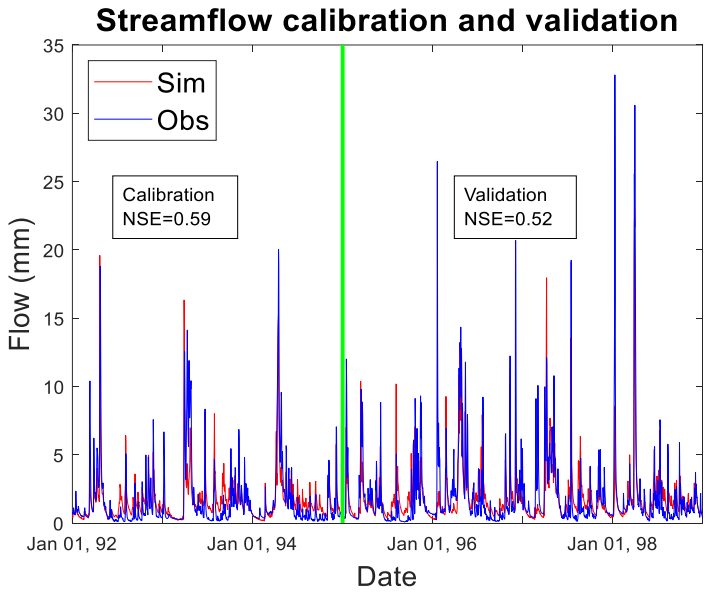

Figure 3.5 Simulated and observed streamflow for calibration and validation periods.

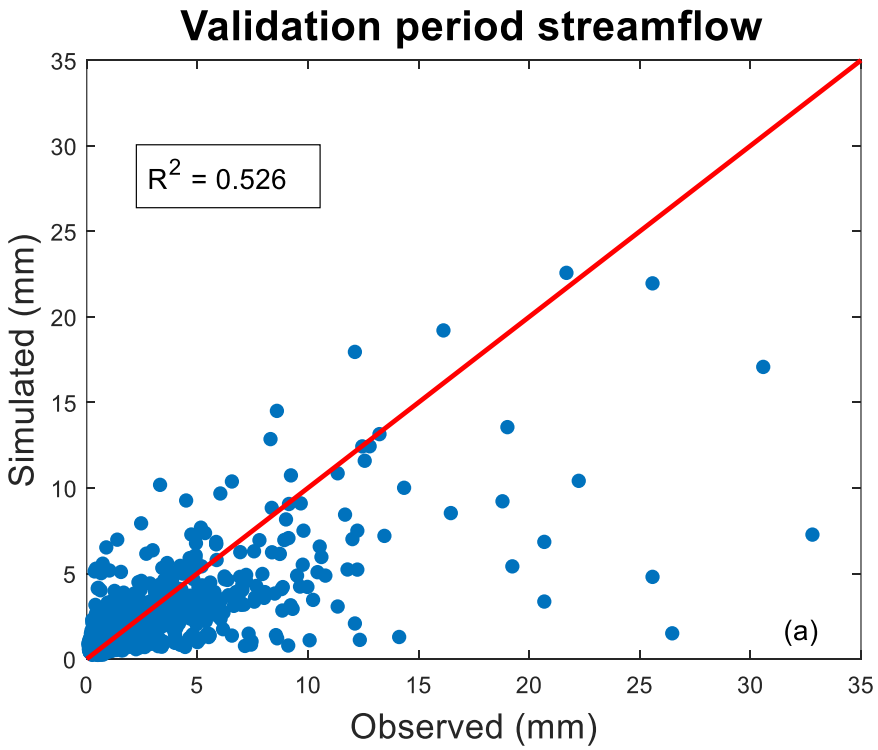

Figure 3.6 Scatter plot for streamflow

3.3.2. Projected streamflow

Annual streamflow showed great variability during the projected period of 2021 – 2050 under all climate and land use scenarios (Figure 3.7). Under the same GCM, all land use scenarios had similar annual streamflow patterns for the same RCP, although with some variation. Under the same LUCC scenario, different GCMs had different annual streamflow patterns and fluctuation magnitudes (Figure 3.7). This indicates that climate change had larger impacts on annual streamflow than LUCC in Missisquoi River watershed during the period of 2021 – 2050.

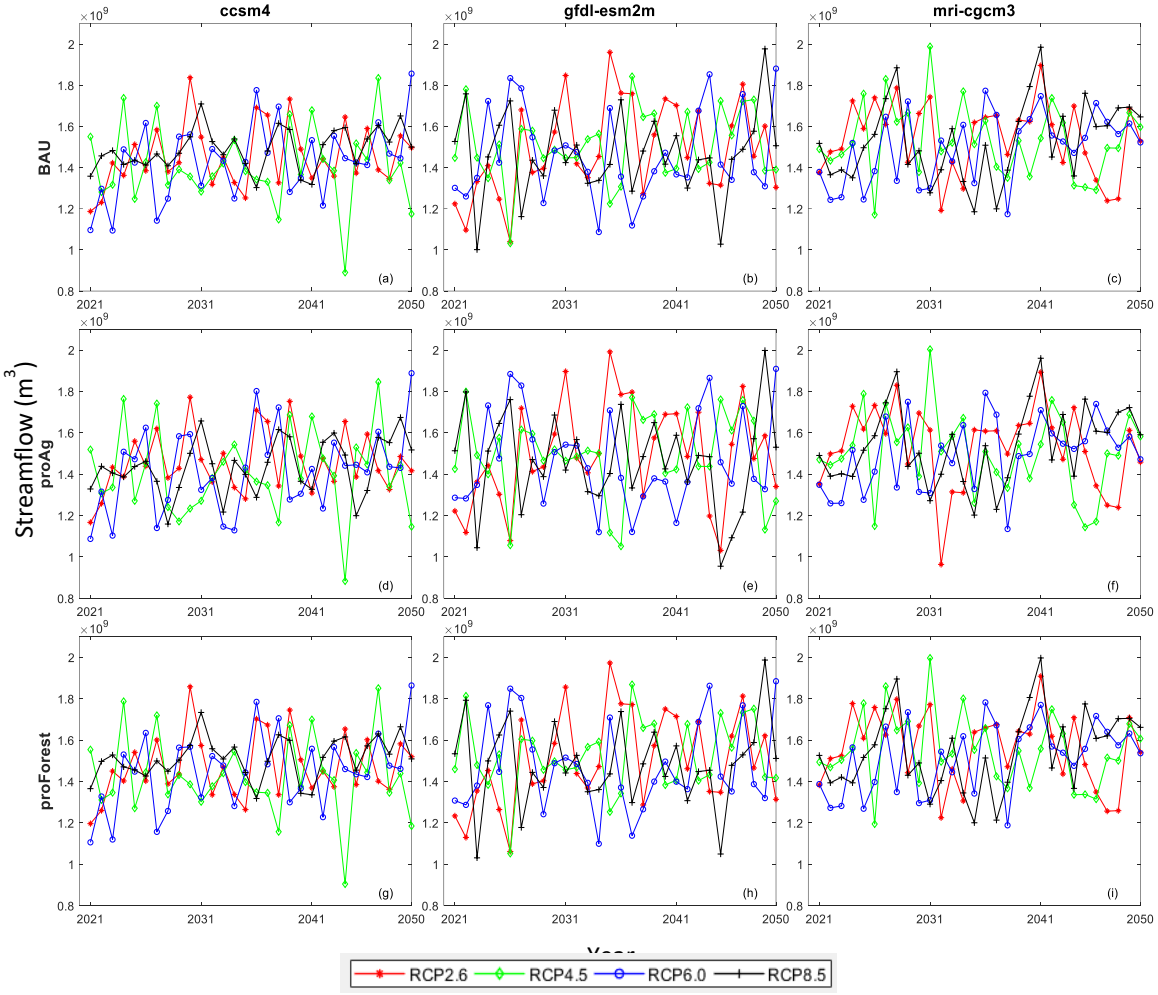

Figure 3.7 Projected annual streamflow under different climate change and LUCC scenarios from 2021 to 2050

Annual streamflow boxplots also showed climate scenarios had a stronger influence than LUCC (Figure 3.8). For the same GCM and RCP, annual streamflow boxplots showed similar patterns under different LUCC. Under all LUCC scenarios, ccsm4 had a median annual flow of around 1.4 $\times 10^9$ m^3 with a narrow interquartile range for all RCPs; gfdl-esm2m had a median annual flow of around 1.4 $\times 10^9$ m^3 but

with a bigger interquartile range for all RCPs; mri-cgcm3 had higher median annual flow of around 1.5 $\times 10^9$ m^3 with a median interquartile range in the 3 GCMs.

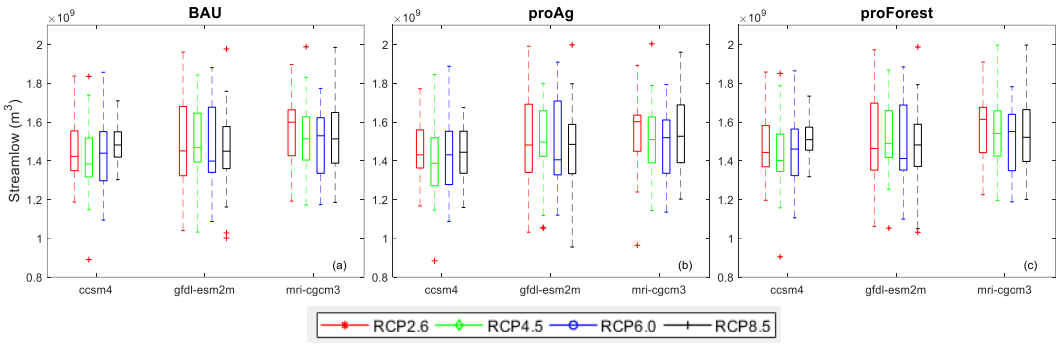

Figure 3.8 Projected annual streamflow boxplot under different climate change and LUCC scenarios for the period of 2021 – 2050

Annual streamflow boxplots for the 3 decades of 2021 – 2050 were studied under all climate and LUCC scenarios (Figure 3.9). In each decade, streamflow under the same climate scenario showed similar patterns under different LUCC, but quite different patterns under different GCMs (Figure 3.9). This indicated climate had a stronger influence on than LUCC in each of the 3 decades.

Generally, under all scenarios, there is no clear increasing or decreasing streamflow trend from the first decade to the third decade, which is consistent with the lack of an upward trend in projected annual stream flows across all three decades (Figure 3.7).

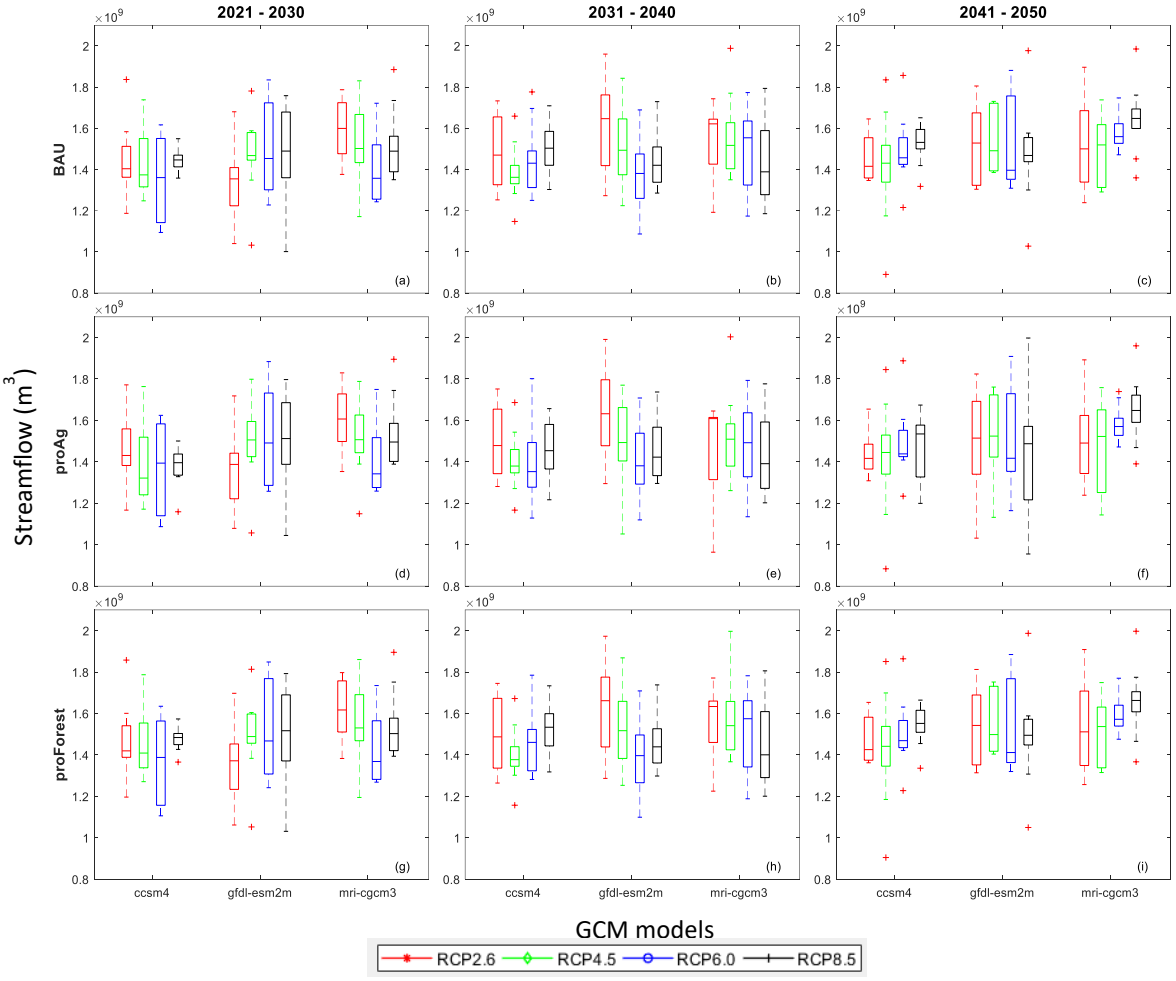

Figure 3.9 Projected annual streamflow boxplot under different climate change and LUCC scenarios for decades of 2021 – 2030, 2031 – 2040 and 2041 – 2050

In addition to annual streamflow, I studied quarterly streamflow to examine potential within year changes in streamflow (e.g., in wintertime or low summer flows Figure 3.10 and Figure 3.11). Under BAU and proForest, all climate scenarios had an increasing trend from quarter 1 (January to March) to quarter 4 (October to December; Figure 3.10), with quarter 1 streamflow significantly lower than other quarters. ProAg shows different characteristics. Under proAg, quarter 1 to quarter 3 (July to September)

streamflow was similar under all climate scenarios, but quarter 4 had higher stream flows than the other 3 quarters.

GCMs also predicted different quarterly extremes. The ccsm4 and gfdl-esm2m models had more extremes in quarter 3 under all LUCCs. The mri-cgcm3 model had the most extremes in the quarter 2.

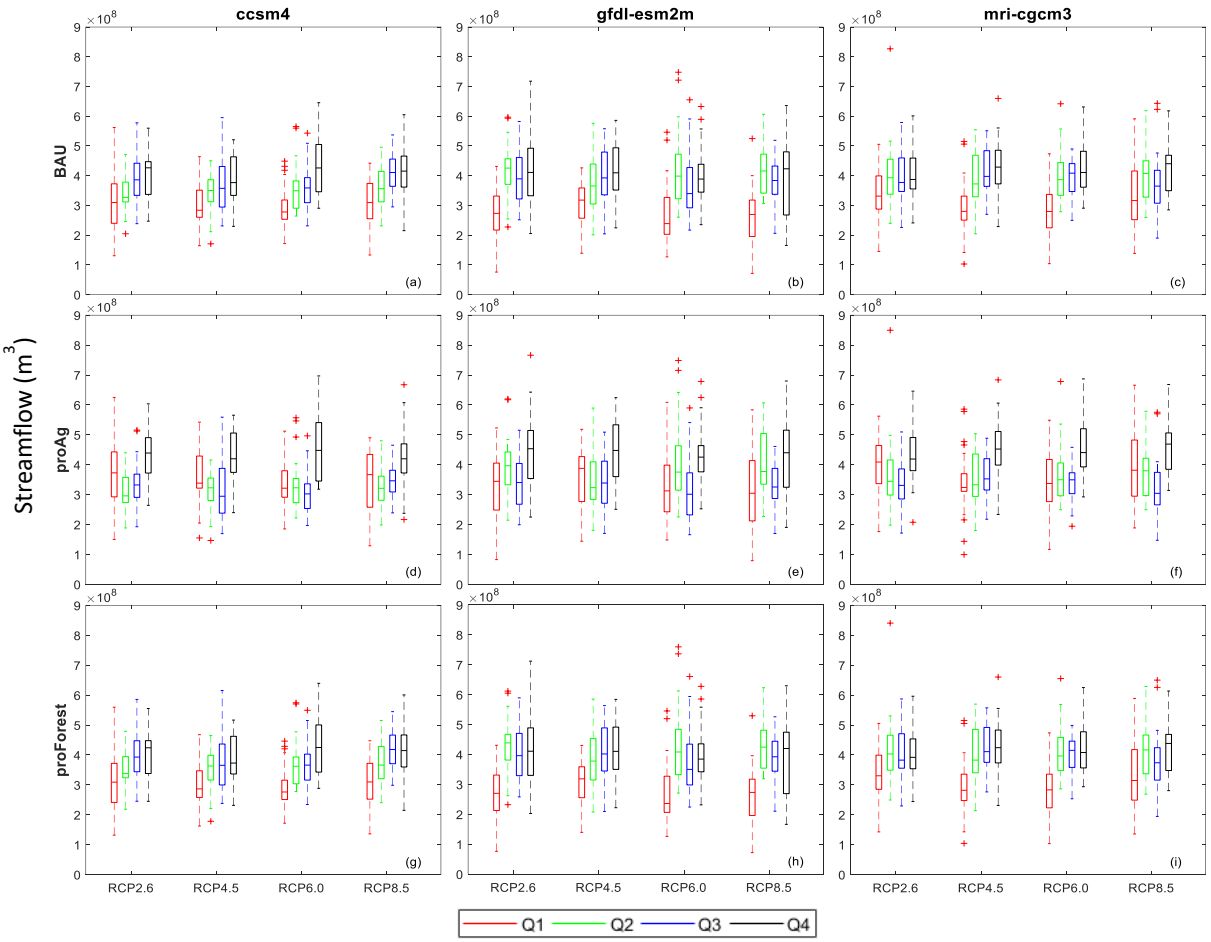

Figure 3.10 Projected quarterly streamflow boxplot under different climate change and LUCC scenarios. Q1 is from January to March, Q2 is from April to June, Q3 is from July to September, and Q4 is from October to December

Figure 3.11 shows the quarterly streamflow in each of the three decades between 2021 and 2050. For each RCP, all 3 GCMs results were combined to represent each RCP result. In all decades, under BAU and proForest, streamflow generally increased from quarter 1 to quarter 4 under all RCPs. Under proAg, streamflow in quarters 1 to 3 were similar, but quarter 4 had higher streamflow than the other 3 quarters.

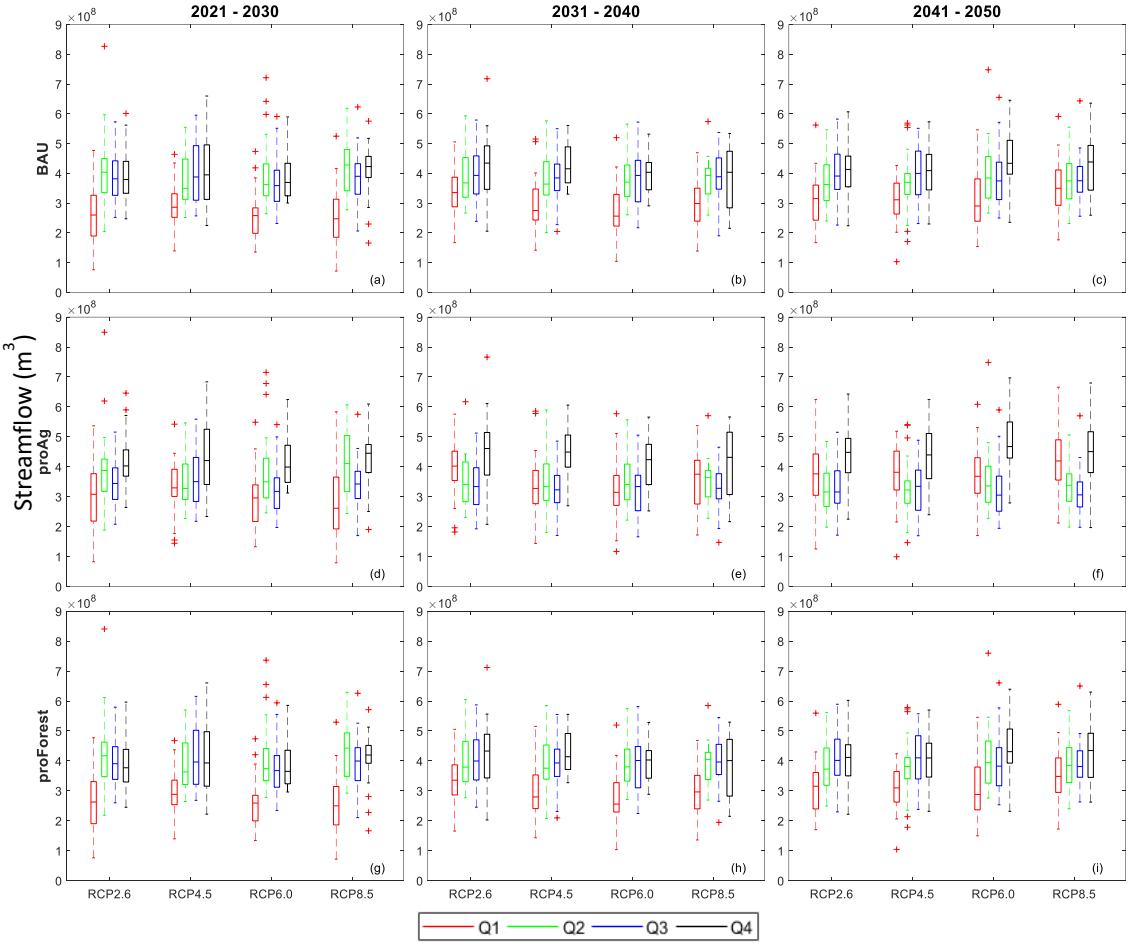

Figure 3.11 Projected quarterly streamflow boxplot under different LUCC scenarios for decades of 2021 – 2030, 2031 – 2040 and 2041 – 2050, for each RCP scenario, all 3 GCMs data were merged in each box

We used annual flow standard deviation to compare the impact of LUCC, RCP climate scenarios, and GCM model choice on streamflow (Figure 3.12). The standard deviation of annual streamflow from 2021-2050 for the 3 LUCCs in each RCP across all GCMs was relatively small (all medians < 0.5 $\times 10^8$ m^3). The standard deviations for annual streamflow for the RCPs (within each LUCC) and for the GCMs (within each RCP) were substantially higher than for LUCCs (medians were approximately 1.5 $\times 10^8$ m^3), indicating that substantially more variation in streamflow was associated with climate scenarios and GCM climate projections. The standard deviation spread of LUCCs was shorter than that of RCPs and GCMs, indicating the impacts on streamflow of LUCCc were stable across the 30 years compared with RCPs and GCMs. One notable thing was that the standard deviation medians and spreads were similar between RCPs and GCMs, meaning the impacts on streamflow of RCPs and GCMs were comparable.

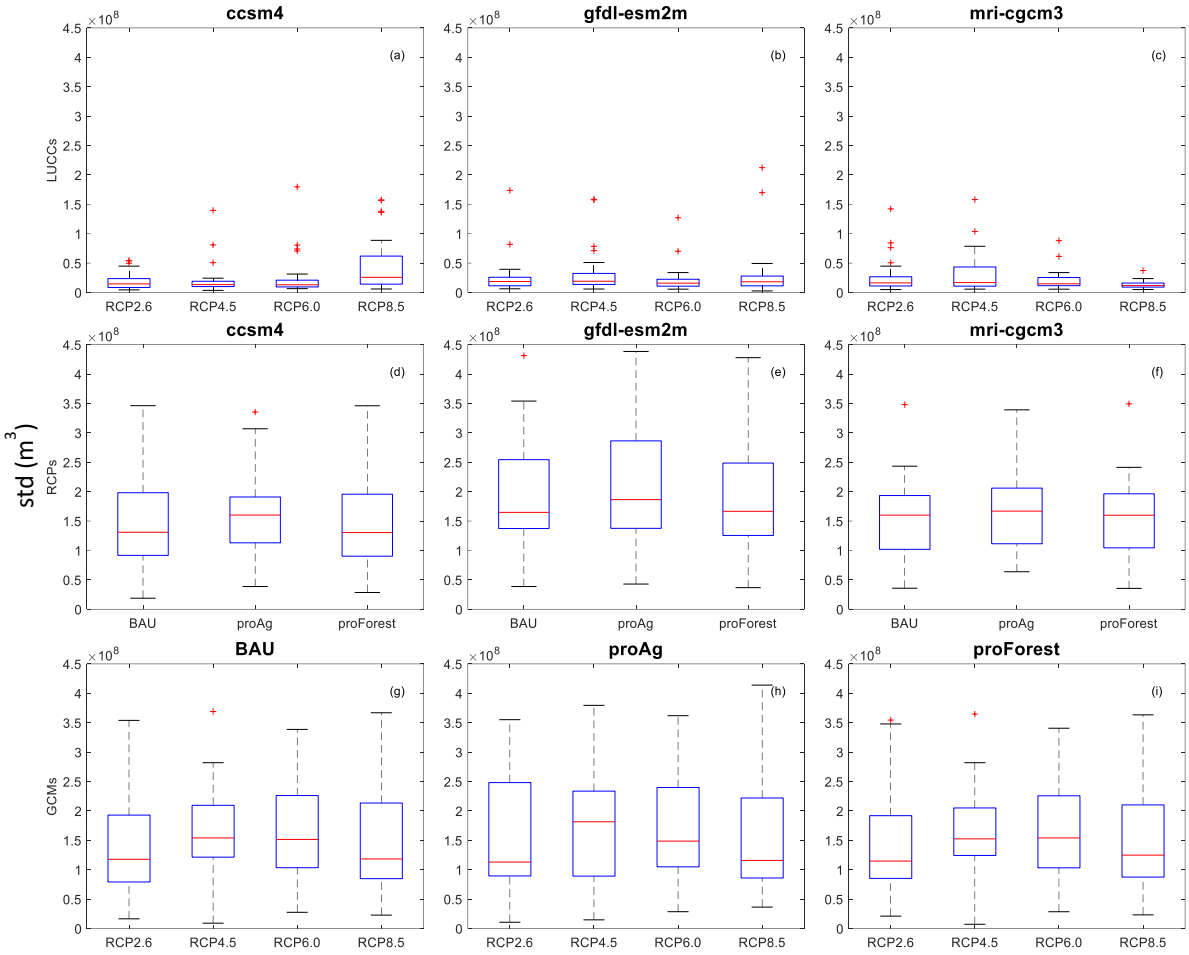

Figure 3.12 Standard deviation of annual streamflow (2021-2050) by land use cover change (LUCC) scenarios, representative concentration pathway (RCP) climate scenarios, and general circulation models (GCMs). The top row shows the standard deviation of LUCCs, the middle row shows the standard deviation of RCPs and the bottom row shows the standard deviation of GCMs

3.4. Discussion

3.4.1. RHESSys performance on streamflow

Although RHESSys has been widely used for watershed simulation (Godsey et al., 2014; Hanan et al., 2017; Hwang et al., 2008; Martin et al., 2017; Saksa et al., 2017), and showed RHESSYs could capture streamflow dynamics, our study showed RHESSys

had low performance in some years (Table 3.2). Guilbert (2016) had similar problems using RHESSys in the Mad River watershed of Vermont, US. He found that NSEs were greater than 0.5 for only 9 of the 49 validation years. This unstable simulation performance suggests that multiple years' data are necessary for RHESSys calibration and that a well-calibrated RHESSys model may still perform poorly in any given simulation year. This situation likely leads to uncertainty surrounding model results and the appropriate level of reliance on these results for predicting the impacts of climate change and LUCC on streamflow. Unfortunately, RHESSys does not come with a diagnostic tool to analyze model uncertainty. Here, we attempt to analyze the potential sources of uncertainty.

The first reason is that RHESSys combines processed-based and empirical water cycle frameworks for ground water. Specifically, the empirical framework is the simple reservoir model for deep ground water, while the process-based framework is for ground water. The problem here is that while the process-based ground water framework is based on real-world processes, the deep ground water seems to only function for tuning streamflow – it cannot be mapped to a real-world process. However, RHESSys calibration relies heavily on the deep ground water parameters (*gw1* and *gw2*). The outcome of the calibration is that even though the model can capture the observations during the calibration period, the calibrated model could still perform poorly in validation or simulation years because the calibrated model does not reflect real-world processes.

The second reason is the mismatch between the input data temporal scale and simulation time step. In this study, precipitation is daily, but RHESSys runs hourly processes internally. When lacking hourly time step data, RHESSys assumes the precipitation is evenly distributed throughout the day. This assumption will underestimate rain intensity, especially for storms, and likely reduces the ability of the model to capture observed high streamflow.

Therefore, future model development should improve the water cycle framework by replacing the empirical module with a process-based module. Furthermore, for precipitation input data, hourly data should be prioritized, especially for investigations of extreme precipitation events.

3.4.2. Climate change and LUCC impacts on streamflow in Missisquoi river watershed

Using projected RCP climate scenarios and LUCC simulations generated by an agent-based land transition model (Y. Tsai et al., 2015), we found that annual discharge was more sensitive to climate than to LUCC. Annual discharge under the same LUCC with different climate data had quite different annual discharge patterns (Figure 3.7 and Figure 3.12). Discharge under different LUCC scenarios with the same climate data had similar patterns, indicating annual discharge is relatively insensitive to land use change at this time scale. Furthermore, streamflow showed little variation in response to LUCC, while it showed large variability in response to climate data from the RCPs and different

GCMs (Figure 3.12). This suggests that streamflow is more sensitive to climate than to LUCC, despite the fact that no overall trend or response to the RCPs was observed over the 2021-2050 period. This result is consistent with Ling et al. (2015) and Alaoui et al. (2014), who found that climate change rather than LUCC were primarily responsible for the hydrological variations. Although land use change can alter ET in the water cycle, which could further influence discharge, compared with climate influence (i.e., direct precipitation input and temperature change), the LUCC scenarios did not play a dominant role in altering discharge.

A further question we explored was the impacts of climate change and GCMs. Climate change is represented as RCPs. However, future climate projection is produced by a specific GCM. This means climate change impacts on streamflow carry over the bias from GCM. Therefore, it is necessary to use multiple GCMs to study the impacts of climate change. In this study, we used 3 GCMs to study and all the 3 GCMs showed the annual streamflow responded RCPs stronger than LUCC, which meant climate change had stronger impacts on streamflow than LUCC. However, we noticed the standard deviation of GCMs were comparable with that of RCPs. This means GCMs options could lead to big variances. Multiple GCMs should be used to provide an uncertainty range from GCMs.

While there were no overall responses of streamflow to the different RCPs, there were some indications that the number of extreme flow events may increase over time in the various RCPs. DESCRIBE THESE RESULTS BRIEFLY HERE. Also, why no

overall response to the RCPs if streamflow is so responsive to climate? Perhaps because the scenarios do not diverge substantially from one another by 2050. Perhaps also because of the variation between GCMs in predicting the different scenarios.

3.4.3. Limitations

Although my study followed the advanced philosophy of simulating real-world dynamic processes, there are still some limitations. The limitations can be categorized into three main categories: model input data, RHESSys intrinsic processes and simulation processes.

Some model input data limitations are common across model applications, but some are specific to this study. First, spatial data aggregation is based on majority rule and this process may have caused some information loss, e.g., regarding soil texture and land use. Second, climate reanalysis data may have contained inaccuracies. The GCM climate data were downscaled to 1 / 8 degree. Winter et al. (2016) pointed the downscaled data absolute bias was noisy at low elevations, and the climate data could be underestimated or overestimated without clear relationship with elevation. The error in precipitation can directly affect watershed water input and reflect in the streamflow. Gombault et al. (2015) found annual precipitation increases of 7 to 12% resulted in streamflow increases of 11 to 21% in an agricultural watershed study of southern Quebec (Canada). These two limitations are common across model simulations. The specific limitation to this study is that lack of hourly precipitation input can't reflect precipitation

intensity, and further affect infiltration and overland flow processes, especially for storms.

There are several RHESSys intrinsic limitations. The first one is RHESSys uses empirical reservoir ground water model, which was mentioned in section 3.4.1. The second limitation is that RHESSys does not include in-stream routing processes, once water reaches any stream, the water automatically exits from the outlet. For small watersheds, this assumption may not result in large errors, because the time for water to travel to the outlet is short. However, for large watersheds, precipitation in one day may reach the outlet in the next day. This mismatch between simulation and observation can make shift simulation streamflows from observed streamflows by several days. The third limitation is that RHESSys does not dynamically change CO_2 concentration and does not fully integrate the interactions between climate and vegetation. High CO_2 concentration reduces leaf stomatal conductance and affects plant transpiration, which further alters streamflow. Luo et al. (2013) integrated CO_2 effects on plants in the SWAT model and showed that doubling CO_2 reduced evapotranspiration (ET) by 10.6% for agricultural land, 5.7% for deciduous forest, and 4.2% for rangeland. Therefore, long-term simulation projections without dynamic CO_2 change can overestimate ET and underestimate streamflow. Growing season length increases due to climate change in mid-high latitude of the northern hemisphere has also been documented since the 1960s (Jeong, Ho, Gim, & Brown, 2011; Kolarova, Nekovar, & Adamik, 2014; Menzel & Fabian, 1999; Piao, Friedlingstein, Ciais, Viovy, & Demarty, 2007), the longer growing season length could also potentially impact the watershed water cycle through water uptake and ET.

RHESSys uses fixed growing season starting day and end day to determine the growing season length, thus the fixed growing season length will not interact with future climate change, which will affect ET and further affect streamflow.

Our simulations are also limited by abrupt LUCC transitions during the land use change year. In this study, we changed patch land use code based on a new land use map in the transition year. This can make the patches with new land use characteristics. However, we kept the patch state variables as the same as before land use change. For example, if a patch changed from grass land to forest land, the patch will carry grass patch states into forest patch. And grass pools will go to corresponding forest pools. If forest pools are not balanced well, the forest patch growth could be affected in the next few years.

These limitations necessarily result in streamflow uncertainly for future projections. To overcome this limitation, more effort needs to be put into improving ecosystem simulation processes in RHESSys.

3.5. Conclusion

This study coupled LUCC and climate change with 3 GCMs to study their impacts on Missisquoi River watershed streamflow dynamics with RHESSys. The study

first evaluated RHESSys performance on streamflow. The model performed moderately well: simulated daily streamflow had an NSE of 0.59 (0.41 – 0.77 for individual year) and RMSE of 1.5054 mm (1.1873 – 1.8737 mm for individual year) in the calibration period, NSE of 0.52 (0.41 – 0.61for individual year) and RMSE of 2.1031 mm (1.4655 – 2.5737 mm for individual year) in the validation period. Second, we evaluated how climate change and LUCC impact on Missisquoi River watershed streamflow. Major results were: (i) For streamflow, medians of standard deviation of annual streamflow was around 1.5×10^8 m^3 for RCPs and 0.2×10^8 m^3 for LUCC, indicating climate had a stronger influence than LUCC; (ii) climate variation in the RCPs and GCMs had comparable influences on streamflow, and had a stronger impact on streamflow than LUCCs; (iii) the stronger impact of climate on streamflow suggests that future, and increasing, climate change will likely have a larger impact on streamflow than changes in LUCC; and (iv) The standard deviation of GCMs was similar to RCPs, indicating GCMs could be an important source of uncertainty source..

CHAPTER 4. CLIMATE CHANGE AND LAND USE/COVER CHANGES IMPACTS ON NITROGEN LOAD IN MISSISQUOI RIVER WATERSHED

4.1 Introduction

Anthropogenic activities have greatly modified the nitrogen cycle through fixing nitrogen as fertilizer, which converts inert nitrogen (N_2) to reactive nitrogen. By 2010, 75% of reactive nitrogen was created on the land by human activities (Galloway et al., 2014). The fixed reactive nitrogen increased agricultural crops yield and supported the growing global population (S. Seitzinger, 2008). However, fertilizer application also provides nitrogen sources for emission into the atmosphere as greenhouse gases (M. Gao et al., 2014) or transport to rivers, leading to water quality degradation (Vitousek et al., 2009). Indeed, agricultural non-point source pollution is a main nutrient source for surface water. Therefore, agricultural land as a nutrient source has received great attention (M. Gao et al., 2014; Jiang et al., 2014).

At the same time, the climate has been warming, especially since 1980, and the global warming trend is projected to continue into the 21st century, which potentially dramatic changes in future temperature and precipitation patterns (Pachauri et al., 2014). Hydrological regimes are closely related to temperature and precipitation, and some studies have shown that projected climate change will affect hydrological regimes in the future (Fan & Shibata, 2015; Zhang et al., 2015). Since hydrology is closely coupled with nitrogen transport, understanding how hydrological regime change will affect nitrogen export is significant for future adaptation. Jeppesen et al. (2011) used the IPCC A2 scenario to study the climate change effects on nitrogen loading and found that the

projected climate change will likely increase the nitrogen load to lakes in Northern Europe at the end of 21st century (2071 – 2010). A study in Eastern Canada showed projected climate change will not only increase annual nitrogen load, but also lead to more nitrogen load in earlier spring by 2100 (Dayyani et al., 2012).

Land use/cover change (LUCC) is another important factor influencing watershed nitrogen loads (El-Khoury et al., 2015; Fan & Shibata, 2016). Different land use types have different nitrogen cycling pathways and characteristics: forest and grass land can intercept and absorb nitrogen; crop land receives fertilizer, making crop land a potential nitrogen source; urban lands with impervious area cannot retain as much nitrogen as vegetated land. Thus, land use change from one to another type leads to different nitrogen cycling pathways and to further changes in watershed nitrogen outputs.

Climate change and LUCC are likely to occur jointly in the future (Ling et al., 2015). Therefore, in this study, we couple LUCC from an agent-based land transition model – Interactive Land Use Transition Agent-Based Model (ILUTABM) (Y. Tsai et al., 2015) – with climate change projections to study their joint impacts on nitrogen loads in the Missisquoi river watershed in Vermont, US. We expect LUCC to have larger impacts on nitrogen loading than climate change scenarios due to fertilizer application in cropland. Thus, the more agricultural land in the land use scenarios, the more nitrogen load the watershed will output. Using a spatially explicit model to understand the relative impacts of climate change and LUCC on watershed nitrogen loading will improve will support stakeholder decisions around land management and policy making. The novelty

of this study is coupling the climate change with dynamic LUCC process, and our experiment design can investigate the relative importance of LUCC, climate change due to RCPs and GCMs.

4.2. Data and methods

4.2.1. Study area

The Missisquoi River watershed is located along the border of the US and Canada and covers 2,200 km^2 (Figure 4.1). The altitude in this area ranges from 17 to 1172m. In 2001, the predominant land cover was forested (~ 70%). Pasture/hay land cover was ~14% and crop land cover was ~5%. The Missisquoi River drains into Missisquoi Bay, which is in the northern part of Lake Chaplain.

A USGS streamflow gauge (#04294000) is located at 44°55'00" N and 73°07'44" W (North American Datum 1927) near the Missisquoi river outlet. The gauge has recorded daily streamflow from March 1st, 1990 until now. The Lake Champlain Long-term Monitoring program also set up a sampling point at the streamflow gauge and recorded nutrient data from 1990 – Now (https://anrweb.vermont.gov/dec/_dec/LongTermMonitoringLakes.aspx).

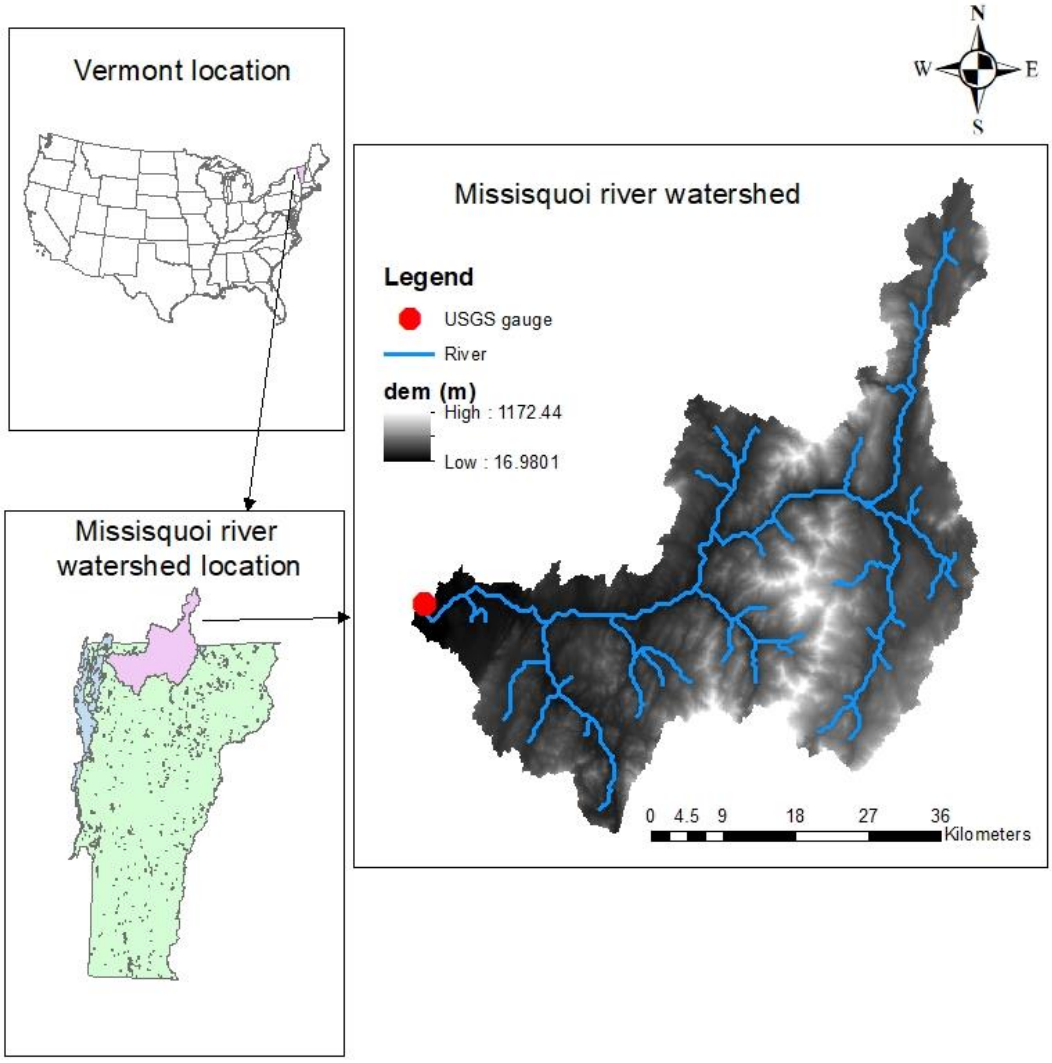

Figure 4.1 Missisquoi river watershed location, USGS gauge #04294000 is located at the outlet of Missisquoi river

4.2.2. RHESSys model description

We used the Regional Hydro-Ecologic Simulation System (RHESSys) (C. L. Tague & Band, 2004), version 5.20 for this study. RHESSys is a Geographical Information System (GIS)-based hydro-ecological model, simulating watershed water,

carbon and nutrient dynamics. RHESSys adopts a hierarchical structure to represent landscapes, which includes basins, hillslopes, zones, patches and canopy strata.

The basin is the whole watershed area. Stream and nutrient routing processes occur at this level, and the routing process iteratively occurs from the highest patch to the lowest patch. The hillslope is the area draining into one side of a stream reach. Groundwater lateral flow is processed at the hillslope level. Deep ground water is simulated as a linear reservoir model. On a daily basis, a fraction of the deep ground water enters its connected stream reach as base flow. Zones are areas with a similar climate. Meteorological data is processed at the zone level by linking the zone with a base station, which provides climate data. The MT-CLIM model (S. W. Running et al., 1987), which uses one climate base station linked to a zone, the topography, slope and aspects etc. to estimate each zone's meteorological data, is integrated at the zone level. The patch is the smallest spatial unit and the basic modeling unit in RHESSys. Patches represent homogeneous soil and land cover characteristics. Vertical water movement is simulated at the patch level, including infiltration in the root zone (for vegetated patches) and unsaturated zone, and recharge to the saturated zone. Soil nutrient fluxes are also simulated at the patch level, such as plant uptake, leaching, decomposition, nitrification and denitrification. Canopy strata have the same spatial area as patches but represent the vertical aboveground vegetation layers. BIOME-BGC (Steven W Running & Hunt, 1993) is integrated at the canopy strata level to simulate plant growth and element fluxes.

RHESSys provides a tool, GRASS2WORLD in GRASS (Geographic Resources Analysis Support System) GIS environment, that partitions the landscape into different structure levels using a Digital Elevation Model (DEM), land cover map, and soil texture, and then generates a text file called worldfile, which represents the landscape structure. This worldfile is used as an input file to RHESSys.

4.2.3. Data

4.2.3.1 Climate data

RHESSys requires at least daily minimum temperature (Tmin), daily maximum temperature (Tmax) and daily precipitation as climate data input. Historical climate data are from Daymet version 3 (Thornton et al., 2017), which provides 1-km grid daily data from 1980 to 2016 for North America. Because future projected downscaled climate data from general circulation models (GCM) have much courser spatial resolution (1/8 degree), Daymet data were resampled at 1/8 degree to be consistent with projected climate data (Figure 4.2).

Three GCM models were chosen based on the model credibility for Northeast United States (Thibeault & Seth, 2015): ccsm4, mri-cgcm3, and gfdl-esm2m. Each GCM has four projected climate datasets from 2020 – 2050 based on the four Representative Concentration Pathways (RCPs): RCP2.6, RCP4.5, RCP6.0 and RCP8.5. All climate data were downscaled to 1/8-degree bias correction with constructed analogs dataset (Zia et al., 2016). Thus, in total, 12 climate scenarios were used for future climate data.

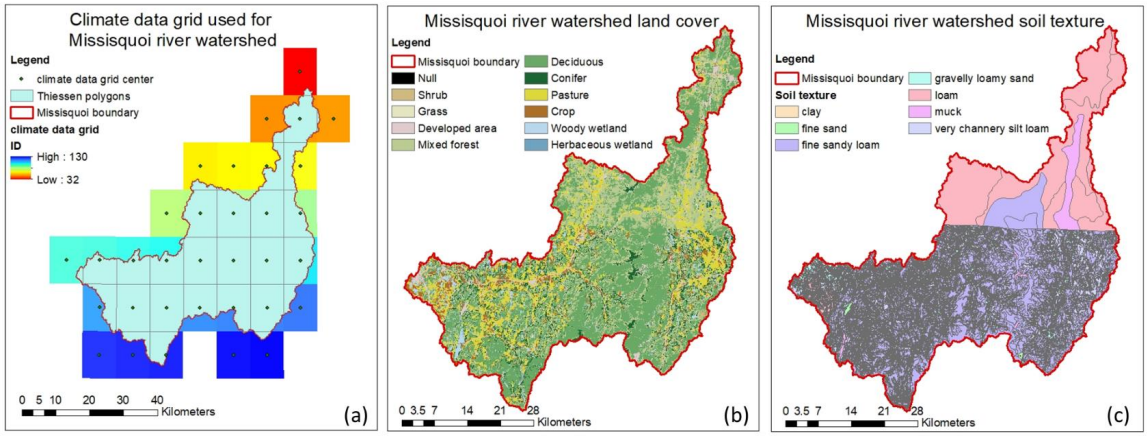

Figure 4.2 RHESSys input data. (a). 1/8 degree grid data used, the grid center points were used to generate Thiessen polygons for spatial climate data input. (b). Missisquoi river watershed land cover, U.S. side is from the year 2001, and Canada side is from the year 2000. (c). Missisquoi river watershed surface soil texture map.

4.2.3.2 Land use/cover data

The land use/cover map combined the US portion (National Land Cover Database, 2001) and Canadian portions (circa 2000, http://www.geobase.ca/) of the Missisquoi River watershed. This land use/cover map was used for RHESSys calibration with historical climate data and gauge data (Figure 4.2).

For the future period (2020 – 2050), we used the ILUTABM model (Y. S. Tsai et al., 2015) to generate three different land use scenario maps (Figure 4.3): Business As Usual (BAU), Prefer Forest (proForest) and Prefer Agriculture (proAg). The ILUTABM model can output land use map every year, but for this study, we outputted one land use map every 10 years. Thus, for each land use scenario, there were three land use maps for

the period of 2020 to 2050 (Figure 4.3). Prior to model input, all land use/cover data were reclassified as RHESSys land use/cover types.

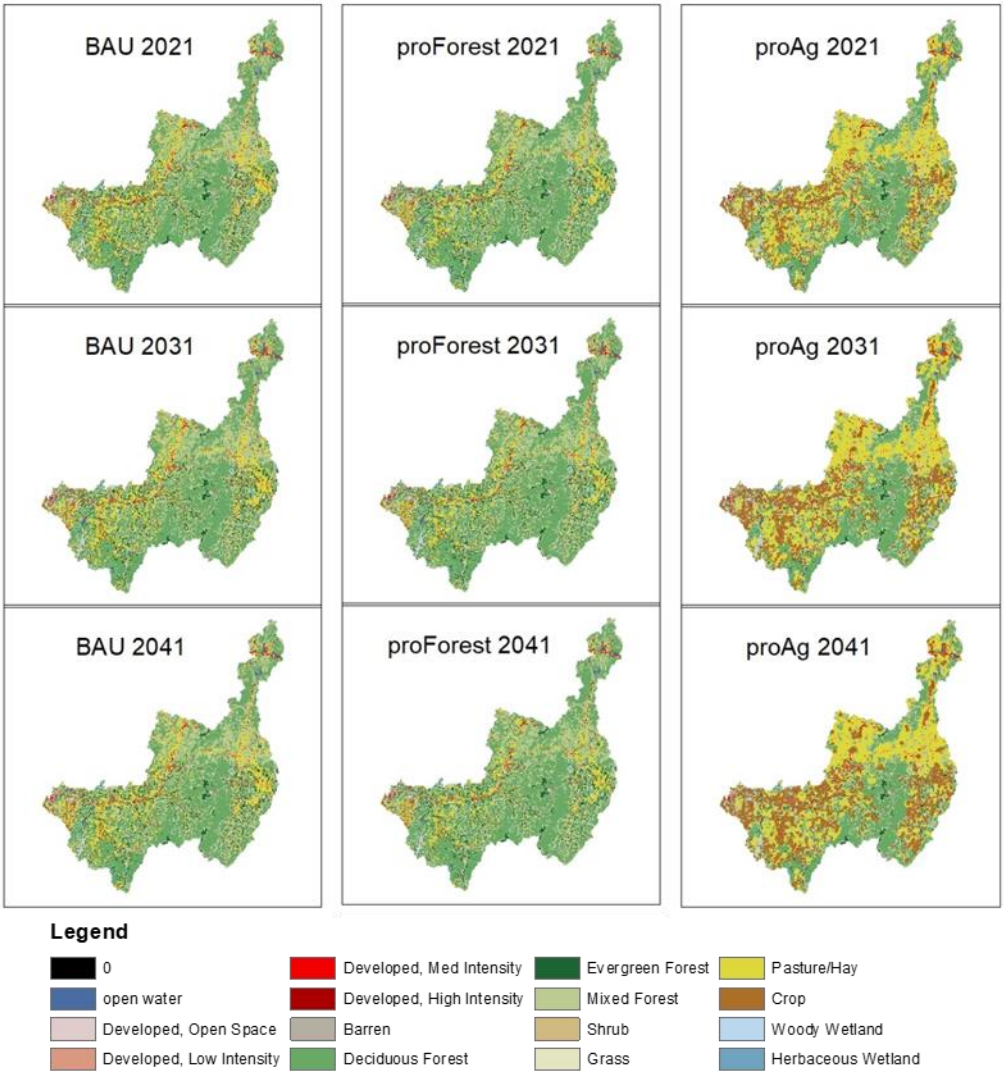

Figure 4.3 Projected land use of the year 2021, 2031 and 2041 for the three land use scenarios: Business As Usual, prefer forest and prefer agriculture.

4.2.3.3 Other input data

For the Missisquoi watershed, a Digital Elevation Model (DEM) of 1 arc-second (approximate 30 meters) from the American National Elevation Dataset was used (Figure 4.1). The DEM was used to generate slope, aspect, west and east horizon grid data. Surface soil texture data were from Vermont Center for Geographic Information (http://vcgi.vermont.gov/) and Soil Landscapes of Canada (http://sis.agr.gc.ca/cansis/nsdb/slc/index.html). Agriculture land management practice data (fertilizer/manure application, harvest date) were from surveys (Department of Plant and Soil Science, the Universithy of Vermont). Due to lack of spatial agriculture land management practice data, we assumed all agriculture land had the same management practices. Atmospheric nitrogen deposition data was from National Atmospheric Deposition Program (http://nadp.slh.wisc.edu/). The total nitrogen deposition for Missisquoi river watershed is 1g N/m^2/year.

4.2.4. Experiment design for climate change and LUCC impacts assessment

I spun-up the RHESSys model for about 1500 years to let plants and soil carbon and nitrogen pools reach equilibrium states. Then, the spun-up model was calibrated for streamflow, streamflow NO_3-N and streamflow NH_4-N at the outlet of Missisquoi river watershed. Finally, with the calibrated parameter set, the model was run with different climate and LUCC scenarios. In this study, 12 climate scenarios (three GCMs with four

RCPs for each GCM) and 3 LUCC scenarios were used, so 36 total climate-LUCC scenarios were used.

4.2.4.1 Calibration and validation

Four parameters were used to calibrate RHESSys: *m*, *K*, *gw1* and *gw2*. *m* is the decay of hydraulic conductivity with depth (dimensionless), *K* is the surface lateral hydraulic conductivity (*m*/*day*), *gw1* is the proportion of net inflow water moving to the deep ground water store (dimensionless), and *gw2* is the proportion of water from deep ground water store moving to the stream. The four parameter ranges used in this study were *m* (0 – 0.2), *K* (0 – 300), *gw1* (0 – 0.9) and *gw2* (0 – 0.9) (Saksa et al., 2017).

Monte Carlo simulations were used to calibrate RHESSys. 5040 parameter sets were generated using the Latin-Hypercube sampling technique with even distribution for each parameter over the parameter range. The 5040 parameter sets were used to drive RHESSys model on NCAR Cheyenne cluster (Laboratory, 2017). The Nash-Sutcliff coefficient (NSE) was used to assess parameter sets performance.

Due to data availability, streamflow, streamflow NO_3-N and streamflow NH_4-N were calibrated and validated with different years' data at a daily timestep (Table 4.1). Model fit during the calibration and validation periods was assessed using the Naash-Sutcliffe efficiency value (NSE) and RMSE. NSE is in the range of $-\infty$ to 1, NSE = 1 means perfect match and NSE = 0 means the model performance is equivalent to the average of observed data, and NSE < 0 means model performance is worse than the

average of observed data. A threshold value of 0.6 for daily streamflow NSE is considered good fit (Guilbert, 2016). RMSE measures the average differences of simulated and observed data. The smaller the better.

Table 4.1 Calibration and validation period

	Calibration	Validation
Runoff	1992.1.1 - 1994.12.31	1995.1.1 - 1999.12.31
NO3-N	1993.1.1 - 1993.12.31	1994.1.1 - 1994.12.31
NH4-N	1993.1.1 - 1993.12.31	1994.1.1 - 1994.12.31

4.2.4.2 Future projection under different climate and LUCC scenarios

Once the best parameter set was determined, it was used to drive RHESSys for all projected scenarios. For all scenarios, the historical land use (US 2000, and Canada 2001) was used to run 2011.1.1 to 2020.12.31 for model warm up. From 2021.1.1, projected land use of 2021 was used to run RHESSys until 2050.12.31. The land use map was updated every 10 years. The same processes were applied to other land use transition years.

In RHESSys, the worldfile is used to describe basin states. Land use change can affect 3 items in the worldfile: the base station a patch attached to, patch land use type, and patch vegetation type. The base station controls agricultural land management practices, such as fertilizer application. Land use type controls common land

management configurations and vegetation type controls vegetation physiology characteristics. Changing these 3 items reflects the LUCC in the RHESSys model.

At the land use transition year, a new worldfile with a new land use map was used to compare with old worldfile (with old land use map). If any of the 3 items were different for the same landscape unit, the item value from new worldfile was used to replace the corresponding value in the old worldfile. In this way, land use change was integrated into model configuration.

4.2.4.3 Future projection results analysis

We used boxplots to show multiple temporal streamflow distribution characteristics under all climate change and LUCC scenarios. To test our hypothesis, we used annual streamflow standard deviations of RCPs, GCMs and LUCCs to study which factor was the dominant impacting factor on streamflow. This analysis further factored climate into RCPs and GCMs and would provide insights on climate change impacts on streamflow.

4.3. Results

4.3.1. Calibration and validation

Monte Carlo simulation was used to calibrate RHESSys with 5040 parameter sets. Model fit was examined using the streamflow NSE relationship with each parameter

(Figure 4.4). Parameter *m* ranged from 0 to 20 and NSE increased with *m* in this range (Figure 4.4 a). Parameter *K* had no uniform relationship with NSE and most NSE values were above zero (Figure 4.4 b). Parameter *gw1* had a parabola relationship with NSE, with the NSE peak is in the range between 0.3 and 0.6 (Figure 4.4 c). Like parameter *m*, the NSE increased with parameter *gw2* (Figure 4.4 d).

Based on the NSE values of all parameter sets, the parameter set with the best overall NSE value for streamflow, NO_3-N and NH_4-N was chosen, and this parameter set was used for calibration, validation and future projections. The parameter values for the selected set were 19.2 for *m*, 206.08 for *K*, 0.299 for *gw1* and 0.888 for *gw2*.

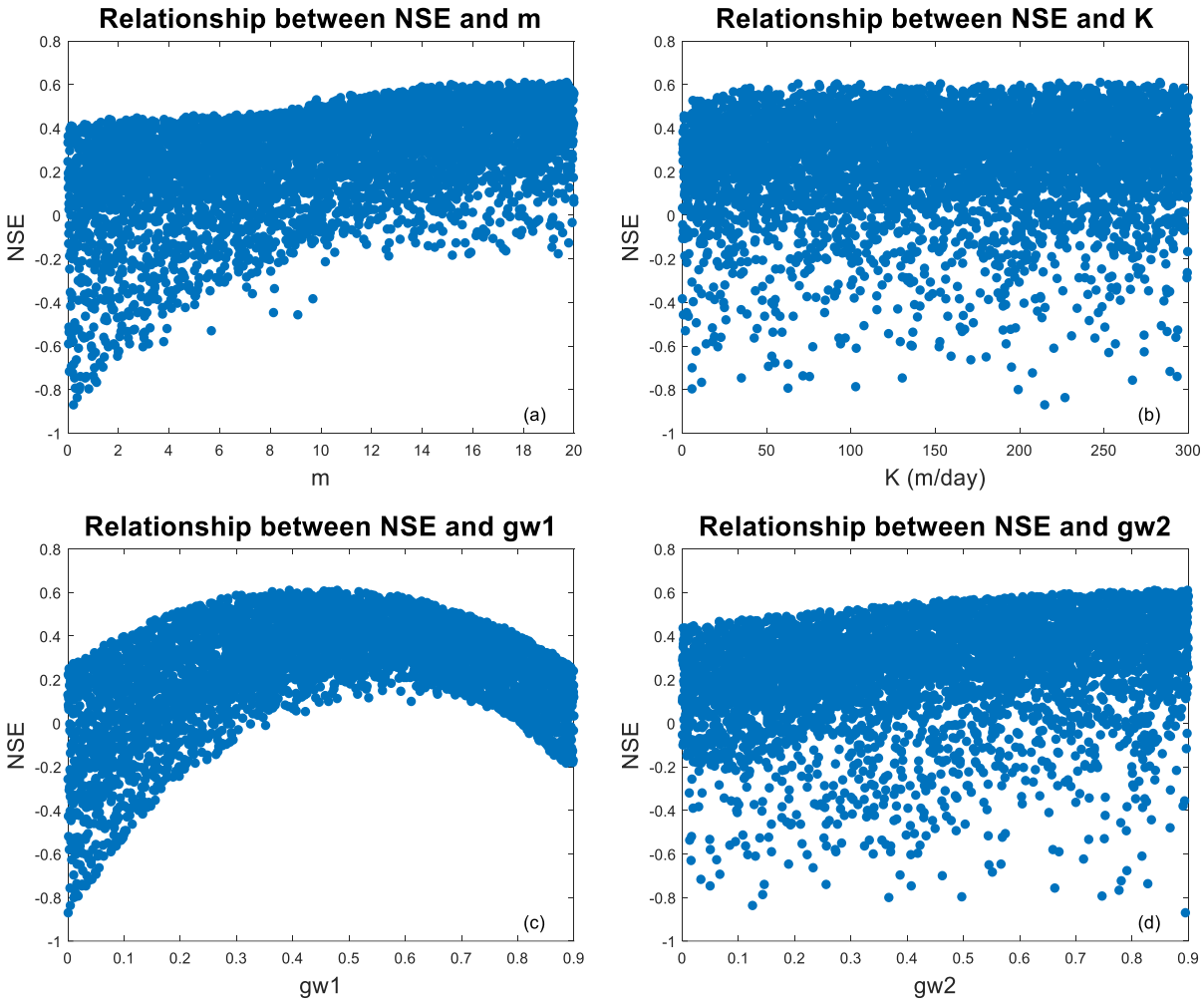

Figure 4.4 Daily streamflow NSE relationship with the 5040 calibrated parameter sets (m, K, gw1, and gw2) in the calibration period (1992.1.1 – 1994.12.31). (a) Parameter m. (b) Parameter K. (c) Parameter gw1. (d) Parameter gw2.

During the streamflow calibration period (01/01/1992 –12/31/1994), NSE was 0.59 and RMSE was 1.5054 mm. In the validation period (1/1/1995 – 12/31/1998), NSE was 0.52, RMSW was 2.1031 mm and the R^2 was 0.526 (Figure 4.6 a).

Mineral nitrogen fluxes were calibrated with 1993 data and validated with 1994 data (Figure 4.5 b-c). In both calibration and validation periods, simulated NO_3-N captured the general observed NO_3-N trend (Figure 4.5 b). The RMSE was 0.0032 g/m^2 in the calibration period and 0.0020 g/m^2 in the validation period. However, in the validation period, the R^2 was 0.007 (Figure 4.6 b). The low R^2 value was due to several simulated values that were lower than the observed values in April of 1994. Similar to NO_3-N, simulated NH_4-N generally was consistent with observed NH_4-N (Figure 4.5 c). The RMSE was 0.00025 g/m^2 both in the calibration period and validation period. In the validation period, the R^2 was 0.494.

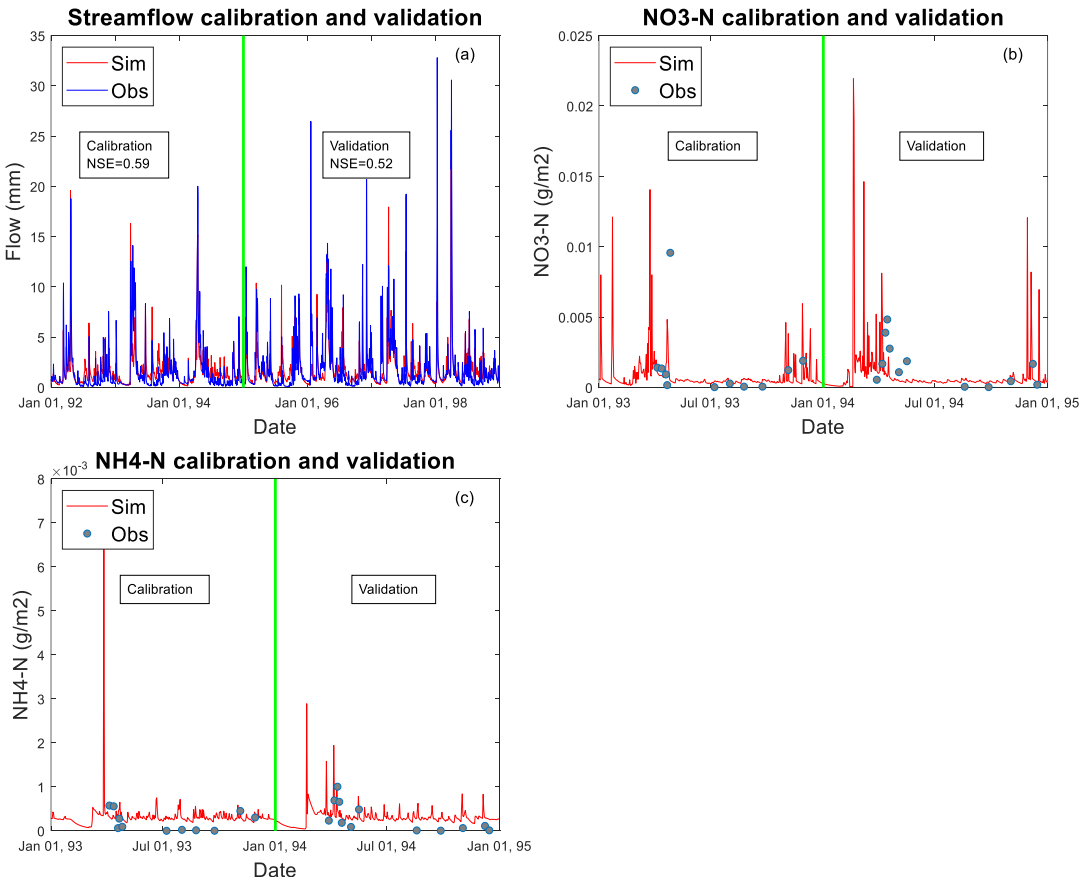

Figure 4.5 Simulated and observed data for calibration and validation periods. (a) streamflow. (b) NO_3-N. (c) NH_4-N.

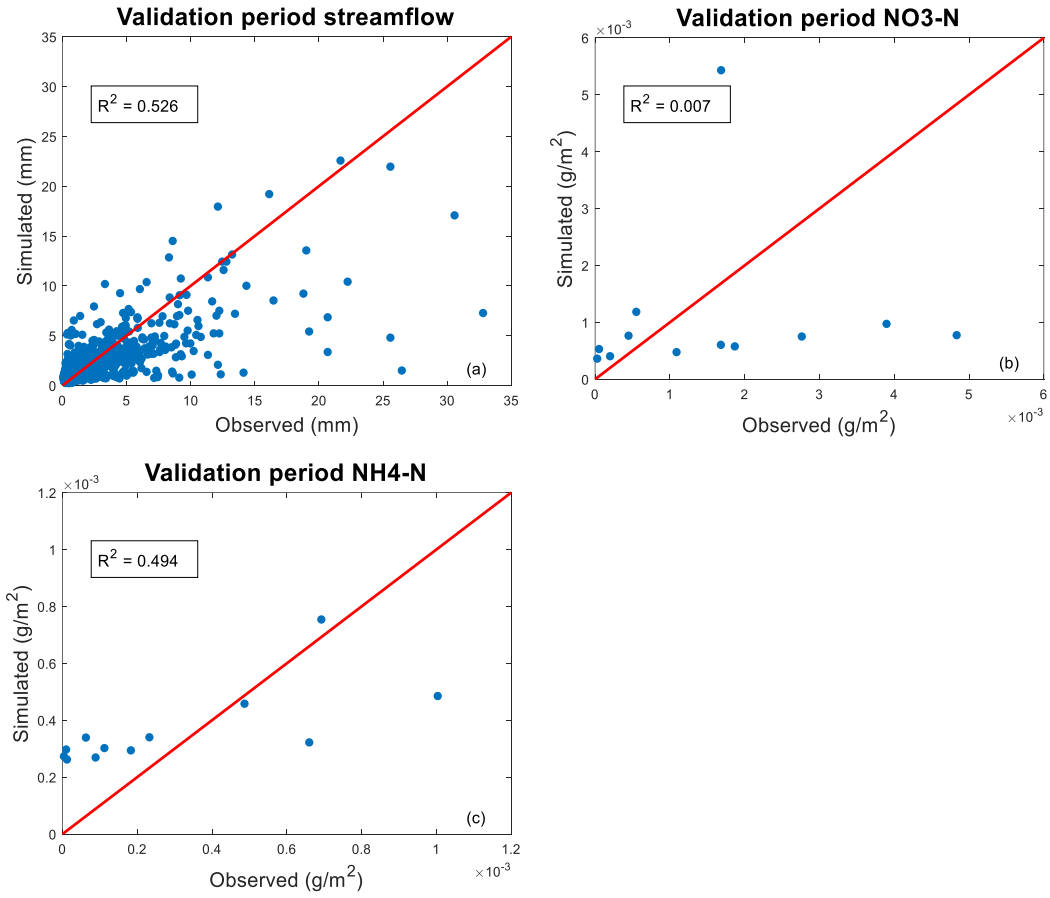

Figure 4.6 Scatter plot for streamflow, NO_3-N, NH_4-N and DOC in the validation period. (a) streamflow. (b) NO_3-N. (c) NH_4-N.

4.3.2. Projected NO3-N

Annual NO_3-N load (Figure 4.7) showed similar patterns and magnitudes under BAU and proForest LUCC scenarios, fluctuating around 5 $\times 10^5$ kg. The annual loads under proAg scenario were two times higher than BAU and proForest and had large variance during the period of 2021 – 2050. In contrast, the RCPs had little impact on N lodading, either among scenarios or over time (Figure 4.7 and Figure 4.8). Thus, LUCCs

(especially proAg) had a much stronger influence on annual NO_3-N load than climate change.

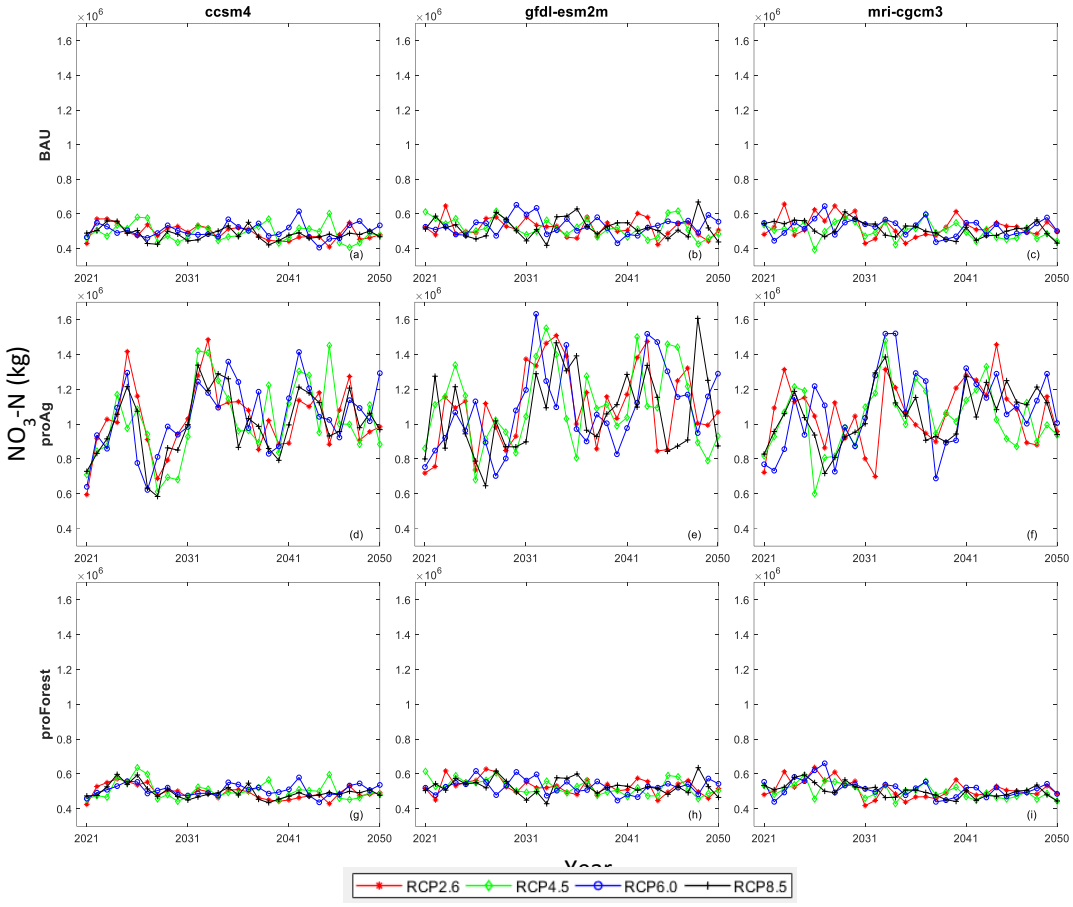

Figure 4.7 Projected annual NO_3-N under different climate change and LUCC scenarios from 2021 to 2050

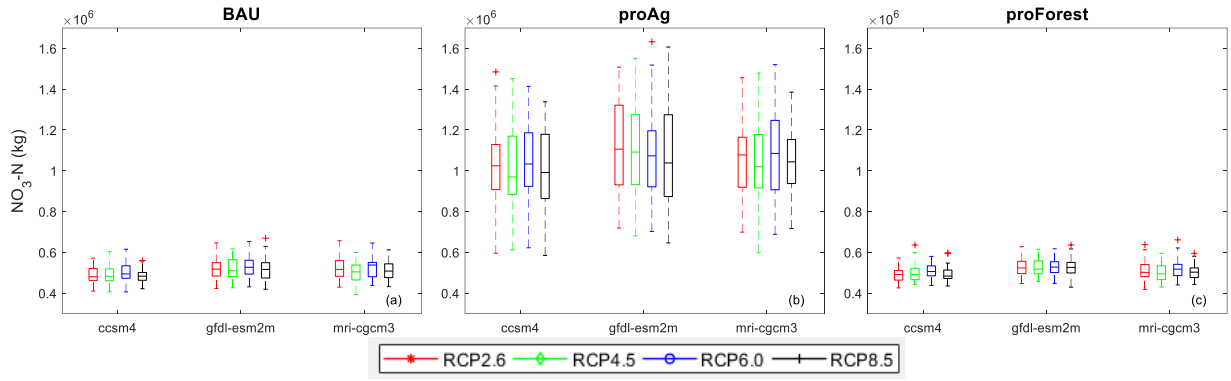

Figure 4.8 Projected annual NO_3-N load boxplot under different climate change and LUCC scenarios for the period of 2021 – 2050

The median annual NO_3-N load from 2021 – 2050 (Figure 4.8) for the proAg scenario was around 2 times larger than the BAU and proForest scenarios. BAU and proForest annual loads had similar patterns under all climate scenarios. Under the proAg scenario, annual median loads in the gfdl-esm2m and mri-cgcm3 models were slightly higher than in the ccsm4 model.

In all climate scenarios, median annual loads for the BAU and proForest scenarios showed similar distribution patterns in all the three decades with median of around 5×10^5 kg (Figure 4.9). Under the proAg scenario, both the median and variance were larger than under BAU and proForest scenarios (Figure 4.9). For the ccsm4 and gfdl-esm2m models, annual loads in decades of 2031 – 2040 and 2041 – 2050 showed a slight increase compared with the decade of 2021 – 2030. However, the mri-cgcm3 did not show this pattern.

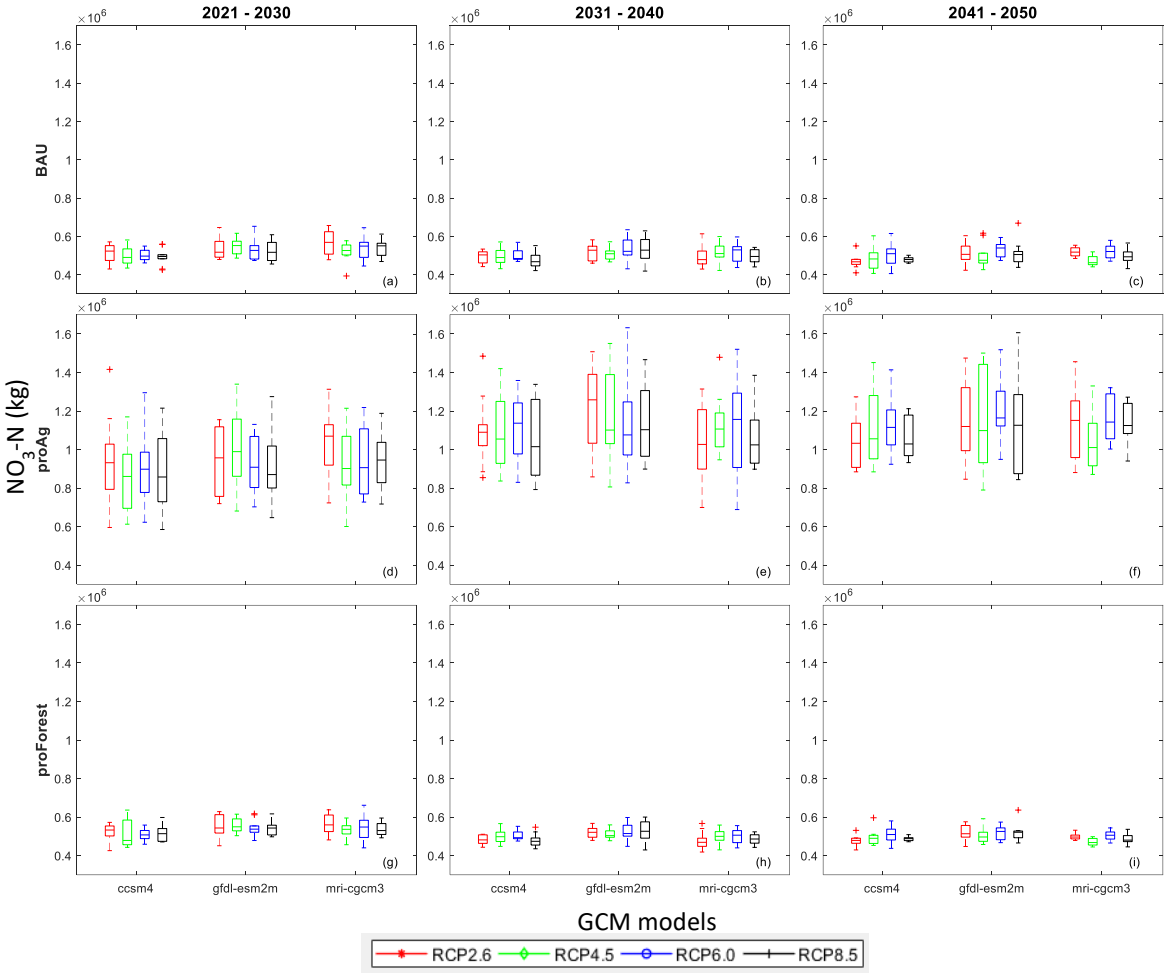

Figure 4.9 Projected annual NO_3-N boxplot under different climate change and LUCC scenarios for decades of 2021 – 2030, 2031 – 2040 and 2041 – 2050

Quarterly NO_3-N loads between 2021 and 2050 in all scenarios showed a consistent pattern although with different magnitudes (Figure 4.10). The highest loads were in Q1 and Q4 and lowest loads in Q2 and Q3 (i.e. parabolic). Otherwise, trends were similar to the annual loads. All climate scenarios showed similar distributions in the same quarter. Under proAg, quarterly loads were higher than the corresponding quarterly loads of BAU and proForest, and with bigger ranges.

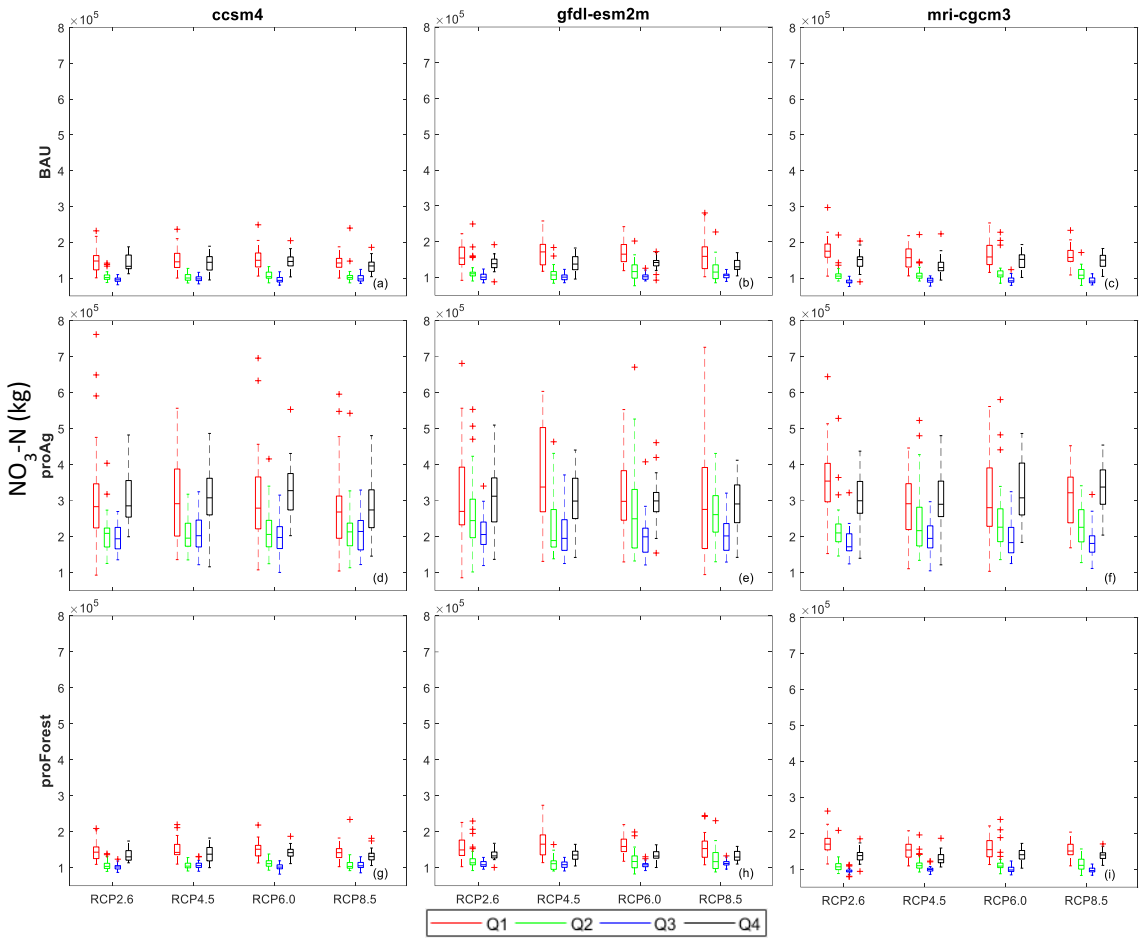

Figure 4.10 Projected quarterly NO_3-N boxplot under different climate change and LUCC scenarios. Q1 is from January to March, Q2 is from April to June, Q3 is from July to September, and Q4 is from October to December

The 3 GCM models (ccsm4, gfdl-esm2m and mri-cgcm3) result were grouped on RCPs to reduce feature dimensions for quarters' loads in each decade (Figure 4.11). Under all LUCCs, medians of Q1 to Q4 also form parabola shape in the 3 decades, with Q1 and Q4 higher than Q2 and Q3.

Under BAU and proForest, quarterly loads showed similar distribution in the 3 decades for all RCPs. Under proAg, generally quarterly loads in the decade of 2031 –

2040 and 2041 – 2050 were higher than the corresponding quarterly loads in the decade of 2021 – 2030. In the same decade and LUCC, different RCPs had similar load distributions for the same quarter, indicating RCPs had slight influences on quarterly loads.

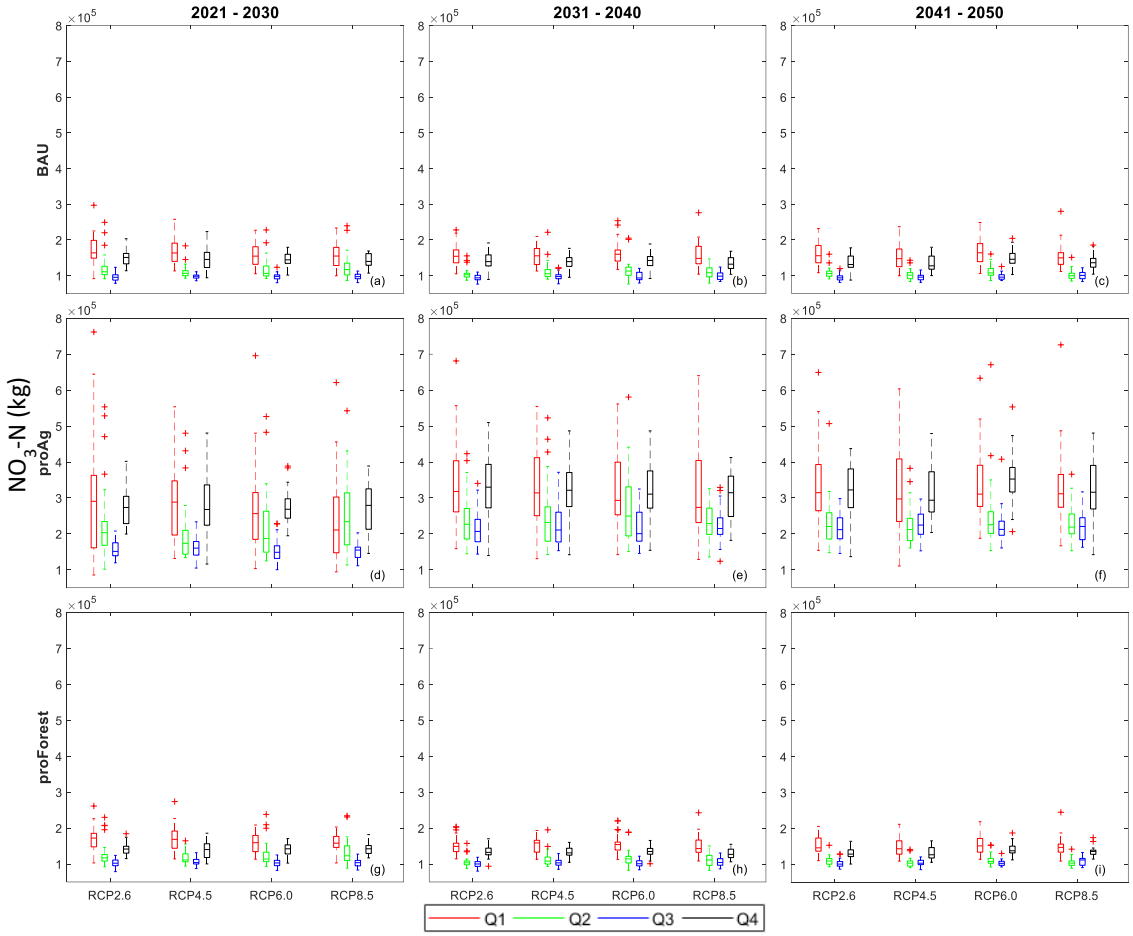

Figure 4.11 Projected quarterly NO_3-N boxplot under different LUCC scenarios for decades of 2021 – 2030, 2031 – 2040 and 2041 – 2050, for each RCP scenario, all 3 GCMs data were merged in each box.

We used the standard deviation of annual NO_3-N loads to compare which factors – LUCC scenario, RCP scenario, or GCM choice – were dominant for creating variability in NO_3-N loads during 2021 - 2050 (Figure 4.12). Most of the variation in NO_3-N loads was responding to LUCC scenario (medians standard deviation was around 3×10^5 kg). Much less variation in NO_3-N loads was in response to the climate data associated with the RCPs and GCMs (Figure 4.12). However, there was more climate-induced variation in NO_3-N loads in the proAg scenario than in the proForest or BAU scenarios (Figure 4.12). BAU and proForest had similar, and relatively low standard deviations in response to RCPs and GCMs when compared to the proAg standard deviations. Our results indicate that LUCCs are the dominant factor for NO_3-N loading rather than responses to climate. However, the wider spread and higher median standard deviations in the proAg scenario indicates that future climate change could play an important role in the proAg LUCC.

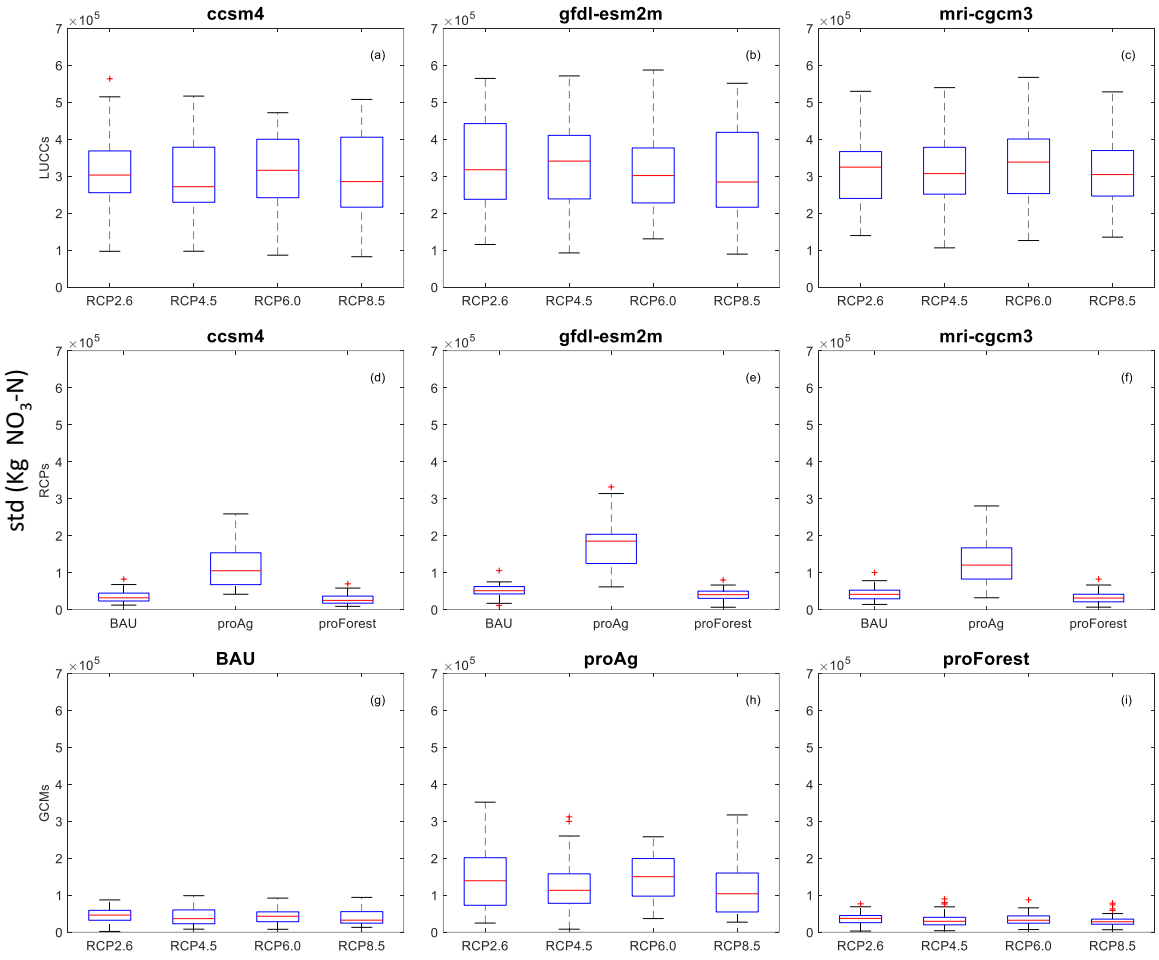

Figure 4.12 Annual NO3-N standard deviation of different factors. The top row shows the standard deviation of LUCCs, the middle row shows the standard deviation of RCPs and the bottom row shows the standard deviation of GCMs

4.3.3. Projected NH4-N

Annual NH_4-N loads were differentially impacted by the different LUCCs (Figure 4.13), with different trends between 2021 – 2050. Under BAU, annual NH_4-N loads increased slightly in all climate. Under proAg, annual NH_4-N loads dramatically increased from approximately 2.2×10^5 kg in 2021 to approximately 3.2×10^5 kg in

2050 under all climate scenarios. Under all climate scenarios, the rate of the proAg increase was steeper from 2021 to 2030 than in subsequent decades. Under proForest, annual NH_4-N loads fluctuated around 2.4×10^5 kg without increasing trends in all climate scenarios.

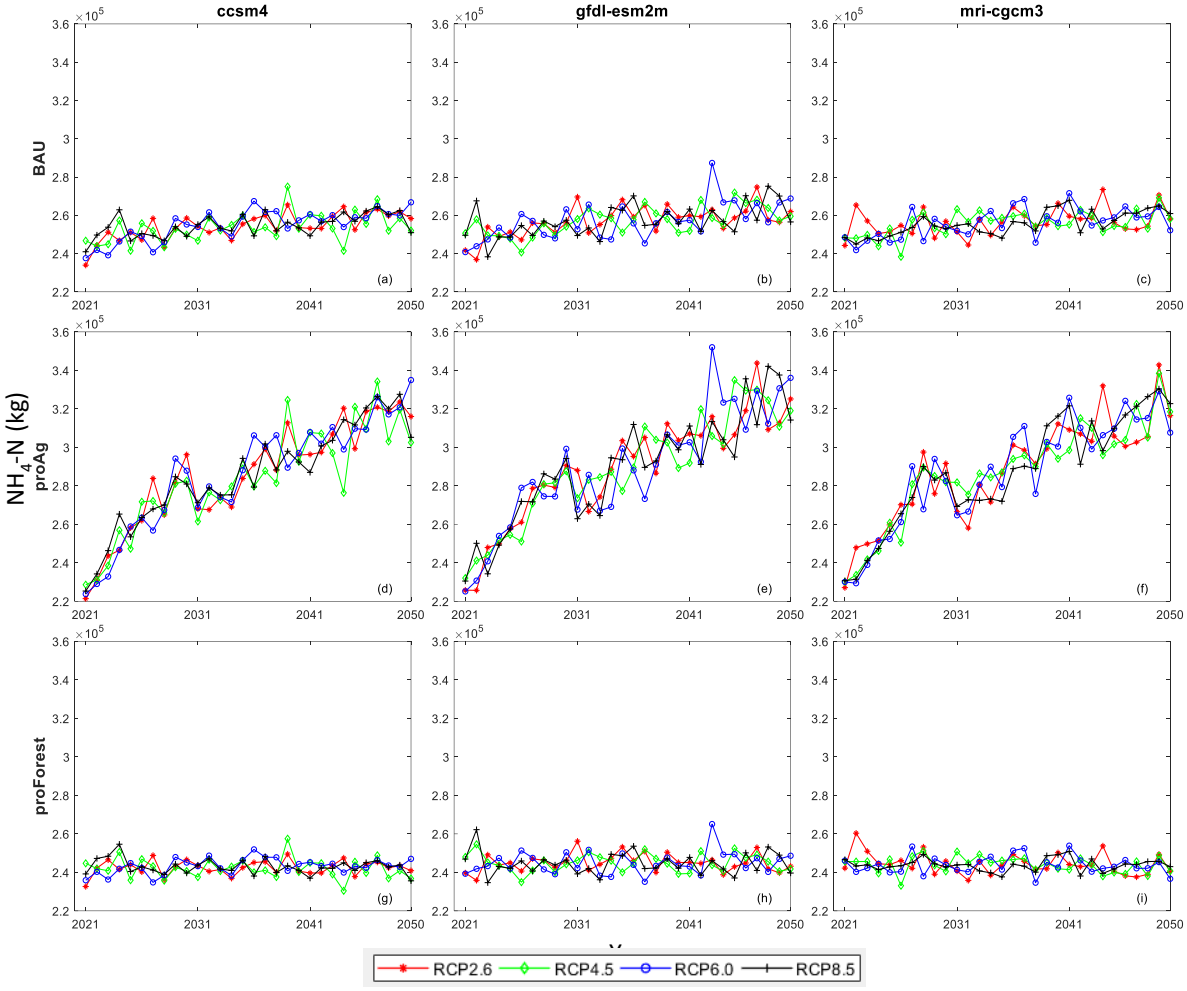

Figure 4.13 Projected annual NH_4-N under different climate change and LUCC scenarios from 2021 to 2050

Median annual NH_4-N loads for the period of 2021 – 2050 (Figure 4.14) were greatest for proAg, followed by BAU and then proForest. The same order also applied to annual loads spread under the 3 LUCCs. The three GCMs showed similar trends within each LUCC. Similarly, annual loads were similar among all four RCPs. These results indicate that LUCCs had a stronger influence on NH_4-N load than climate during 2021 – 2050.

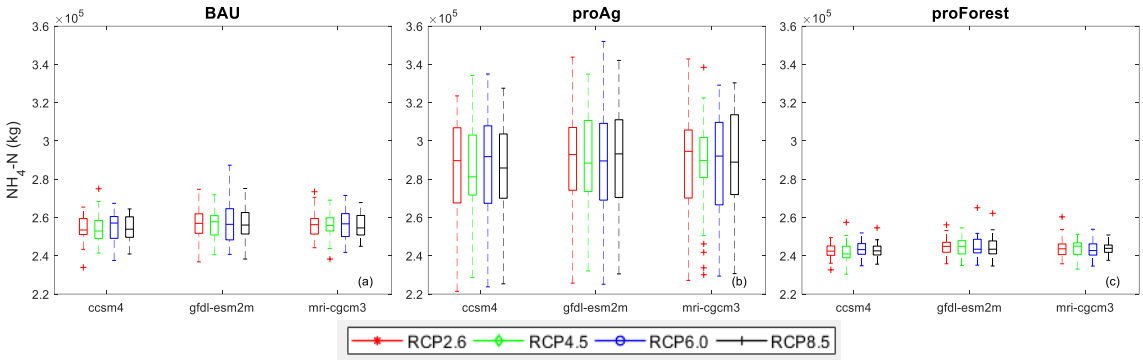

Figure 4.14 Projected annual NH_4-N load boxplot under different climate change and LUCC scenarios for the period of 2021 – 2050

Annual loads in each decade between 2021 - 2050 revealed some decadal patterns (Figure 4.15). Under BAU, annual NH_4-N loads increased slightly from the 1st decade to the 3rd decade. Under proAg, annual NH_4-N loads increased sharply from the 1st decade to the 3rd decade. Under proForest, annual NH_4-N loads were similar across all three decades. One notable characteristic is that the variation in annual NH_4-N loads in the 1st decade was wider than the 2nd and 3rd decades under proAg scenario.

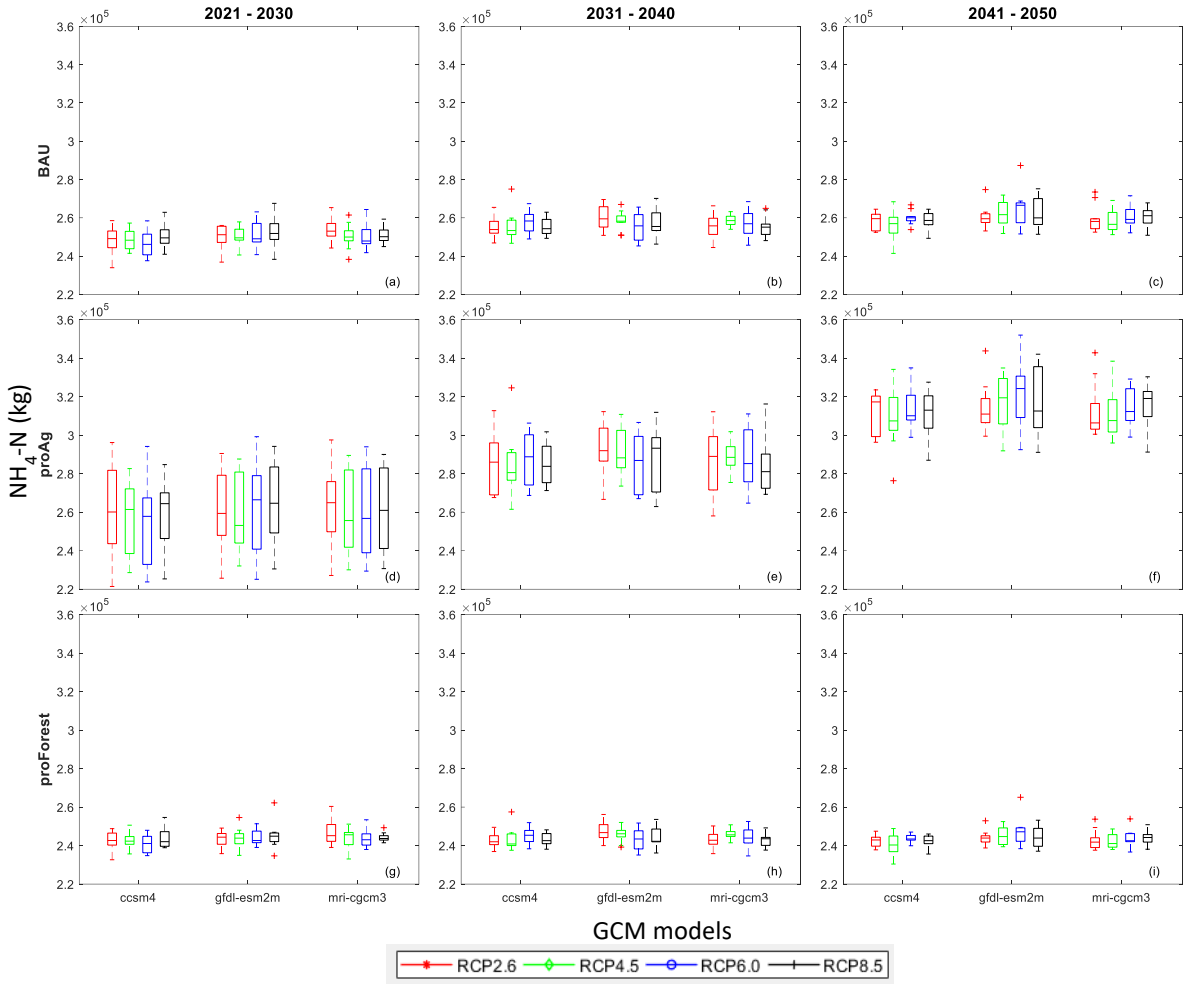

Figure 4.15 Projected annual NH_4-N load boxplot under different climate change and LUCC scenarios for decades of 2021 – 2030, 2031 – 2040 and 2041 – 2050

Quarterly NH_4-N loads for 2021 – 2050 under all climate and LUCC scenarios were lowest in Q2, which was consistent with quarterly NO_3-N load characteristics (Figure 4.16). Under the same LUCC, however, there were no substantial differences in quarterly NH_4-N loads among the different climate scenarios for the same quarter (Figure

4.16). Under the same climate scenario, quarterly load under proAg was the largest, with BAU as the 2nd largest, and proForest as the lowest.

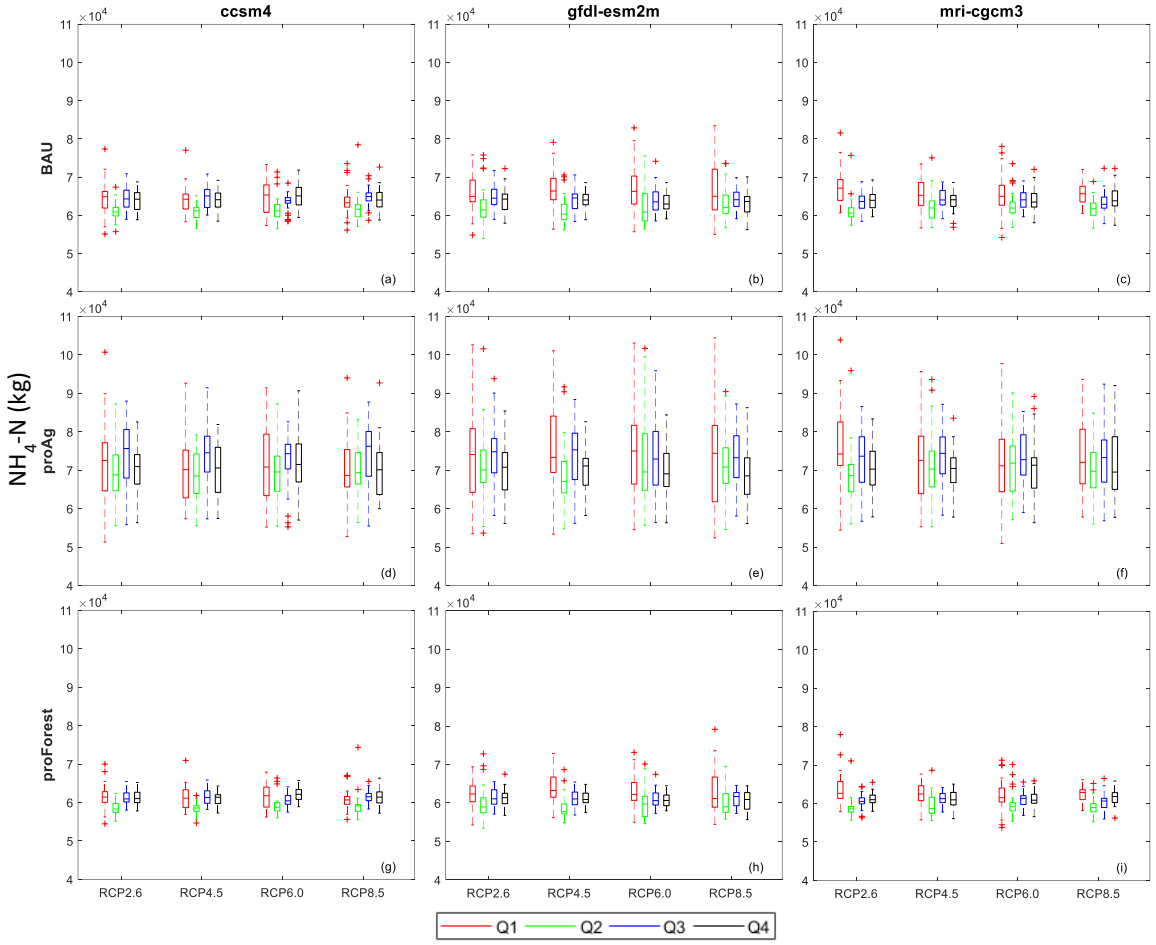

Figure 4.16 Projected quarterly NH_4-N load boxplot under different climate change and LUCC scenarios. Q1 is from January to March, Q2 is from April to June, Q3 is from July to September, and Q4 is from October to December

Under BAU, quarterly NH_4-N load generally increased slightly from the 1st decade to the 3rd decade for the same quarter under all RCPs; Under proAg, quarterly NH_4-N load increased dramatically from the 1st decade to the 3rd decade for the same

quarter under all RCPs; Under proForest, quarterly NH_4-N loads were comparable in the 3 decades for the same quarter (Figure 4.17). In the 3 decades, Q2 NH_4-N loads were lowest compared with other quarterly loads.

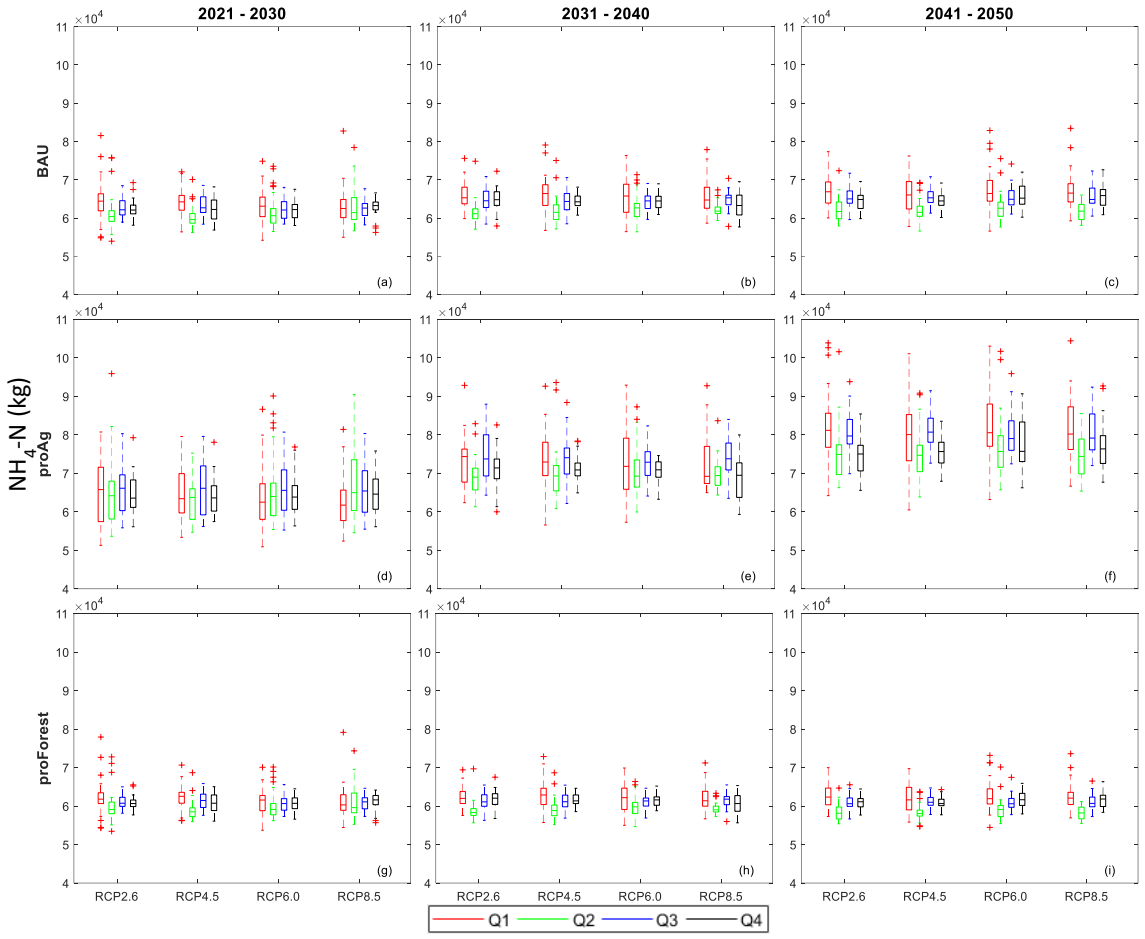

Figure 4.17 Projected quarterly NH_4-N load boxplot under different LUCC scenarios for decades of 2021 – 2030, 2031 – 2040 and 2041 – 2050, for each RCP scenario, all 3 GCMs data were merged in each box.

We used annual NH_4-N standard deviation to compare which factors were dominant for producing variation in NH_4-N load during 2021 - 2050 (Figure 4.18). The largest standard deviations were associated with LUCC (Figure 4.18). Standard deviations for annual NH_4-N loads were much smaller for RCP scenarios and different

GCMs (Figure 4.18). However, as for annual NO_3-N loads there was more climate-induced variation for annual NH_4-N loads in the proAg scenario than in the proForest or BAU scenarios (Figure 4.18). BAU and proForest had similar, and relatively low standard deviations in response to RCPs and GCMs compared to proAg, indicating that, while LUCCs are the dominant factor for NH_4-N loading, the wider spread and higher median standard deviations in the proAg scenario for RCPs and GCMs indicates that future climate change could play an important role in the proAg LUCC.

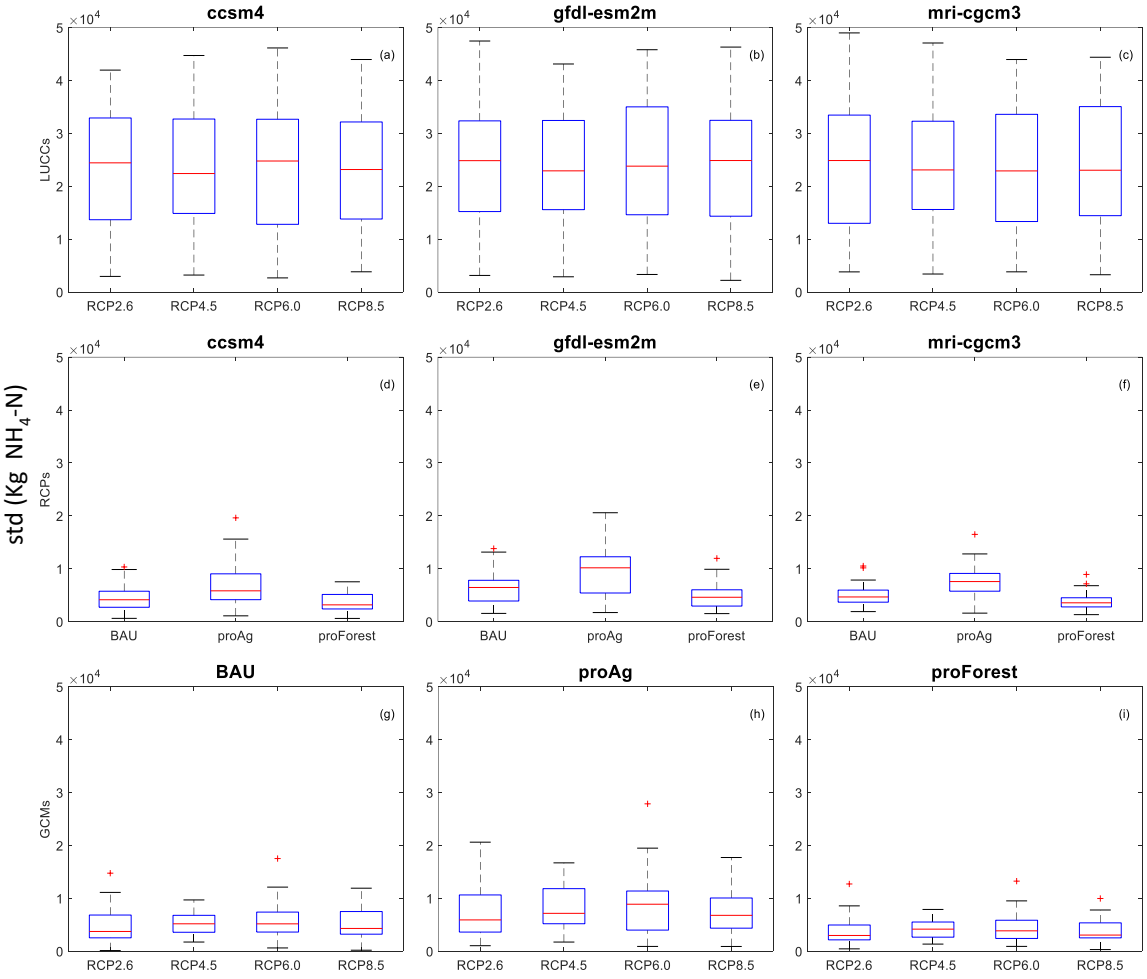

Figure 4.18 Annual NH_4-N standard deviation of different factors. The top row shows the standard deviation of LUCCs, the middle row shows the standard deviation of RCPs and the bottom row shows the standard deviation of GCMs

4.4. Discussion

4.4.1. RHESSys performance on streamflow and nitrogen

Although RHESSys has been widely used for watershed simulation (Godsey et al., 2014; Hanan et al., 2017; Hwang et al., 2008; Martin et al., 2017; Saksa et al., 2017), most have used it for streamflow simulation. Few have used it to study terrestrial carbon (Vicente-Serrano et al., 2015) or streamflow nutrient loads (Hanan et al., 2017). Therefore, as an eco-hydrological model, the strength of RHESSys as a biogeochemistry model has not been widely validated or applied. C. L. Tague and Band (2004) applied RHESSys in a small forest watershed for NO_3-N simulation, but the simulated NO_3-N loads were much higher than observed NO_3-N – some simulated NO_3-N loads were 7 times observed loads or even higher. Hanan et al. (2017) used RHESSys to study fire impacts on nitrogen export in a California watershed, but simulated nitrogen export was not verified with observed nitrogen data. Overall, the ability of RHESSys to accurately simulate watershed N loads has not been verified.

We systematically evaluated RHESSys performance for simulating streamflow, NO_3-N and NH_4-N after incorporating land use and management data in Missisquoi River watershed. We found that, for nutrient export, model simulations generally captured the observed patterns, but R^2 values were low during the validation period except for NH_d-N. This indicates that RHESSys lacks some mechanisms for simulating nutrient processes. One possible reason for the discrepancy is that the model does not have a sediment module, so transport of particulate nutrients is not simulated in RHESSys. A second potential reason is that RHESSys has not fully incorporated nutrient

in-stream routing process. Thus, there are no in-stream nutrient transformations, including nitrogen mineralization and nitrification. The third potential reason is that, currently, to calculate total soil nutrient content, the vertical distribution of nutrients in soil is assumed to decay exponentially. In this way, when soil nutrients in one patch are transported to a neighbor patch through groundwater flow, the nutrient vertical distribution of current patch will be redistributed based on the exponential function. This vertical distribution of nutrients may not reflect the real nutrient vertical movement. In addition, RHESSys runs at a daily time step, but there is a user-defined routing time for one day (currently at 24 times/day) to achieve model stability. The combined effects could lead to nutrient export simulation errors. Therefore, future work could reconstruct the soil nutrient vertical distribution framework and take into account of in-stream routing processes to improve the nutrient export simulation results.

Another potential restriction on using RHESSys to study nutrient export is that the model input data requires spatially explicit land management practices for agricultural land, such as fertilizer application date and amount, harvest date etc. The finest spatial-scale for land management in RHESSys is patch-level. Such extensive data collection may not available. In this study, we did not have sufficient land management data for the Missisquoi river watershed. We therefore applied our survey data from a subset of farmlands in the watershed to the whole watershed. In addition to the data sources, there is no standard procedure how to use the land management data in RHESSys. Future efforts should focus on improving the RHESSys biogeochemistry module performance.

4.4.2. Climate change and LUCC impacts on Missisquoi river watershed nitrogen export

Using projected climate scenarios and LUCC simulations generated by an agent-based land transition model (Y. Tsai et al., 2015), we found that LUCC was the dominant factor rather than climate change for NO_3-N and NH_4-N export. In this study, the median annual NO_3-N load (2021 – 2050) under proAg was two times larger than the medians under BAU and proForest scenarios. Similarly, the median annual NH_4-N load under proAg (2021 – 2050) was 1.16 times larger than the median under the BAU and 1.20 times larger than the median under proForest scenario. The large impact of LUCC is likely because agricultural land is a large non-point nitrogen source due to fertilizer and manure applications (Fan & Shibata, 2015). Thus, more agricultural land means more nitrogen inputs to the watershed. However, NO_3-N and NH_4-N export did not increase at the same rate under the proAg scenario. NO_3-N export initially increased more quickly than NH_4-N export. This is likely because plants have uptake preference. And current land use change transition can change plants to unmatured states. The unmatured states need several years to grow and then its uptake ability grows along the time.

In addition, we compared annual NO_3-N and NH_4-N standard deviation of LUCCs, RCPs and GCMs (Figure 4.12 and Figure 4.18). The standard deviation of RCPs and GCMs were lower than the LUCCs, indicating LUCCs were the dominant factor for creating variation in NO_3-N and NH_4-N loads rather than climate. The standard deviation of annual loads across RCPs was comparable to those across GCMs, indicating that climate impacts on nitrogen load were comparable with GCM model usage. This

uncertainty associated with GCM choice could mask the climate change impacts on nitrogen load, meaning more GCMs need to be used to reduce the uncertainty from GCMs. One interesting finding was that proAg scenario had higher standard deviation than BAU and proForest. This suggests that climate may play a more important role in driving nitrogen loads in proAg than in BAU or proForest.

4.4.3. Limitations

Although this study followed the advanced philosophy of simulating real-world dynamic processes, there are still some limitations. The limitations can be categorized into three main categories: model input data, RHESSys intrinsic processes and simulation process.

Some model input data limitations are common across model applications, but some are specific to this study. First, spatial data aggregation is based on majority rule and this process may have caused some information loss, e.g., regarding soil texture and land use. Second, climate reanalysis data may have contained inaccuracies. These two limitations are common across model simulations. The specific limitation to this study is from fertilizer application data. Because spatially explicit fertilizer application data is not available, we assumed all agricultural land had the same land management practices. This could be a significant uncertainty source for simulating nitrogen export.

As discussed above, intrinsic limitations for RHESSys include no stream-routing processes, assuming soil nutrient content always follows an exponential decay function,

which result in unreasonable vertical nutrient movement, no separate calibration procedures for nutrients and no widely verified ecosystem module performance on carbon and nitrogen simulation.

Simulation limitations include short term observation data and LUCC transitions at the land use change year. Only two years of stream NO_3-N and NH_4-N observations were collected for this study. And the low determined coefficient between simulated and observed nutrient loadings likely introduced uncertainty.

Our simulations are also limited by abrupt LUCC transitions during the land use change year. In this study, we changed patch land use code based on a new land use map in the transition year. This can make the patches with new land use characteristics. However, we kept the patch state variables as the same as before land use change. For example, if a patch changed from grass land to forest land, the patch will carry grass patch states into forest patch. And grass pools will go to corresponding forest pools. If forest pools are not balanced well, the forest patch growth could be affected in the next few years. To overcome this limitation, more efforts need to put into ecosystem simulation processes in RHESSys.

4.5. Conclusion

This study coupled LUCC and climate change to study their impacts on nitrogen loads in the Missisquoi River watershed with RHESSys. The study evaluated RHESSys performance for simulation of streamflow nitrogen loads. Although simulated nutrient loads generally captured the observed patterns, the R^2 values were low in the validation period, indicating more work is needed to improve the nitrogen simulation modules. Another focus of this study was how climate change and LUCC might interact to impact on nitrogen loads in the Missisquoi River watershed. Major results were: (i) Fertilizer application in agricultural lands is a major source for nitrogen export, therefore, LUCC scenarios with more agricultural land had higher nitrogen loads. Indeed, LUCC scenarios had larger impacts on nitrogen loads than climate change; (ii) Climate variation in the RCPs and GCMs had comparable impacts on nitrogen loads, suggesting that both caused substantial variation in nitrogen loads; (iii) In the proAg LUCC scenario, climate had larger impacts on N loading than in the other two LUCC scenarios. This suggests that further changes in climate might have larger impacts on agricultural nitrogen loading than in other land use types. Our resultsindicated BAU or proForest in Missisquoi watershed were acceptable for Lake Chaplain water quality, while proAg would export too much nitrogen and lead to water quality deterioration.

CHAPTER 5. CLIMIATE ACHANGE AND LUCC IMPACTS ON DISSOVLED PHOSPHORUS USING RHESSYS-P: A NEW RHESSYS MODEL WITH DISSOVLED PHOSPHORUS MODULE

5.1 Introduction

Phosphorus is an essential element for life (Correll, 1998), but excess phosphorus entering freshwater aquatic systems can cause eutrophication, which has become a worldwide environmental problem (Han et al., 2011; Huang & Hong, 2010; Ulen et al., 2007). Particulate and dissolved phosphorus (DP) are the two forms of phosphorus exported to aquatic systems. Particulate phosphorus is accompanied by soil erosion. Globally, soil erosion accounts for 2.1-3.9 Tg yr^{-1} organic phosphorus and 12.5-22.5 Tg yr^{-1} inorganic phosphorus flux (Quinton et al., 2010). Dissolved phosphorus is the total phosphorus in solution which can pass 0.45 μm filter (Haygarth & Sharpley, 2000). In aquatic systems, dissolved phosphorus is readily available for algal growth and can directly accelerate eutrophication (Ekholm et al., 1999).

Non-point phosphorus sources, especially non-point agricultural sources, are considered major contributors to excess phosphorus loads (Zhernwei Li et al., 2015; Ongley et al., 2010; Ulen et al., 2007). Because agricultural land has been identified as a significant phosphorus source area due to fertilizer application (Fan & Shibata, 2015), land use/cover change (LUCC) is an important factor in determining watershed phosphorus loads. LUCC can also change phosphorus loadings by affecting hydrologic processes, which can alter the phosphorus transport processes.

At the same time, climate change may impact watershed phosphorus export (Fan & Shibata, 2015; Mehdi et al., 2015; Ockenden et al., 2017; Sha et al., 2018) by changing precipitation amount and patterns, which can alter phosphorus biogeochemistry and transport processes leading to phosphorus load change. For example, Sha et al. (2018) found that a hotter and wetter climate will generate more total dissolved phosphorus in a sub watershed of Yangtze River basin. In contrast, Mehdi et al. (2015) found that climate change will reduce annual total phosphorus loads by 2050 due to lower streamflow. These contrasting results demonstrate the complexity of climate change impacts on phosphorus loads. In reality, climate change and LUCC are highly likely to happen concurrently. Therefore, studying their combined impacts on phosphorus load can provide insights for future phosphorus loads.

At the watershed scale, models are important tools to understand phosphorus export for water quality management. Generally, such models have three categories: Simple statistical models, semi process-based models and process-based models. A simple statistical model such as the Export Coefficient Model (ECM) (Malve et al., 2012), uses a statistical relationship between land use and nutrient loads. While this model is easy to use, ECM is area specific and does not take account eco-hydrologic processes, which restricts its applications. In comparison, semi process-based models have moderate computation complexity and don't need extensive input data. These models can simulate key phosphorus dynamics, such as sources and transport. Examples of semi-process-based models are the Spatially and Temporally Distributed Empirical

model for Phosphorus Management (STEM-P) (S. Li et al., 2017) and SPAtially Referenced Regression On Watershed attributes (SPARROW) (Kim et al., 2017). Process-based models are the most complex models but incorporate main eco-hydrologic processes. Models in this category can help users understand phosphorus biogeochemistry and provide insights for watershed management practices. Many climate change and land use/cover change impacts on watershed phosphorus loads have been studied with models in this category.

RHESSys is a process-based spatially distributed eco-hydrological model, which has integrated watershed hydrology, carbon, and nitrogen processes. However, phosphorus has not been simulated in RHESSys. DayCent (Parton et al., 1998) is a non-spatially explicit terrestrial ecosystem model that simulates carbon, nitrogen and phosphorus. RHESSys and DayCent have a similar carbon and nitrogen framework, which provides the potential to integrate the phosphorus module into RHESSys. In this study, we constructed a model, RHESSys-P by integrating dissolved phosphorus module from DayCent into RHESSys. Then, we used RHESSys-P to study how climate change and LUCC will jointly impact on dissolved P loads in the Missiquoi River watershed from 2021 to 2050. We expected LUCC would be a dominant factor impacting DP loads rather than climate change, because the main DP source is from agricultural land fertilizer application.

5.2 Theory and methodology of RHESSys-P

Briefly, in the new version of RHESSys, hereafter RHESSys-P, phosphorus was coupled with carbon processes to simulate phosphorus interactions between plants and soil. The current water routing method in RHESSys was be used to route dissolved phosphorus. Since the current RHESSys version does not model sediment, the phosphorus module only includes Dissolved Inorganic Phosphorus (DIP) and Dissolved Organic Phosphorus (DOP). The following sections will detail the phosphorus module development, including infrastructure (data structure for phosphorus), soil-plant continuum processes and phosphorus routing processes.

5.2.1 Basin routing

Water and nutrient routing occur at the basin level in RHESSys. Within RHESSys, two approaches are used for routing. The first uses the quasi-spatial TOPMODEL (Beven & Kirkby, 1979), and the second is an explicit routing model adapted from Distributed Hydrology Soil Vegetation Model (DHSVM) (Wigmosta et al., 1994). RHESSys-P uses explicit DHSVM for routing. The utility function cf (CREATEFLOWPATHS) in RHESSys generates the flow table, which describes patch connectivity.

Within a basin, routing starts from the highest elevation patch and then iterates through all patches in the order of patch elevation (Figure 5.1). Every patch routes water and nutrient to its neighbor patches through subsurface and surface flow. Once the water and nutrients reach the stream patch, they automatically exit the basin outlet.

In RHESSys, there are three types of patches: land patches, road patches, and stream patches. However, in practice, due to the small size of road pixels, the aggregation process to create patches often masks out the road patches. Therefore, RHESSys-P only processes phosphorus routing for land and stream patches.

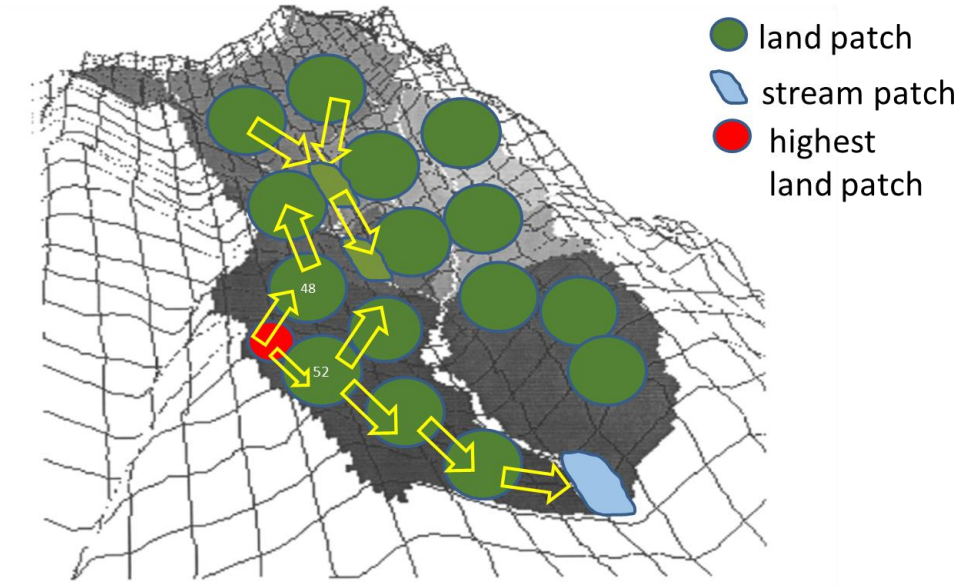

Figure 5.1 Explicit routing scheme for RHESSys-P, adjusted from Parton et al. (1996)

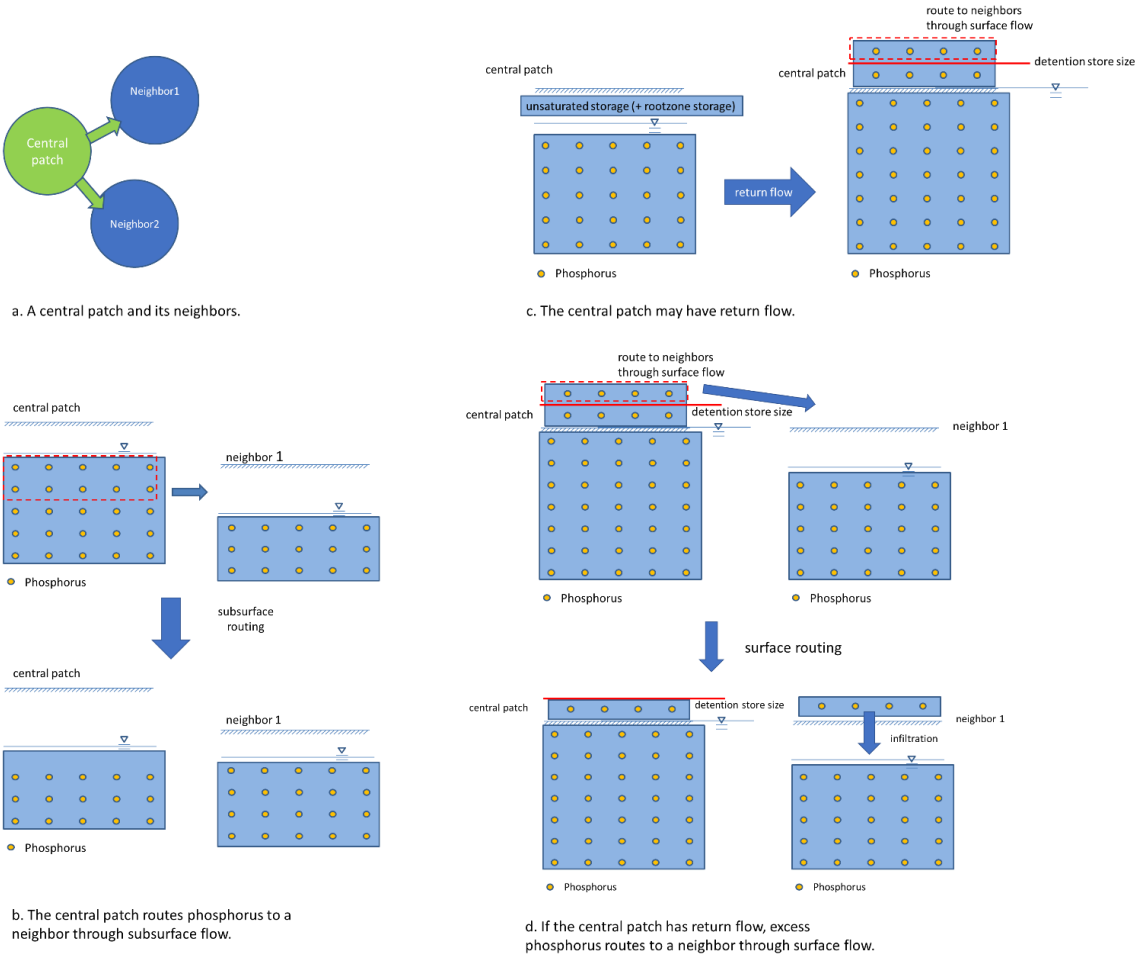

Figure 5.2 Land patch phosphorus routing processes. a. For a specific patch (central patch), flow table indicates the flow direction and flow proportion to the central patch neighbors. b. Subsurface routing occurs at the saturated flow layer, water and phosphorus flow from the central patch to the neighbor patch. c. For the central patch, if the unsaturated water (and rootzone water for vegetation patch) is greater than the patch saturation deficit, return flow occurs. Groundwater with phosphorus moves up to the patch surface. d. If the central patch has return flow, aboveground excess water flows to its neighbor patch surface, and then the surface water on the neighbor patch infiltrates into the soil.

5.2.1.1 Land patch routing

Land patch routing includes subsurface flow and surface flow. Figure 5.2 shows the land patch routing process. For a specific patch, which we will call the central patch,

the patch has its downstream neighbor patch connectivity defined by the flow table. For both subsurface and surface flow, the flow table also indicates the proportion of flow each neighbor can receive from the central patch. The proportion each neighbor patch receives is denoted as γ_i , where *i* is the neighbor patch index. For a central patch, all of its neighbors γ_i sum to 1. In Figure 5.2, for example, possible γ_i values for the two neighbor patches are $\gamma_1 = 0.6$ and $\gamma_2 = 0.4$, indicating that neighbor 1 receives 60% of the total flow out of the central patch and neighbor 2 receives 40%.

Subsurface routing

Subsurface flow occurs at the saturated layer. The flow quantity from the central patch to a neighbor patch is determined by equation (1) (C. L. Tague & Band, 2004).

$$Q_{c,n} = -T_{c,n} \tan \beta_{c,n} w_{c,n} \quad (1)$$

Where $Q_{c,n}$ is the saturated flow quantity from the central patch to a neighbor patch, $T_{c,n}$, is the transmissivity between the central patch and the neighbor patch, $\tan \beta_{c,n}$ is the slope between the two patches, which is also assumed to be the local hydrologic gradient and $w_{c,n}$ is the flow width between the central patch and neighbor patch.

The soil transmissivity, $T_{c,n}$, is calculated with equation (2) and is the integration of soil conductivity from the bottom of soil to the water table depth.

$$T_{c,n} = \int_{-\infty}^{Z_{sat}} K_{sats}(z)dz \quad (2)$$

where Z_{sat} is the water table depth, and $K_{sats}(z)$ is the saturated hydrologic conductivity at the depth *z*. $K_{sats}(z)$ is assumed to follow an exponential decay as in equation (3):

$$K_{sats}(z) = K_{sats0} \exp^{(-\frac{z}{m})} \quad (3)$$

where K_{sats0} is the saturated hydrologic conductivity at the soil surface, which is defined in soil properties or defined by user. z is the soil depth, and m is the decay coefficient of hydraulic conductivity with depth.

In the RHESSys and RHESSys-P code, flow quantity between patches is not calculated directly with equation (1). In the code, the total amount of subsurface flow out of the central patch is calculated, and then distributed according to the neighbor patch γ_i value.

Soil phosphorus is assumed to decline exponentially with soil depth as in equation (4):

$$soil_P(z) = P_{surface} \exp^{-P_{decay} z} \quad (4)$$

where $soil_P(z)$ is the soil phosphorus amount at the depth z, $P_{surface}$ is the soil phosphorus amount at the surface, P_{decay} is the soil phosphorus decay coefficient, and z is the soil depth.

Using equation (4), total soil phosphorus can be computed as equation (5):

$$soil_P = \int_0^{Z_{soil}} soil_P(z)dz \tag{5}$$

where $soil_P$ is the total soil phosphorus amount, and Z_{soil} is the soil depth.

In RHESSys-P, $soil_P$ is a state variable for a given patch. After rearranging equation (5), $P_{surface}$ is expressed as equation (6):

$$P_{surface} = \frac{soil_P P_{decay}}{1 - \exp(-P_{decay} z_{soil})} \tag{6}$$

With equation (6), soil phosphorus for any soil layer can be calculated with equation (7):

$$soil_{P\_z_1-z_2} = \int_{z_1}^{z_2} P_{surf} \exp(-P_{decay} z)dz = \frac{P_{surf}}{P_{decay}}(\exp(-P_{decay} z_1) - \exp(-P_{decay} z_2)) \tag{7}$$

where $soil_{P\_z_1-z_2}$ is the total phosphorus amount from soil depth z_1 to z_2.

Soil phosphorus below the water table has two states: adsorbed or in solution. The adsorbed state is phosphorus adsorbed to soil particles. The adsorbed phosphorus of

any layer under water table does not move with lateral flow and is determined by equation (8):

$$P_{adsorbed\_z_1-z_2} = n_0(z_2 - z_1)P_{adsorbRate}\rho_b \quad (8)$$

where $P_{adsorbed\_z_1-z_2}$ is the adsorbed phosphorus amount for the soil layer from depth z_1 to z_2, n_0 is the soil average porosity, z_2 is the soil layer bottom depth, z_1 is the soil layer top depth, $P_{adsorbRate}$ is the soil-specific coefficient describing how much phosphorus can be adsorbed by unit weight soil, and ρ_b is soil bulk density.

Adsorbed phosphorus below the water table is expressed as $P_{adsorbed\_z_{sat}-z_{soil}}$. It is calculated by plugging $z_2 = z_{soil}$, and $z_1 = z_{sat}$ into equation (8), where z_{soil} is the soil depth, z_{sat} is the water table depth.

Solution state phosphorus is the remaining phosphorus, which is assumed to be well mixed in the saturated water. Solution state phosphorus is also called available phosphorus, because solution state phosphorus can be routed to neighbor patches. The available phosphorus of any layer under water table is calculated by equation (9):

$$P_{avail\_z_1-z_2} = soil_{P\_z_1-z_2} - P_{adsorbed\_z_1-z_2} \quad (9)$$

where $P_{avail\_z_1-z_2}$ is the solution state phosphorus of the layer from soil depth z_1 to z_2, z_1 is the soil layer top depth, z_2 is the soil layer bottom depth, $soil_{P\_z_1-z_2}$ is the

soil phosphorus from soil depth z_1 to z_2 calculated by equation (7), $P_{adsorbed\_z_1-z_2}$ is the absorbed state phosphorus amount from soil depth z_1 to z_2 calculated by equation (8).

Equation (9) gives a general form for the available phosphorus of any layer. A special form is the available phosphorus in the saturated layer, $P_{avail\_z_{sat}-z_{soil}}$, which is calculated with equation (9) by plugging in $z_2 = z_{soil}$, and $z_1 = z_{sat}$.

With subsurface flow $Q_{c,n}$ and saturated layer solution state phosphorus $P_{avail\_z_{sat}-z_{soil}}$, the phosphorus routing from the central patch to its neighbor patch can be calculated with equation (10):

$$P_{c,n} = \frac{Q_{c,n}}{Q_{sat}} P_{avail\_z_{sat}-z_{soil}} S_{patch} \quad (10)$$

where $P_{c,n}$ is the phosphorus amount moving from central patch to its neighbor patch through subsurface flow, $Q_{c,n}$ is the saturated flow quantity from the central patch to a neighbor patch, and Q_{sat} is the saturated layer water quantity in the central patch. The transported phosphorus, $P_{c,n}$, will be added to the neighbor soil phosphorus pool, S_{patch} is the central patch area.

Surface routing (overland flow)

If the unsaturated water (plus rootzone water for vegetation patch) is greater than the saturation deficit, return flow occurs (Figure 5.2 c). Return flow, Q_{return}, is calculated with equation (11):

$$Q_{return} = Q_{unsat} + Q_{rootzone} - W_{sat} \quad (11)$$

where Q_{return} is the return flow quantity, Q_{unsat} is the unsaturated soil layer water, $Q_{rootzone}$ is the rootzone layer water for vegetation land use, and W_{sat} is the patch water saturation deficit.

RHESSys-P describes soil porosity using equation (12):

$$n(z) = n_0 \exp^{-\frac{z}{p}} \quad (12)$$

where $n(z)$ is the soil porosity at soil depth z, n_0 is a soil specific parameter describing the soil surface porosity, and p is the soil porosity decay coefficient.

For the saturated layer, integration of equation (12) provides the water content for the layer as equation (13):

$$Tn_{z_1-z_2} = \int_{z_1}^{z_2} n_0 \exp(-z / p)dz = pn_0(\exp(-z_1 / p) - \exp(-z_2 / p)) \quad (13)$$

where $Tn_{z_1-z_2}$ is the total porosity from depth z_1 to z_2, z_1 is the starting depth, and z_2 is the ending depth.

For return flow, RHESSys-P assumes that the return flow source is from the top soil layer, specifically, from soil surface to some depth z_{return} . Using the porosity equation (14), z_{return} is calculated as equation (14):

$$z_{return} = -p \times \log(1 - \frac{Q_{return}}{n_0 p}) \quad (14)$$

The return flow layer is from the soil surface to z_{return} . The return flow Q_{return} is computed using equation (13) and substituting in z_{surf} for z_1 and z_{return} for z_2 . Soil phosphorus in the return flow layer, $soil_{P\_z_{surf}-z_{return}}$, is calculated with equation (7) by substituting z_{surf} for z_1 and z_{return} for z_2 . The adsorbed phosphorus in the return layer, $P_{adsorbed\_z_{surf}-z_{return}}$, is calculated with equation (8) by substituting z_{surf} for z_1 and z_{return} for z_2 . Equation (9) with $z_1 = z_{surf}$ and $z_2 = z_{return}$, is used to calculate the available phosphorus in the return flow layer, $P_{avail\_z_{surf}-z_{return}}$. Then, $P_{avail\_z_{surf}-z_{return}}$ is moved to the central patch surface with return flow, and the water Q_{return} is added to the central patch detention store pool with equation (15):

$$Q_{det}^{'} = Q_{det} + Q_{return} \quad (15)$$

where $Q_{det}^{'}$ is the new detention store water quantity after return flow moves to the surface, Q_{det} is the old detention store water quantity before return flow moves to the surface, Q_{return} is the return flow. The available phosphorus in the return flow,

$P_{avail\_z_{surf}-z_{return}}$, is added to the central patch phosphorus surface store pool with equation (16):

$$P'_{surf} = P_{surf} + P_{avail\_z_{surf}-z_{return}} \quad (16)$$

where P'_{surf} is the new patch surface phosphorus amount after return flow moves to the surface, P_{surf} is the old patch surface phosphorus amount before return flow moves to the surface, $P_{avail\_z_{surf}-z_{return}}$ is the available phosphorus in the return flow layer. The surface phosphorus is considered well mixed in the patch detention store water.

If the new detention store water Q'_{det} is greater than the detention store size S_{det}, the central patch can't hold the water quantity, and the excess water Q_{det_excess} in equation (17) is routed to its neighbors through overland flow:

$$Q_{det\_excess} = Q'_{det} - S_{det} \quad (17)$$

where Q_{det_excess} is the quantity of water exceeding the detention store size, Q'_{det} is the new quantity of detention store water, and S_{det} is the patch detention store size.

The excess water, Q_{det_excess}, and the phosphorus it contains is routed to its neighbors as overland flow based on the neighbor patch γ_i value from the flow table. Once the neighbor patch receives the overland flow, the neighbor updates its detention store and surface phosphorus. Then, the neighbor patch computes infiltration, and with

infiltration, surface phosphorus enters to neighbor patch soil phosphorus pool (Figure 5.2 d).

5.2.1.2 Stream patch routing

The stream patch routing process is similar to the land patch routing with minor differences. The biggest difference is that stream patches route water and phosphorus as streamflow directly. Figure 5.3 shows the stream routing processes. Although the stream patch still has neighbors, the stream patch does not route water and phosphorus to its neighbors and neighbor connectivity is only used to compute subsurface flow. Similar to land patches, stream patches have subsurface and surface routing processes.

Subsurface routing

For a specific stream patch, which we will call the central patch (Figure 5.3 a), the quantity of subsurface water routed to its neighbors is computed with equation (1). The amount of phosphorus in the subsurface flow is computed with equation (10). Unlike land patch routing, the calculated "subsurface flow" is assumed to be streamflow for that day (Figure 5.3 b).

Surface routing

If a stream patch has return flow, the same procedure as for land patch return flow is used to calculate return flow and the phosphorus brought up to the surface with return flow (Equation 11). After return flow is calculated, if the surface detention store is greater

than the patch detention store size, excess flow with phosphorus is streamflow for that day (Figure 5.3 c).

a. A central stream patch and its neighbor.

b. The central patch subsurface flow routes to streamflow directly.

c. The central patch may have return flow, after processing return flow, surface excess water directly enters streamflow.

Figure 5.3 Stream patch routing processes. a. For a specific patch (central patch), it has neighbors from flow table. b. Subsurface routing occurs at the saturated flow layer, water and phosphorus flow from the central patch and routes as streamflow directly. c. For the central patch, if return flow occurs. Groundwater with phosphorus moves up to the patch surface. And then excess water from the patch surface routes as streamflow.

After processing each stream patch in the basin, streamflow and phosphorus from each stream patch is added up and the sum is the daily streamflow and phosphorus output for that day.

5.2.2 Hillslope

The hillslope spatial unit has two major water fluxes (Figure 5.4). The first is bypass flow, meaning a portion of the hillslope surface water enters the deep ground water pool through soil macro pores. Surface phosphorus is assumed to be well mixed in the surface water, and the bypass flow proportionally adds hillslope surface phosphorus into the deep ground water phosphorus pool. The bypass flow amount is determined by the coefficient *gw1*, which is a parameter to be calibrated.

The second hillslope water flux is the base flow, the portion of the deep ground water that flows to stream as base flow. The phosphorus in the deep ground water store is assumed to be well mixed, so the phosphorus entering the stream with base flow is proportional to the base flow. The portion of the deep ground water that flows to stream as base flow is determined by another coefficient *gw2*, which is also a parameter to be calibrated.

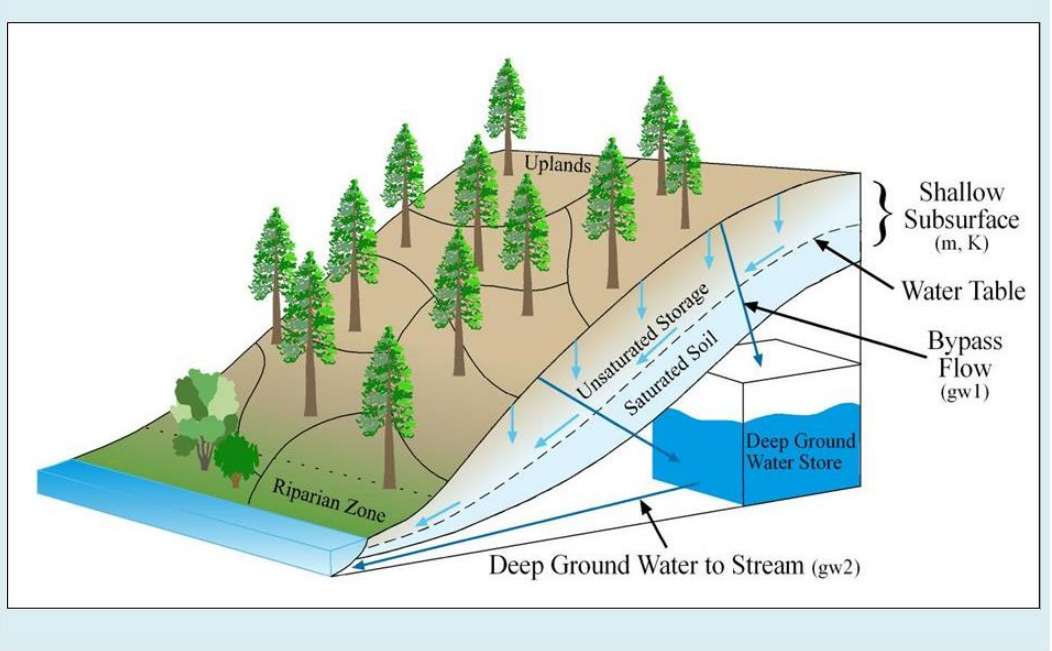

Figure 5.4 Water flux on hillslope. Bypass flow is the water on the hillslope surface entering deep ground water store through macro pores and the flow is determined by the coefficient gw1, and a portion of deep ground water moves to the stream as streamflow and the portion is determined by the coefficient gw2 (https://pdfs.semanticscholar.org/presentation/0c6c/c80fb1dec4bfc8a32528cb3a99a4411610ed.pdf).

5.2.3 Base station

The base station in RHESSys includes spatially explicit time-series climate data and dated agricultural management inputs (fertilizer, irrigation). Although climate data is necessary for model run and dated input data is optional. Base stations don't belong to any specific hierarchical unit (basin, hillslope, zone, patch or stratum), but a base station can be attached to any hierarchical unit. In most RHESSys applications, base stations are attached to zones, and are mainly used to provide climate data (Tmin, Tmax and precipitation) for zones. Although the standard version of RHESSys has the potential to provide fertilizer data, there is no clear procedure for using the base stations to provide

fertilizer data. Since fertilizer is a key source for phosphorus, we developed a method to use spatial-temporal fertilizer application data in RHESSys-P (also applicable for RHESSys), and phosphorus fertilizer functions were added in RHESSys-P to process agriculture land use fertilizer application.

5.2.3.1 Two-level base station construction

In order to use spatial-temporal fertilizer data, we developed a method called the "two-level base station construction". Level one base station construction is based on climate data (real climate station data or reanalysis grid data). This level of base station construction is the same as constructing a base station in standard RHESSys. Level two base station construction is based on the level one base station map but uses an agricultural land use map to construct the level two base station map.

Level 1 base station map

To create the base station map, weather stations or climate reanalysis grid data are used to create Thiessen polygons (Figure 5.5 a). In RHESSys-P, zones are the hierarchical unit for processing climate data. Each zone uses the climate base station for the Thiessen polygon in which it is located (Figure 5.5 b). If the zone lies in multiple Thiessen polygons, majority rule is used to determine which climate base station is used.

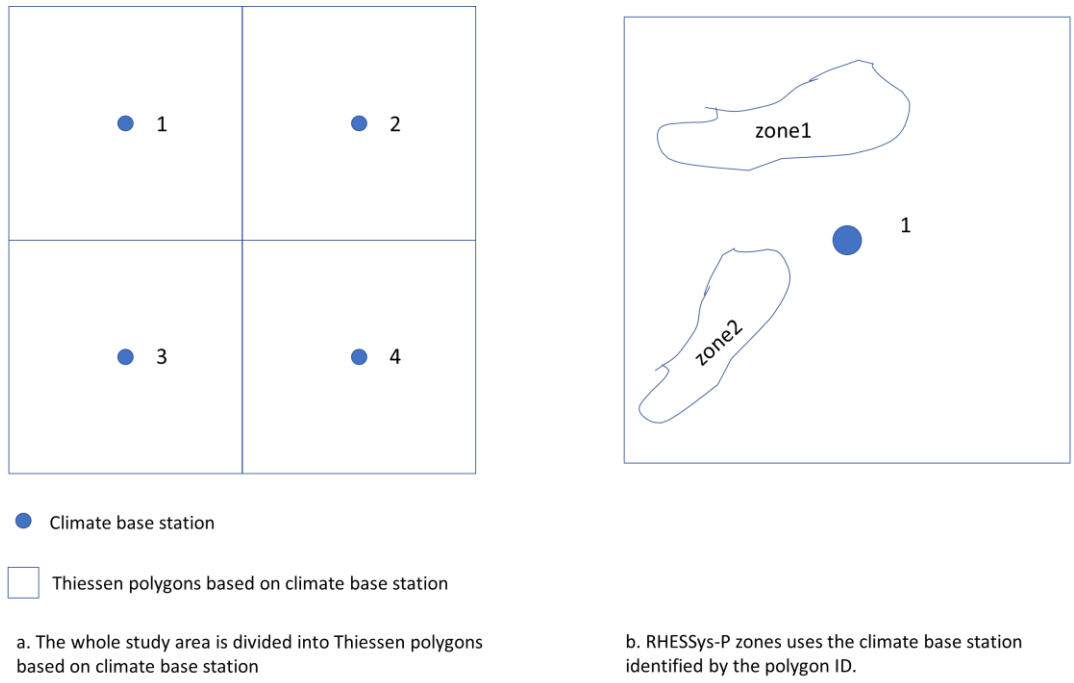

Figure 5.5 Level one base station map. a. Climate base stations are used to create Thiessen polygons. b. RHESSys-P zones use the climate base station based on the polygon ID, which is the same as the base station ID. In the example above, zone1 and zone2 both use the climate base station data associated with polygon 1.

Land management scheme

Before constructing the level two base station map, a land management map needs to be created. For agricultural land use, different land may have different fertilizer application dates, amounts or harvest dates. The combination of all the land management practices is called the land management scheme (Figure 5.6).

The items in the land management scheme are defined by users. Commonly used items include fertilizer application (NO_3-N, NH_4-N, DIP, DOP), and harvest date. Non-agricultural land uses are set to 0, which has no management practices. For agricultural

land use in the study basin, a scheme must be created with details based on the agricultural land management practices (Figure 5.6).

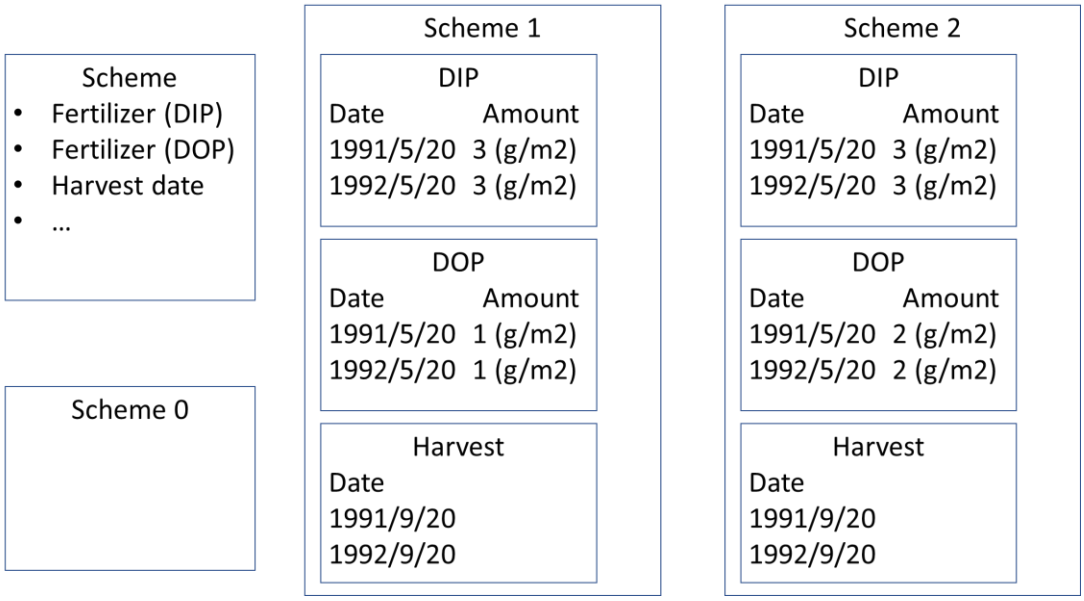

Figure 5.6 Agricultural land use management schemes include different user-defined land use management practices, including fertilization amounts, types, dates and harvest dates. Scheme 0 has no management practices and is used for non-agriculture land. Any difference between two agriculture land management practices leads to a different scheme. In this example, Scheme 1 has a different DOP application amount from Scheme 2.

Figure 5.7 shows an example of the scheme map creating process and how the spatial data is linked with the schemes using polygon 1 as an example. The land use map is first reclassified to agricultural and non-agricultural land (Figure 5.7 a). The agricultural land is then further divided into different schemes based on the agricultural land management (Figure 5.7 b).

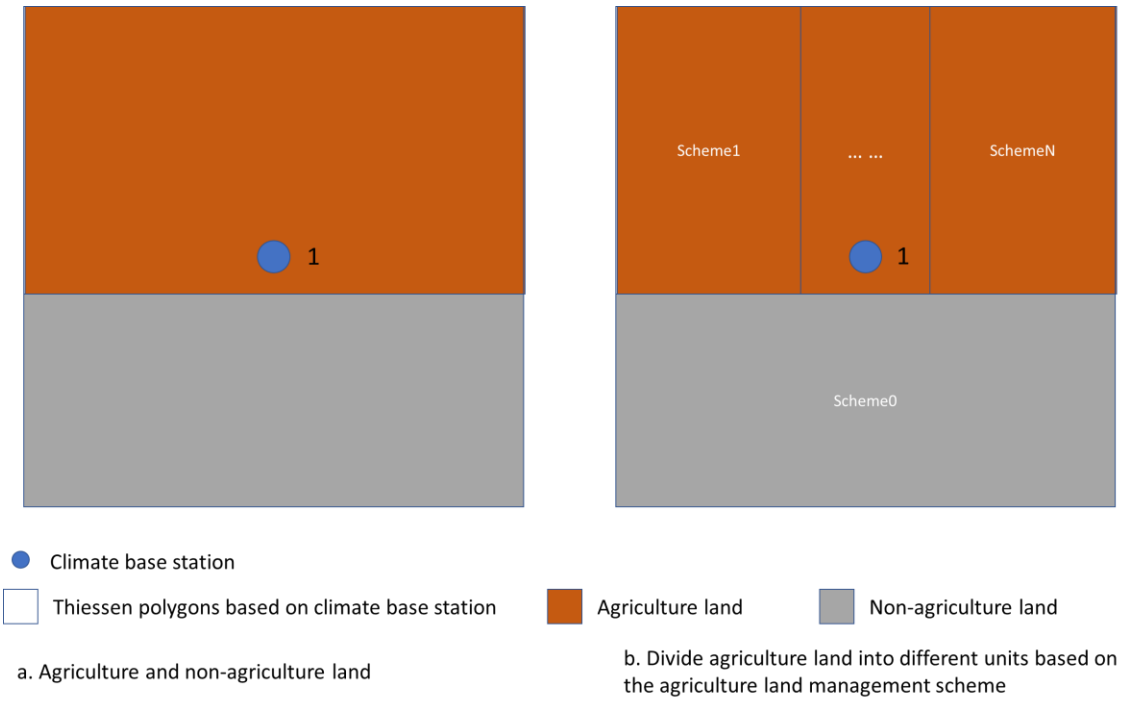

Figure 5.7 Land management scheme creating process, using one Thiessen polygon as an example. a. Divide the study area into agricultural and non-agricultural land. b. Divide the agricultural land into different schemes based on the land management.

Level 2 base station map

Once the land management scheme map is created, concatenating the level 1 base station map with the scheme map creates level 2 base station map for each pixel (Figure 5.8). If we assume there are N schemes and the number N has n digits, the level 2 base station map is calculated with equation (18) using GIS raster calculation:

$$L2 = L1 \times 10^{n} + scheme \tag{18}$$

where $L2$ is the level 2 base station raster map, and $L1$ is the level 1 base station raster map, and $scheme$ is the scheme raster map. A raster calculation with equation (18)

generates the level 2 base station map (Figure 5.9). Each pixel value in the level 2 base station map contains the appropriate climate and land management information.

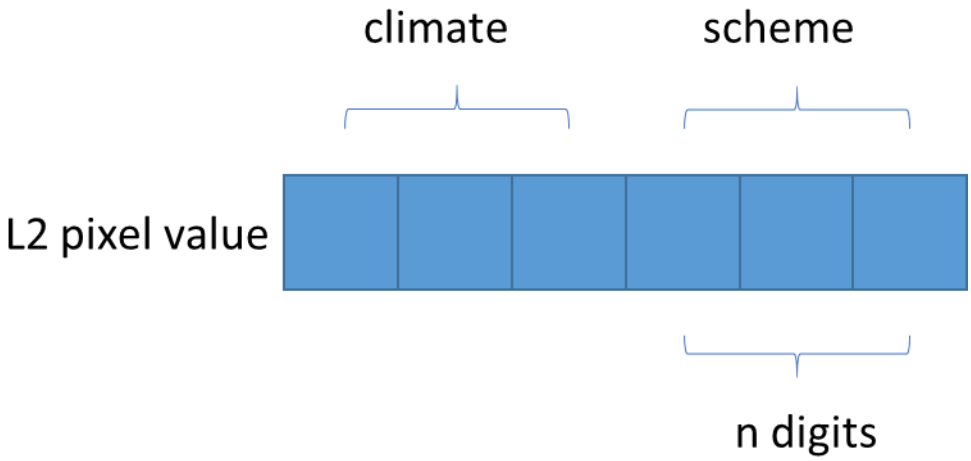

Figure 5.8 Level 2 base station map pixel value is the concatenation of climate base station and management scheme.

Within the level 2 base station map, a climate station is assigned to each pixel using equation (19):

$$climate\_station\_ID = \text{int}(L2 \div 10^{n}) \quad (19)$$

where $climate\_station\_ID$ is the climate base station ID, int is the function to extract integer value, $L2$ is the level 2 base station map, and n is the digit number of the total number of schemes. Each pixel is assigned a management scheme using equation (20):

$$scheme\_ID = L2 \bmod 10^n \quad (20)$$

where $scheme\_ID$ is the land management scheme ID, $\bmod$ is the function to calculate the remainder. Through the encoding and decoding procedures, RHESSys-P can process the spatial-temporal input data.

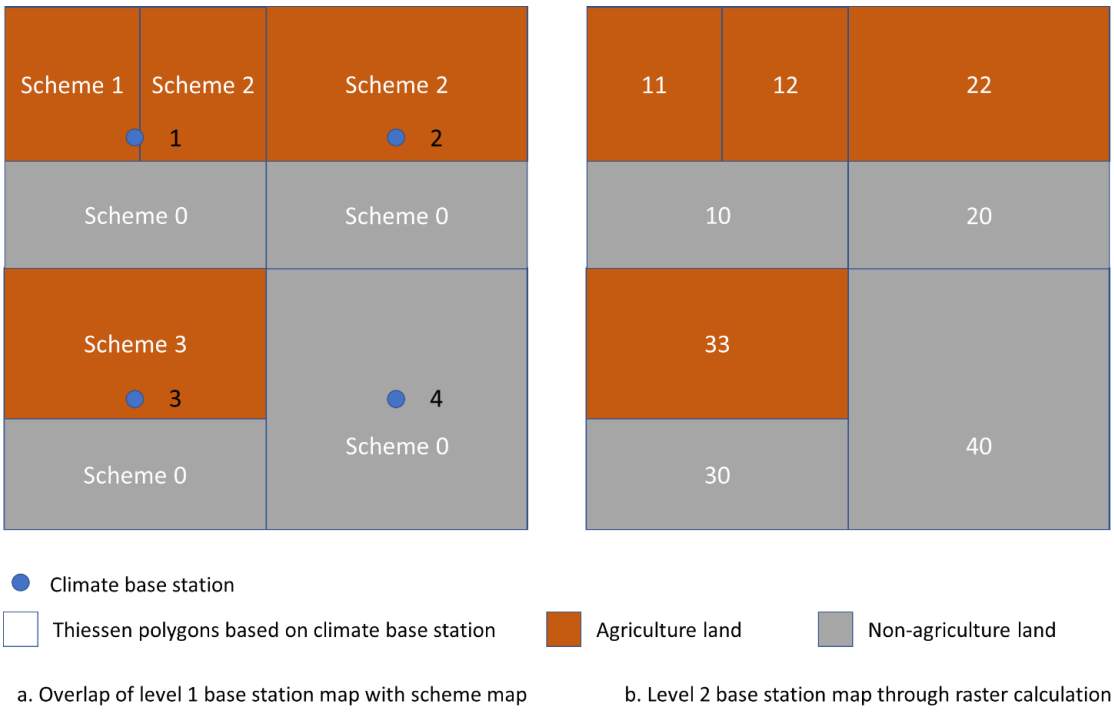

Figure 5.9 Level 2 base station map creating process. a. Overlap the level 1 base station map on the scheme map. b. Concatenating level 1 base station map pixel value with scheme map pixel value to create the level 2 base station map.

5.2.4 Patch

The patch is the basic spatial simulation unit in RHESSys-P. We added several phosphorus pools, processes and fluxes at this level. The added phosphorus pools include the soil surface phosphorus pool, litter phosphorus pool, soil phosphorus pool and soil

organic matter (SOM) phosphorus pool. Added phosphorus processes include rock weathering, surface phosphorus infiltration, decomposition of litter and fertilizer application (Figure 5.10).

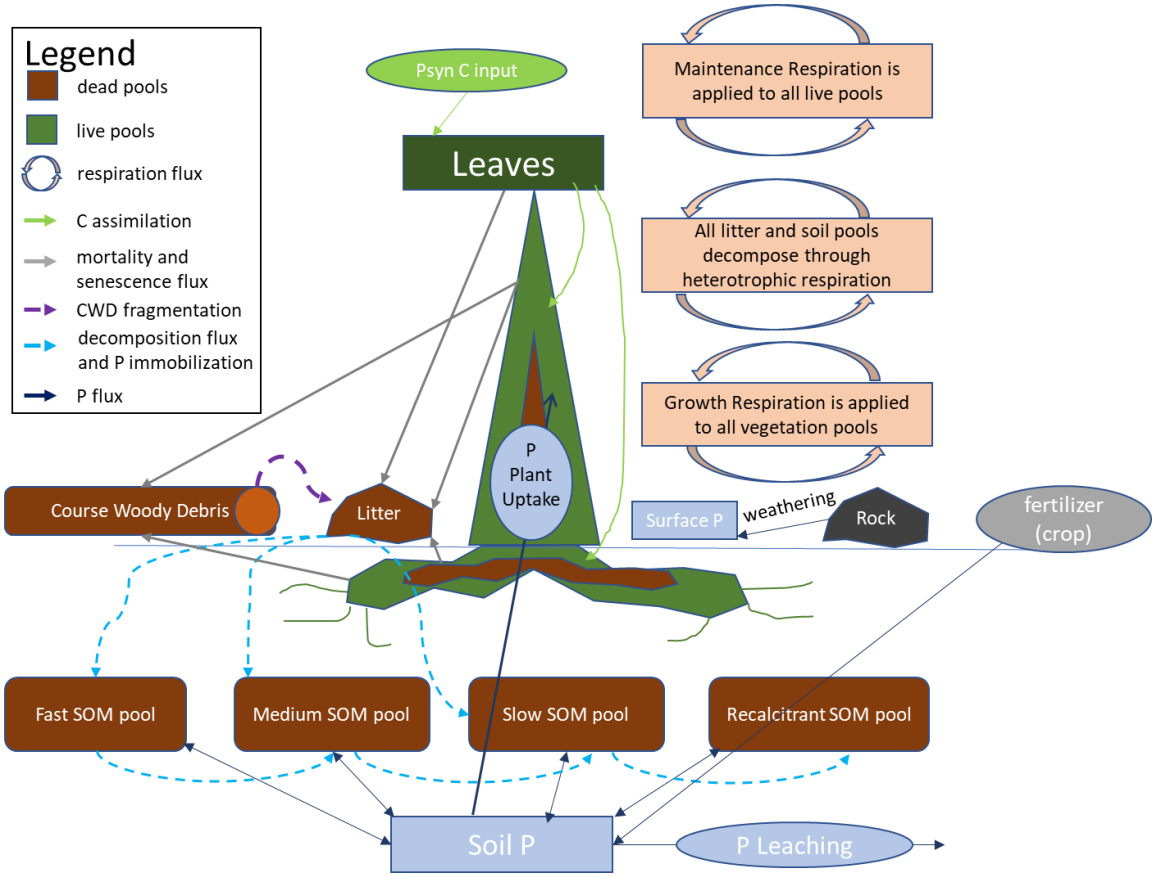

Figure 5.10 Phosphorus pools and fluxes in RHESSys-P, the figure is adjusted from BiomeBGC manual document.

5.2.4.1 Patch phosphorus pools

Soil surface phosphorus pool

The soil surface phosphorus pool is the pool for phosphorus on the soil surface. When the patch detention store is zero (i.e., there is no surface water), phosphorus in the

pool stays static. When the patch detention store has water, surface phosphorus is assumed to be well mixed in the surface water, and the surface phosphorus can move into the soil with infiltration or move to neighbor patch's surface phosphorus pool with overland flow.

Litter phosphorus pool

The litter pool contains phosphorus in dead fallen leaves, branches, or fine roots. Litter is categorized into four types: labile litter, unshielded cellulosic litter, shielded cellulosic litter, and lignin litter. The four litter types are numbered 1, 2, 3, and 4 respectively (Figure 5.11). Phosphorus is determined by the carbon and phosphorus ratio of each pool. Dead leaf C:P ratio varies with vegetation: grass C:P ratio is 565 and tree C:P ratio is 1218 (Sun et al., 2017). The C:P ratios for the remaining litter types are fixed at 500 as in the DayCent model (Parton et al., 1998).

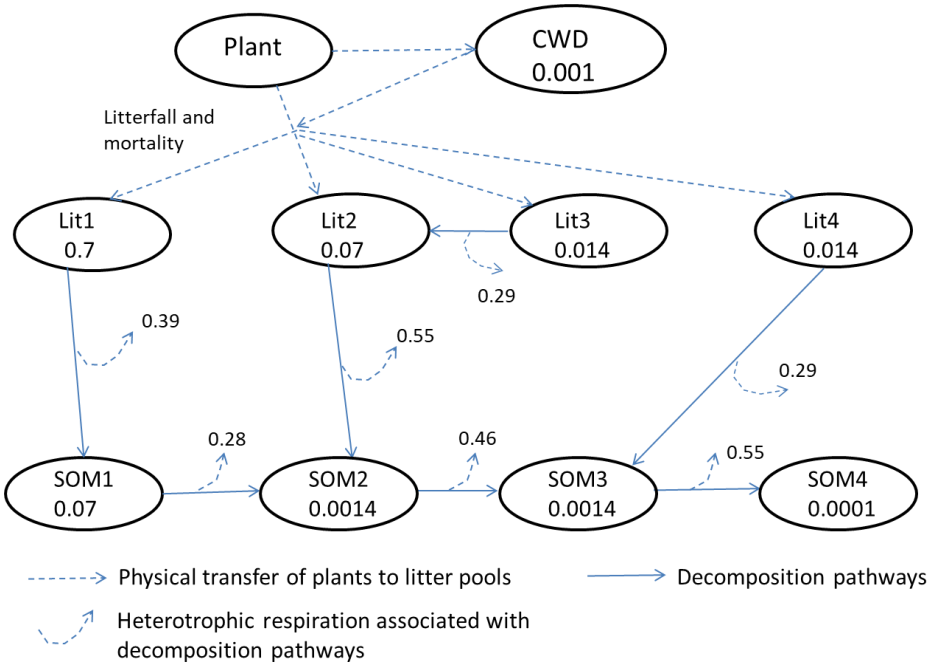

Figure 5.11 Litter (Lit) and soil organic matter (SOM) decomposition pathways (adjusted from BiomeBGC manual document). The value in the oval indicates the base fraction litter or SOM decomposes, the value with the heterotrophic respiration arrow indicates the base fraction used for respiration in the decomposition process. The actual fraction value is adjusted with water and temperature conditions. Lit1, Lit2, Lit3 and Lit4 are the 4 litter types; SOM1, SOM2, SOM3 and SOM4 are the 4 SOM types.

Soil phosphorus pool

The soil phosphorus pool is for belowground phosphorus. Soil phosphorus is assumed to decline exponentially with soil depth as in equation (4). Any change in the soil phosphorus pool generates a new phosphorus profile distribution, whether the change is at the soil surface (return flow) or at the bottom of soil (subsurface flow). The DIP of soil phosphorus pool in vegetation root zone is the phosphorus supply for vegetation.

Soil organic matter phosphorus pool

Soil organic matter (SOM) phosphorus originates from the structural components of vegetation. In RHESSys-P, there are four types of soil organic matter based on their recycling rate (Figure 5.10): fast, medium, slow and recalcitrant. These four types are also labeled as 1, 2, 3 and 4, respectively (Figure 5.11). Soil organic matter phosphorus is determined by fixed C:P ratios, which are 50, 150, 150 and 150 for fast, medium, slow and recalcitrant pools respectively as in the DayCent model (Parton et al., 1998).

5.2.4.2 Patch phosphorus processes

Rock weathering

Rock weathering releases DIP to the patch surface phosphorus pool on a daily time step. The weathering rate is a property of soil type.

Surface phosphorus infiltration

In RHESSys, water in the patch detention store infiltrates into soil with Phillips's infiltration equation (C. L. Tague & Band, 2004). Since the surface phosphorus is assumed to be well mixed in the patch surface detention store, surface phosphorus enters soil phosphorus pools proportionally with infiltration.

Fertilizer application

Every patch is attached to a level-2 base station, which provides user-defined fertilizer application data. When a fertilizer application event happens, the specified amount phosphorus enters the soil phosphorus pool on that specified day.

Decomposition

Litter and SOM decompositions drive phosphorus fluxes among litter phosphorus pools and SOM phosphorus pools (Figure 5.11). The potential phosphorus flux between two pools is calculated with equation (21):

$$pmpf\_p1p2 = p1\_closs * (1.0 - rf\_p1p2 - (cp\_p2/cp\_p1))/cp\_p2 \quad (21)$$

where $pmpf\_p1p2$ is the potential mineral phosphorus flux from pool 1 to pool 2 without soil DIP limit, $p1\_closs$ is the carbon loss in pool 1, rf_p1p2 is the respiration fraction on the decomposition pathway from pool 1 to pool 2, cp_p2 is the ratio of carbon and phosphorus in pool 2, and cp_p1 is the ratio of carbon and phosphorus in pool 1.

A positive $pmpf\_p1p2$ value indicates phosphorus immobilization, which means the decomposition process needs soil DIP to maintain the C:P ratio in pool 1 and pool 2. When soil DIP is not limiting, immobilization proceeds with the potential rate. When soil DIP is limiting for immobilization, a coefficient is used to adjust the flux; A negative $pmpf\_p1p2$ value indicates phosphorus mineralization, which means that after maintaining the C:P ratio in pool 1 and pool 2, there is excess phosphorus in the

decomposition process. The excess phosphorus (DIP) enters the soil phosphorus pool. Since mineralization does not require soil phosphorus, mineralization always occurs at its potential rate.

5.2.5 Canopy strata

The canopy strata level has the same spatial extent as the patch and is used to model plants living on the patch. Plants phosphorus pools were added to RHESSys-P, including leaf phosphorus pool, stem phosphorus pool, fine root phosphorus pool, course root phosphorus pool. We also added plant phosphorus fluxes, including plant growth, mortality, course woody debris decay, leaf fall and cropland harvest. The plant phosphorus fluxes (Figure 5.10) are coupled with plant carbon flux following the C:P ratios shown in **Error! Reference source not found.** (Sun et al., 2017).

Table 5.1 Different components C:P ratio values for vegetation types

	Deciduous	Coniferous	Shrubland	Grassland
Leaf	338	656	393	320
Wood	3125	3125	1875	1875
Root	513	975	513	513

Plant growth

Photosynthesis assimilates carbon into plants, and the potential carbon assimilation rate is calculated with Farquhar model (C. L. Tague & Band, 2004). Using the C:P ratio, potential phosphorus demand is calculated. Since nitrogen and phosphorus can limit plant growth, the following method is used to resolved nitrogen and phosphorus

limitation interactions. In RHESSys-P, if both nitrogen and phosphorus can satisfy plant growth, plants grow at the potential rate; if either one or both can limit plant growth, the most limiting nutrient determines plant growth.

Once the plant growth rate is determined, the assimilated plant phosphorus is allocated to leaf phosphorus pool, stem phosphorus pool, fine root and course root phosphorus pool based on the allocation coefficient in RHESSys vegetation library files.

Mortality process

Mortality applies to all plant components on a daily time step following a mortality coefficient set in the vegetation library files. In this process, the dead leaf phosphorus and fine root phosphorus flows into the patch litter phosphorus pool; dead stem phosphorus and course root phosphorus flows into the coarse woody debris phosphorus pool.

Coarse woody debris decay

Coarse woody debris decay is the physical fragmentation of coarse woody debris into litter (Figure 5.11). Coarse woody debris phosphorus flows into the four litter pools following C:P ratios.

Leaf fall and Harvest

For plants with a leaf fall season (e.g. deciduous forest), leaves fall in a specific time window. In the leaf fall process, leaf phosphorus flows to the patch litter pool.

Harvest only occurs in agricultural lands. Users can specify harvest dates through the land management schemes. When harvest occurs, all aboveground plant phosphorus is removed from the aboveground phosphorus pools.

5.3. Data and methods

5.3.1. Study area

The Missisquoi River watershed is located along the border of the US and Canada covering 2,200 km^2 (Figure 5.12). The altitude in this area ranges from 17 m to 1172 m. In 2001, the predominant land cover was forested (~ 70%). Pasture/hay land cover was ~14% and crop land cover was ~5%. The Missisquoi River drains into Missisquoi Bay, which is in the northern part of Lake Chaplain.

A USGS streamflow gauge (#04294000) is located at 44°55'00" N and 73°07'44" W (North American Datum 1927) near the Missisquoi river outlet. The gauge records daily streamflow data from March 1st, 1990 until now. The Lake Champlain Long-term Monitoring program also set up a sampling point at the streamflow gauge and recorded nutrient data from 1990 – Now (https://anrweb.vermont.gov/dec/_dec/LongTermMonitoringLakes.aspx.)

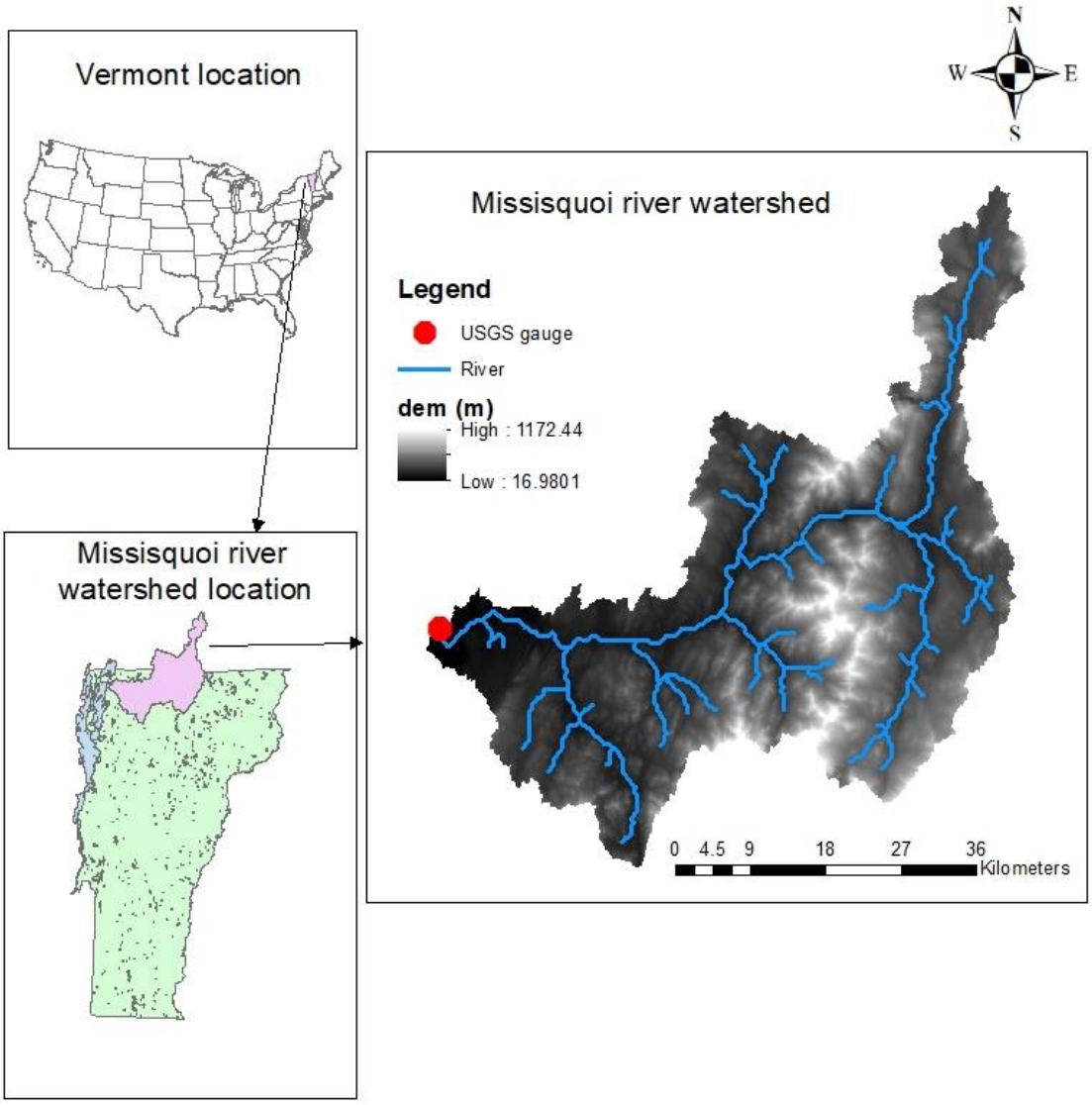

Figure 5.12 Missisquoi river watershed location, USGS gauge #04294000 is located at the outlet of Missisquoi river

5.3.2. Data

5.3.2.1 Climate data

RHESSys-P requires at least daily minimum temperature (Tmin), daily maximum temperature (Tmax) and daily precipitation as climate data input. Historical climate data

are from Daymet version 3 (Thornton et al., 2017), which provides 1-km grid daily data from 1980 to 2016 for North America. Because future projected downscaled climate data from general circulation model (GCM) have much courser spatial resolution (1/8 degree), Daymet data were resampled at 1/8 degree to be consistent with projected climate data (Figure 5.13).

Three GCM models were chosen based on the model credibility for Northeast United States (Thibeault & Seth, 2015): ccsm4, mri-cgcm3, and gfdl-esm2m. Each GCM has four projected climate datasets from 2020 – 2050 based on the four Representative Concentration Pathways (RCPs): RCP2.6, RCP4.5, RCP6.0 and RCP8.5. All climate data were downscaled to 1/8-degree bias correction with constructed analogs dataset (Zia et al., 2016). Thus, in total, 12 climate scenarios were used for future climate data.

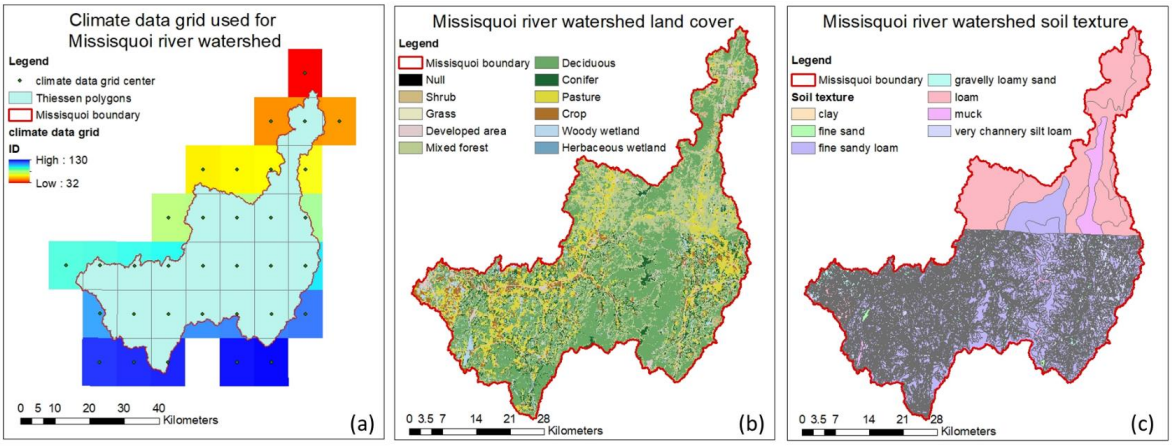

Figure 5.13 RHESSys input data. (a). 1/8 degree grid data used, the grid center points were used to generate Thiessen polygons for spatial climate data input. (b). Missisquoi river watershed land cover, U.S. side is from the year 2001, and Canada side is from the year 2000. (c). Missisquoi river watershed surface soil texture map.

5.3.2.2 Land use/cover data

The land use/cover map combined the US portion (National Land Cover Database, 2001) and Canadian portions (circa 2000, http://www.geobase.ca/) of the Missisquoi River watershed. This land use/cover map was used for RHESSys calibration with historical climate data and gauge data (Figure 5.13).

For the future period (2020 – 2050), we used ILUTABM model (Y. S. Tsai et al., 2015) to generate three different land use scenario maps (Figure 5.14): Business As Usual (BAU), Prefer Forest (proForest) and Prefer Agriculture (proAg). The ILUTABM model can output land use map every year, but for this study, we outputted one land use map every 10 years. Thus, for each land use scenario, there were three land use maps for the period of 2020 to 2050 (Figure 5.14). Prior to model input, all land use/cover data were reclassified as RHESSys land use/cover types.

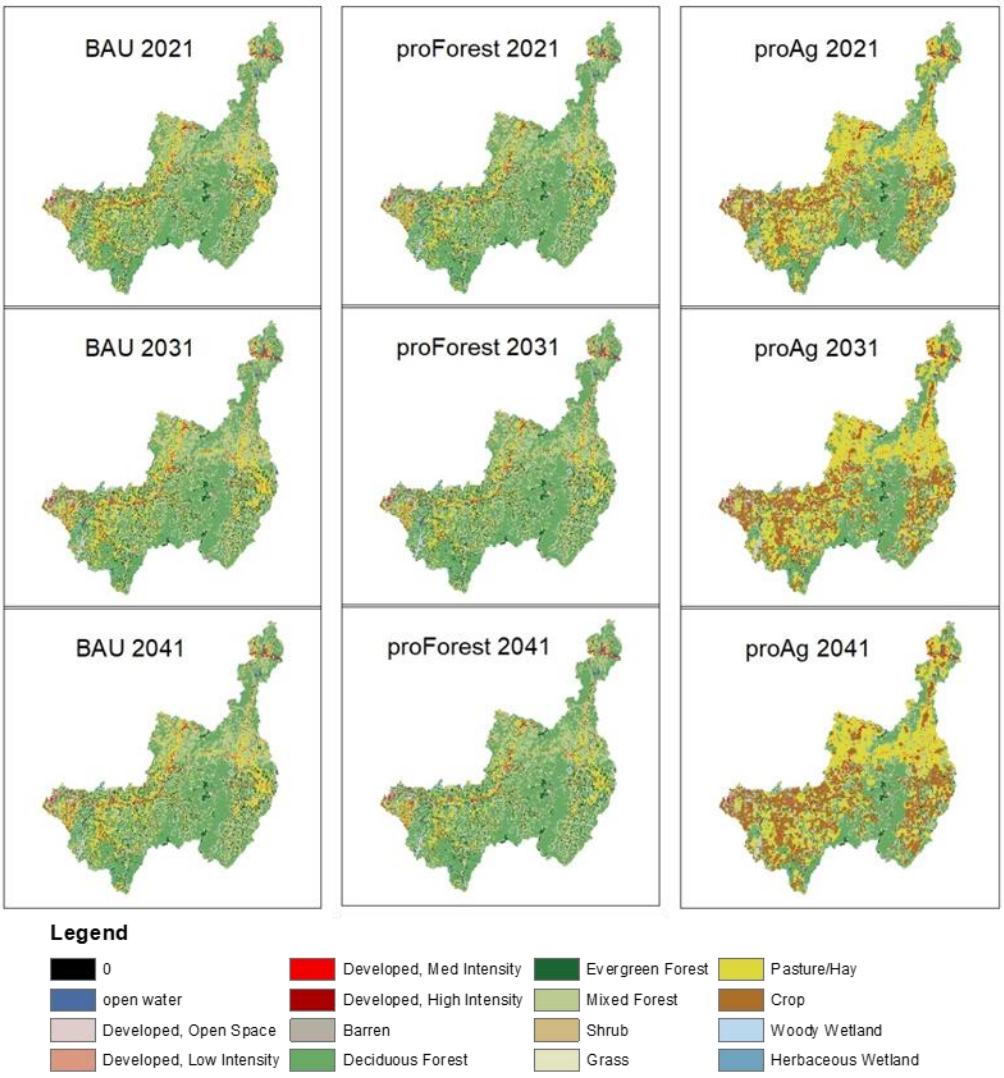

Figure 5.14 Projected land use of the year 2021, 2031 and 2041 for the three land use scenarios: Business As Usual, prefer forest and prefer agriculture.

5.3.2.3 Other input data

For the Missisquoi watershed, a Digital Elevation Model (DEM) of 1 arc-second (approximate 30 meters) from the American National Elevation Dataset was used (Figure 5.12). The DEM was used to generate slope, aspect, west and east horizon grid data. Surface soil texture data were from Vermont Center for Geographic Information

(http://vcgi.vermont.gov/) and Soil Landscapes of Canada (http://sis.agr.gc.ca/cansis/nsdb/slc/index.html). Agriculture land management practice data (fertilizer/manure application, harvest date) were from surveys (Department of Plant and Soil Science, the Universithy of Vermont)). Due to lack of spatial agriculture land management practice data, we assumed all agriculture land had the same management practices. Atmospheric nitrogen deposition data was from National Atmospheric Deposition Program (http://nadp.slh.wisc.edu/). The total nitrogen deposition for Missisquoi river watershed is 1g N/m^2/year.

5.3.3. Experiment design for climate change and LUCC impacts assessment

We spun-up the RHESSys model for about 1500 years to let plants and soil carbon, nitrogen and phosphorus pools reach equilibrium states. Then, the spun-up model was calibrated for streamflow and DP at the outlet of Missisquoi river watershed. Finally, with the calibrated parameter set, the model was run with different climate and LUCC scenarios. In this study, 12 climate scenarios (three GCMs with four RCPs for each GCM) and 3 LUCC scenarios were used, so 36 total climate-LUCC scenarios were used.

5.3.3.1 Calibration and validation

Four parameters were used to calibrate RHESSys-P: *m*, *K*, *gw1* and *gw2*. *m* is the decay of hydraulic conductivity with depth (dimensionless), *K* is the surface lateral hydraulic conductivity (*m*/*day*), *gw1* is the proportion of net inflow water moving to the deep ground water store (dimensionless), and *gw2* is the proportion of water from deep

ground water store moving to the stream. The four parameter ranges used in this study were *m* (0 – 0.2), *K* (0 – 300), *gw1* (0 – 0.9) and *gw2* (0 – 0.9) (Saksa et al., 2017).

Monte Carlo simulations were used to calibrate RHESSys-P 5040 parameter sets were generated using Latin-Hypercube sampling technique with even distribution for each parameter over the parameter range. Then the 5040 parameter sets were used to drive RHESSys-P model on the NCAR Cheyenne cluster (Laboratory, 2017). Nash-Sutcliff coefficient (NSE) was used to assess parameter sets performance.

Streamflow and streamflow DP were calibrated with the data from 2002.1.1 to 2004.12.31. The model was validated with DP data from 2009.1.1 to 2010.12.31. Model fit during the calibration and validation periods was assessed using the Nash-Sutcliffe efficiency value (NSE) and RMSE. NSE is in the range of $-\infty$ to 1, NSE = 1 means perfect match and NSE = 0 means the model performance is equivalent to the average of observed data, and NSE < 0 means model performance is worse than the average of observed data. A threshold value of 0.6 for daily streamflow NSE is considered good fit (Guilbert, 2016). RMSE measures the average differences of simulated and observed data. The smaller the better.

5.3.3.2 Future projection under different climate and LUCC scenarios

Once the best parameter set was determined, it was used to drive RHESSys-P for all projected scenarios. For all scenarios, the historical land use (US 2000, and Canada

2001) was used to run 2011.1.1 to 2020.12.31 for model warm up. From 2021.1.1, projected land use of 2021 was used to run RHESSys-P until 2050.12.31; The land use map was updated every 10 years. The same processes were applied to other land use transition years.

In RHESSys-P, the worldfile is used to describe basin states. Land use change can affect 3 items in the worldfile: the base station a patch attached to, patch land use type, and patch vegetation type. Base station controls the agricultural land management practices, such as fertilizer application. Land use type controls common land management configurations and vegetation type controls vegetation physiology characteristics. Changing these 3 items reflects the LUCC in the RHESSys-P model.

At the land use transition year, a new worldfile with new land use map was used to compare with old worldfile (with old land use map). If any of the 3 items were different for the same landscape unit, the item value from new worldfile was used to replace the corresponding value in the old worldfile. In this way, land use change was integrated into model configuration.

5.3.3.3 Future projection results analysis

We used boxplots to show multiple temporal streamflow distribution characteristics under all climate change and LUCC scenarios. To test our hypothesis, we used annual streamflow standard deviations of RCPs, GCMs and LUCCs to study which

factor was the dominant impacting factor on streamflow. This analysis further factored climate into RCPs and GCMs and would provide insights on climate change impacts on streamflow.

5.4 Results

5.4.1 Calibration and validation

In the streamflow calibration period, the Nash-Sutcliffe efficiency value (NSE) was 0.59 (Figure 5.15 a) and the RMSE was 1.8088 mm. In the validation period, NSE was 0.50 (Figure 5.15 b) and the RMSE was 1.6938 mm, and the R^2 of simulated vs overserved flow was 0.528 (Figure 5.15 e). In both calibration and validation periods, simulated DP basically captured the observed DP. In the calibration period, the NSE was 0.41 and RMSE was 0.00024 g/m^2. In the validation period, the NSE was 0.78, RMSE was 0.00014 g/m^2 and the R^2 of simulated vs overserved DP was 0.788 (Figure 5.15 f).

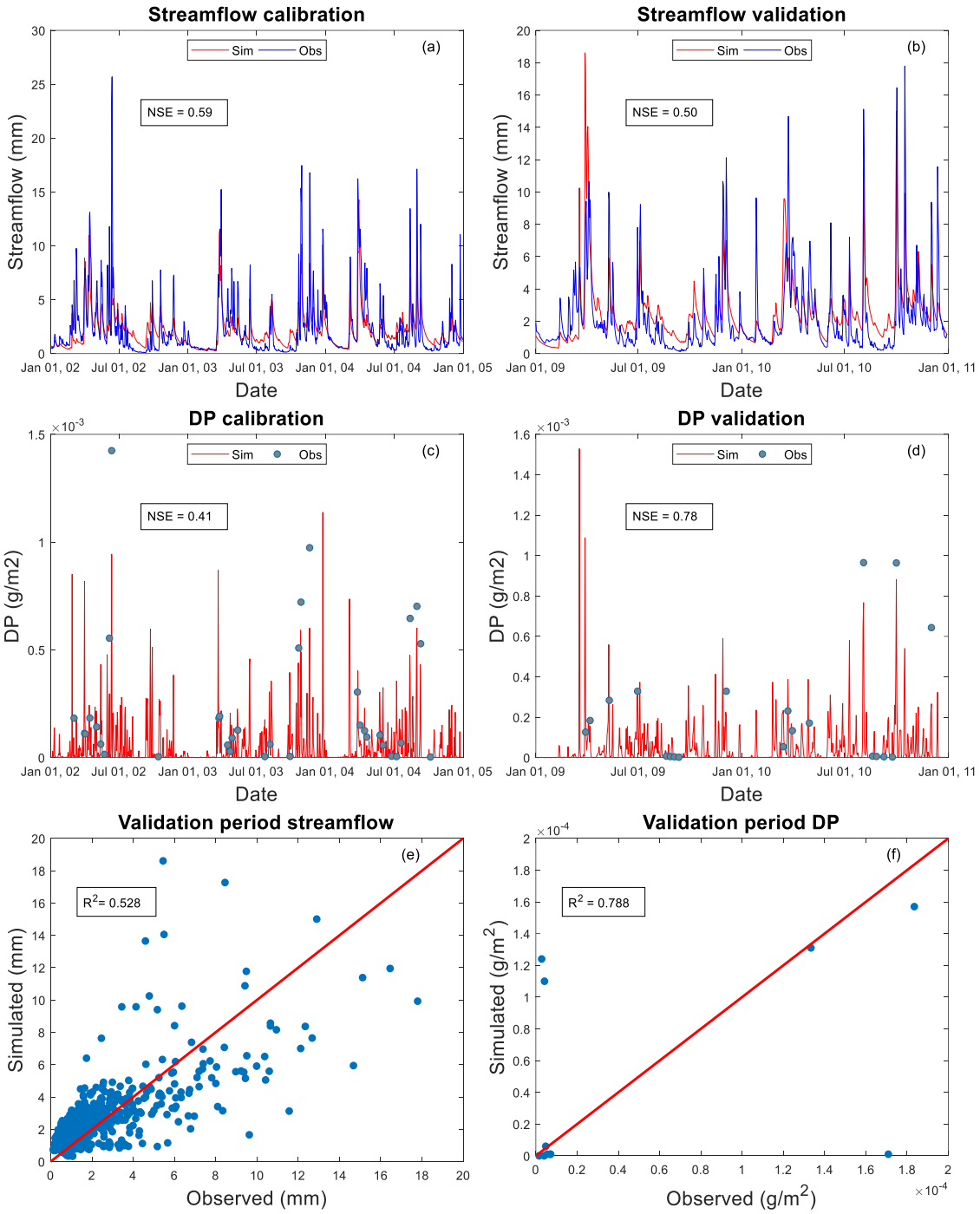

Figure 5.15 Streamflow, streamflow DP calibration and validation results at the outlet of Missisquoi River watershed. (a). Streamflow calibration from 2002.1.1 to 2004.12.31. (b). Streamflow validation from 2009.1.1 to 2010.12.31. (c). Streamflow DP calibration from 2002.1.1 to 2004.12.31. (d). Streamflow DP validation from 2009.1.1 to 2010.12.31. (e). 1:1 line for simulated and observed streamflow for validation period. (f). 1:1 line for simulated and observed streamflow DP for validation period.

5.4.2 Projected DP

Annual DP loads had different time-series trends under different LUCCs during 2021 – 2050 (Figure 5.16). Annual DP loads under BAU had a very gentle increasing trend with around 3.6×10^4 kg at the beginning and 4.0×10^4 kg at the end of simulation period for all climate scenarios. Annual DP loads under proAg increased dramatically from around 3.6×10^4 kg in the year of 2021 to around 1.5×10^5 kg in all climate scenarios. Annual DP loads under proForest were relatively stable, fluctuating around 3.0×10^4 kg without an increasing or decreasing trend between 2021 – 2050 in all climate scenarios. Under the same LUCC, the 3 GCM models had comparable annual loads. This characteristic also applies to the 4 RCPs for the same GCM under the same LUCC.

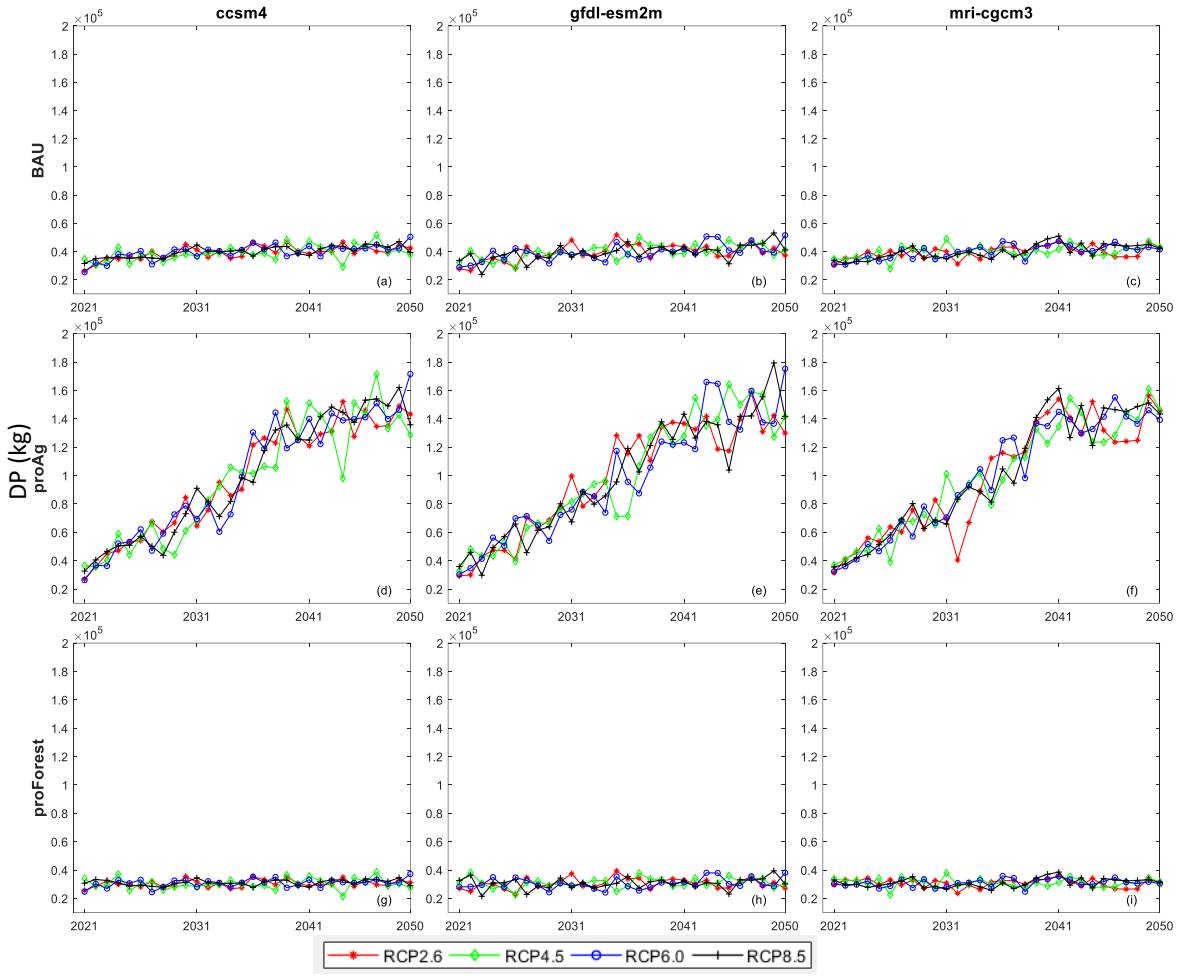

Figure 5.16 Projected annual DP load under different climate change and LUCC scenarios from 2021 to 2050

The medians and ranges in annual DP load also indicated that LUCC had a large impact on loads (Figure 5.17). Annual DP loads under BAU had medians around 4.0×10^4 kg with medium range in the 3 LUCCs. Annual DP loads under proAg had medians around 1.0×10^5 kg with widest range in the 3 LUCCs. Annual DP loads under proForest had medians around 3.0×10^5 kg with smallest range of the 3 LUCCs. Under the same LUCC, the annual loads under the 3 GCMs generally had similar distributions for each

RCP. Similarly, under the same LUCC and GCM, DP loads for all RCPs under BAU and proForest had similar distributions. However, annual loads proAg for different RCPs had variance up to around 2.0 × 10^4 kg.

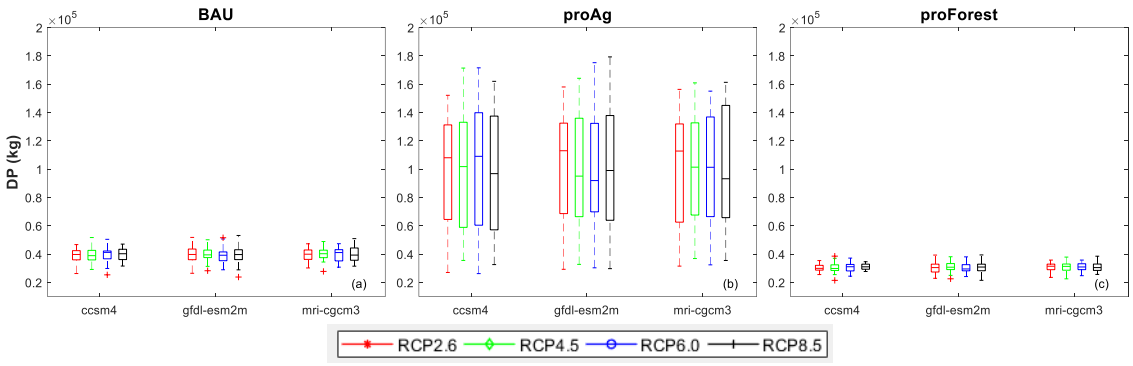

Figure 5.17 Projected annual DP load boxplot under different climate change and LUCC scenarios for the period of 2021 – 2050

Decadal annual DP loads increased in BAU and proAg scenarios, but there was no apparent trend for proForest under any climate scenario (Figure 5.18). Under BAU, medians were around 3.8 × 10^4 kg in the 1st decade, then shifted to 4.0 × 10^4 kg in the 2nd decade, and finally to the 4.1 × 10^4 kg in the 3rd decade. Under proAg, medians were around 5.0 × 10^4 kg in the 1st decade, then jumped to around 1.0 × 10^5 kg, and finally reached 1.3× 10^5 kg. Under proForest, medians were all around 3.0 × 10^4 kg in the 3 decades.

In addition to the medians, annual load ranges had different patterns in the 3 decades for 3 LUCCs. Annual load ranges under BAU and proForest were consistent across the 3 decades. Annual load ranges under proAg shifted during the 3 decades: the

1st decade had a medium interquartile of around 2.0 $\times$ 10^4 kg, and the interquartile increased to around 4.0 $\times$ 10^4 kg in the 2nd decade, and the interquartile shrank to around 1.8 $\times$ 10^4 kg in the 3rd decade.

Under BAU and proForest scenarios, all GCMs had similar patterns across the 3 decades for each RCP (Figure 5.18). For proAg scenarios, annual load patterns under different GCMs and RCPs were different across the decades. In the 1st decade, annual loads were similar for all 3 GCMs under the same RCP; In the 2nd decade, annual load distribution for the 3 GCMs under the same RCP were still comparable but with some exceptions, e.g. gfdl-esm2m under RCP45 has wider ranges than ccsm4 and mri-cgcm3. The 4 RCPs for the same GCM model had different patterns; In the 3rd decade, climate influences on annual loads were similar to the 2nd decade.

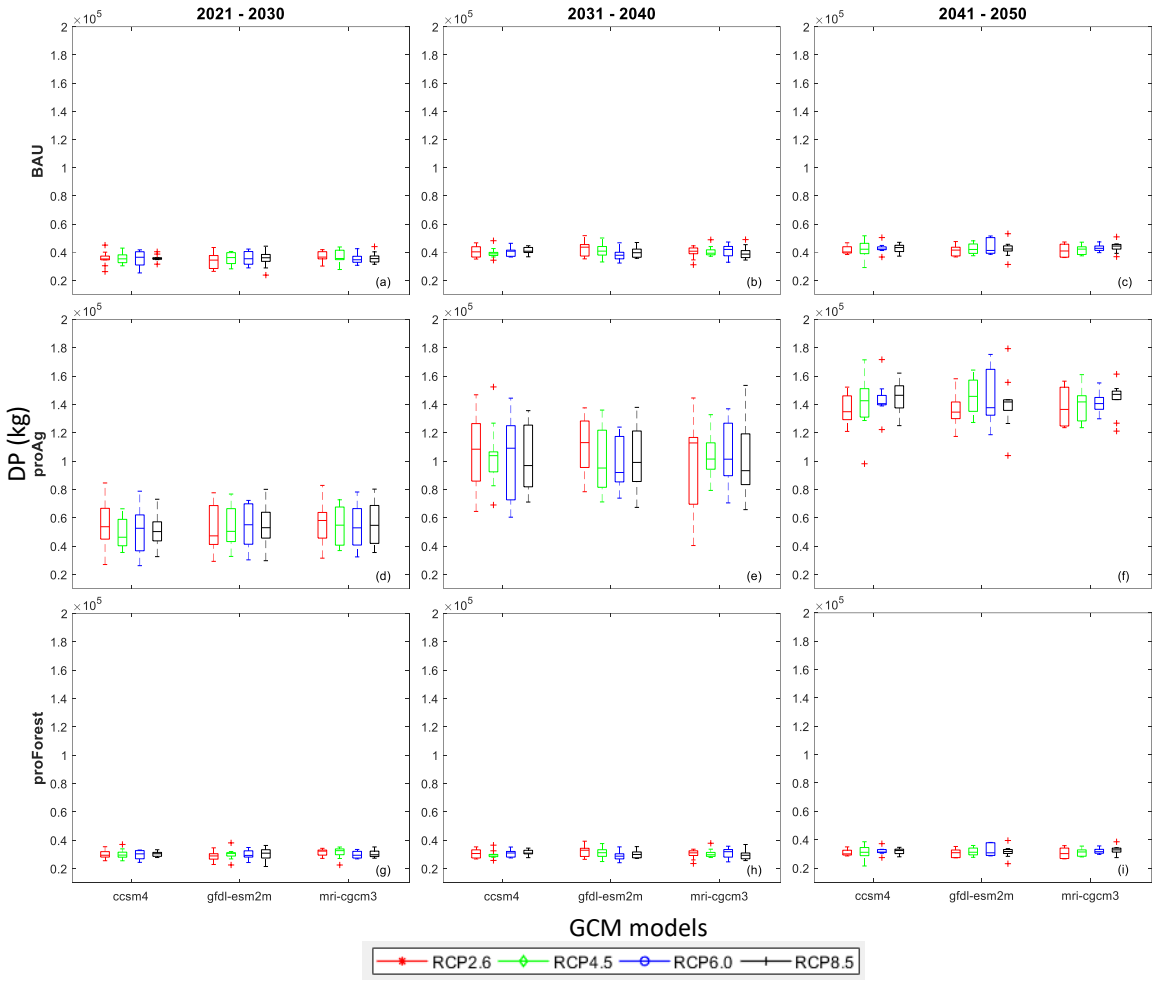

Figure 5.18 Projected annual DP load boxplot under different climate change and LUCC scenarios for decades of 2021 – 2030, 2031 – 2040 and 2041 – 2050

Quarterly DP loads revealed that DP export was typically higher in Q2 and Q3 than in Q1 and Q4 (Figure 5.19). Although there were slight variations among LUCC scenarios, this pattern generally held across LUCC scenarios, RCPs and GCMs (Figure 5.19). Compared with BAU and proForest, quarterly loads under proAg were higher for the same quarter.

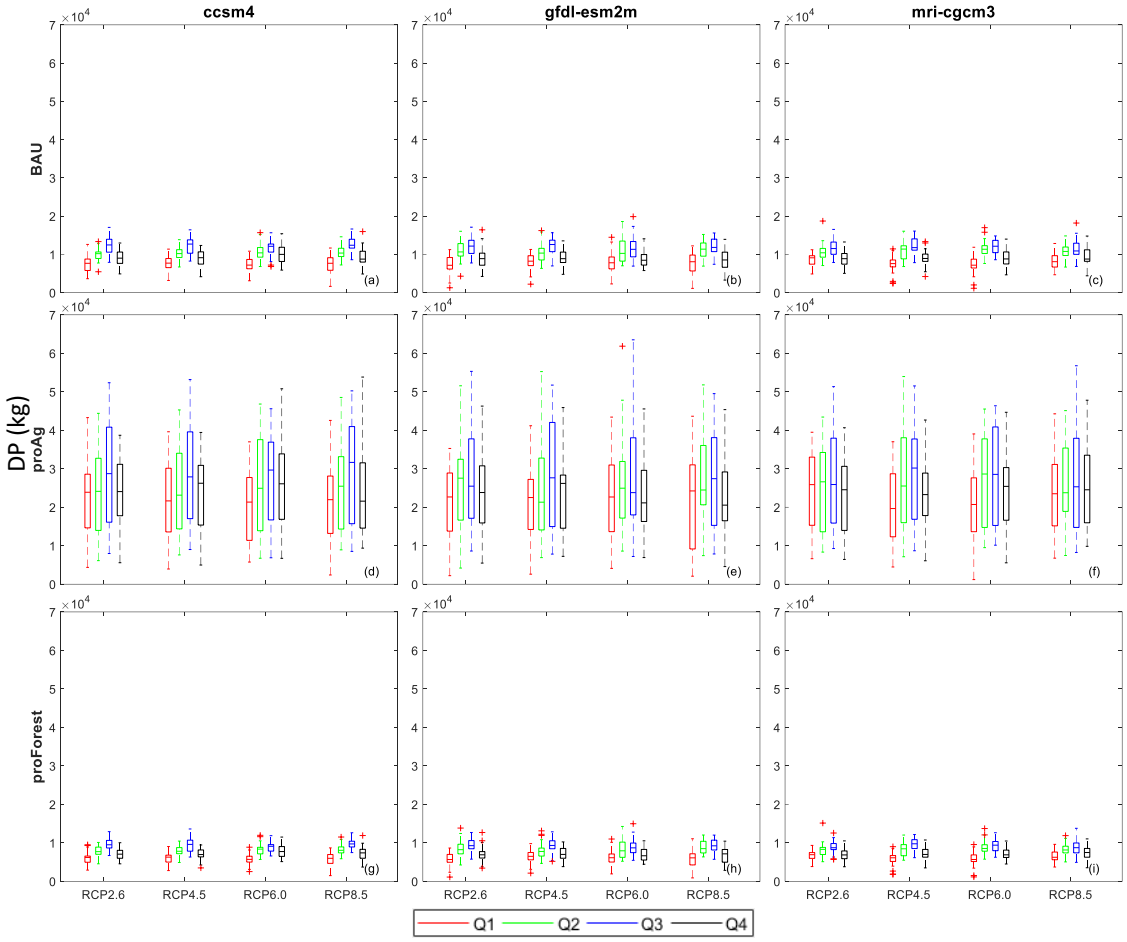

Figure 5.19 Projected quarterly DP load boxplot under different climate change and LUCC scenarios. Q1 is from January to March, Q2 is from April to June, Q3 is from July to September, and Q4 is from October to December

The quarterly loads under 3 GCMs were merged for the same RCP to examine decadal quarterly loads characteristics (Figure 5.20). Under BAU and proForest, the quarterly loads in the 3 decades had similar patterns and magnitudes under the same RCP. Medians of quarterly loads formed a parabolic shape in each of the 3 decades under all RCPs, with Q1 and Q4 loads lower than Q2 and Q3 loads.

In contrast, under proAg, the quarterly loads had different patterns in the 3 decades. In the 1st decade, quarterly loads had a slight increasing trend for all RCPs with medians around 1.0×10^4 kg; In the 2nd decade, medians of quarterly loads increased compared to in the 1st decade. Medians of quarterly loads trends were different for the RCPs (Figure 5.20). Under RCP2.6, the 4 quarterly loads were comparable; for other 3 RCPs, the medians increased in the first 3 quarters and then dropped in Q4; in the 3rd decade, Q1 and Q4 loads under the same RCP were comparable with the corresponding load in the 2nd decade. However, Q2 and Q3 loads dramatically increased, especially Q3 compared with corresponding quarterly loads in the 2nd decade. The quarterly load changes formed a parabola, with lower loads in Q1 and Q4 than Q2 and Q3.

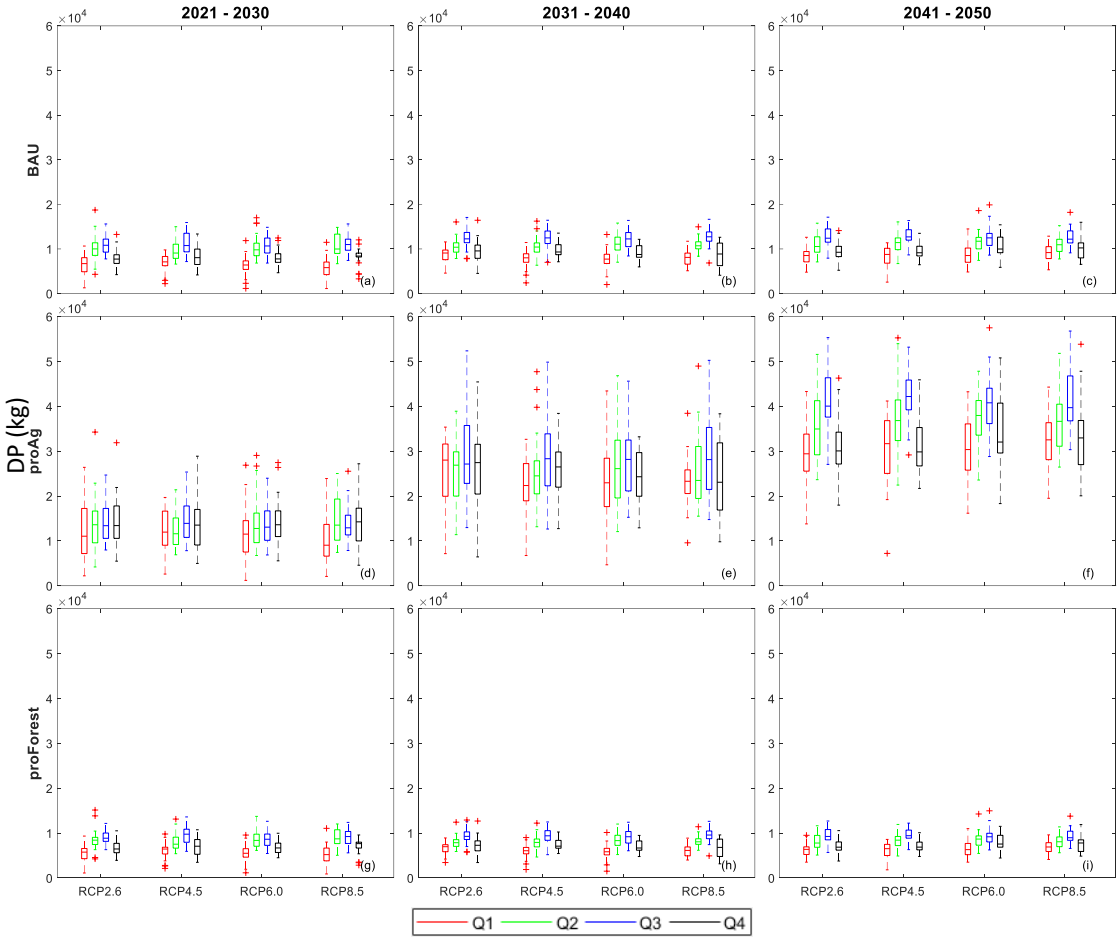

Figure 5.20 Projected quarterly DP load boxplot under different LUCC scenarios for decades of 2021 – 2030, 2031 – 2040 and 2041 – 2050, for each RCP scenario, all 3 GCMs data were merged in each box.

We used annual DP standard deviation to compare which factors – climate, land use, or GCM choice – caused the largest variations in DP load during 2021 - 2050 (Figure 5.21). Across RCPs and GCM models, LUCC caused the most variation in DP load (Figure 5.21), with similar distributions and medians around 4.0×10^4 kg. RCPs and GCMs caused substantially less variation in DP loads, although there was more variation in response the RCP and GCM choice in the proAg scenarios (Figure 5.12). Our results

therefore indicate that LUCCs were the dominant factor for DP load rather than responses to variations in climate.

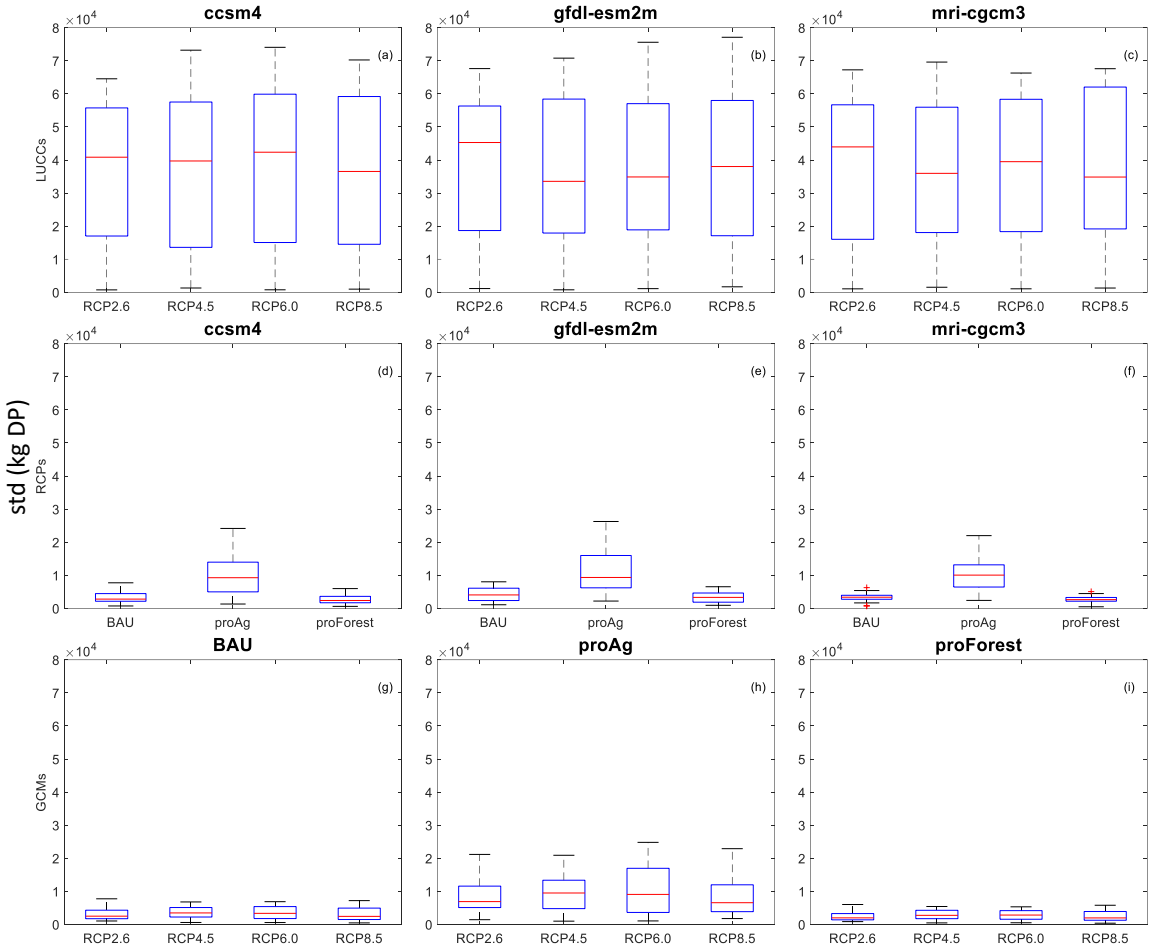

Figure 5.21 Annual DP standard deviation of different factors. The top row shows the standard deviation of LUCCs, the middle row shows the standard deviation of RCPs and the bottom row shows the standard deviation of GCMs

5.4 Discussion

5.3.1 Performance and limitation of RHESSys-P

We developed a process-based RHESSys-P model by integrating the DayCent phosphorus module into the RHESSys model. The DayCent phosphorus module provides dissolved phosphorus processes at the RHESSys patch level, and RHESSys takes care of phosphorus distribution in the soil and transport processes across the landscape. Since RHESSys-P is based on the RHESSys framework, RHESSys-P has inherited limitations. For example, RHESSys-P does not include particulate phosphorus export and does not have in-stream routing processes. One important limitation is the fertilizer/manure application data source, since we used survey data and assumed application rate were the same for all agricultural land, this definitely brought some uncertainty. Another important limitation is from the downscaled climate data. The GCM climate data were downscaled to 1 / 8 degree. Winter et al. (2016) pointed the downscaled data absolute bias was noisy at low elevations, and the climate data could be underestimated or overestimated without clear relationship with elevation. The uncertainty in precipitation can directly affect watershed water input and change the streamflow, which further affect the DP load.

However, our simulation results are promising. RHESSys-P captured observed DP dynamics during the validation period with an R^2 of 79%. Because we only tested the model in Missisquoi River watershed with limited observational data, the model still needs verification in more study areas with observed data. Regardless, our results suggest

that this model provides an alternative tool for phosphorus research and management at the watershed level.

5.3.2 Climate change and LUCC impacts on DP load

Under the combined impacts of climate change and LUCC, land use had larger impacts on dissolved phosphorus loads than did a changing climate. While dissolved phosphorus loads under the proForest land use scenario remained relatively stable under all climate scenarios from 2021 to 2050, dissolved phosphorus loads increased under BAU and proAg scenarios. Dissolved phosphorus loads under BAU increased slightly over time under all climate scenarios; Dissolved phosphorus loads under the proAg scenario increased dramatically over time under all climate scenarios, so that the annual load in 2050 was around 4 times larger than the annual load in 2021. My results therefore suggest that land use is a dominant factor for dissolved phosphorus load compared with climate change. However, this does not mean climate change is not important for dissolved phosphorus load. In the boxplot for the period of 2021 – 2050 (Figure 5.17), dissolved phosphorus load medians under proAg varied by about 20%, but with no consistent trends across GCMs.

Compared with nitrogen, phosphorus biogeochemistry cycle has no gaseous phase. Nitrogen can be lost to the atmosphere as N_2 or N_2O via denitrification; but phosphorus cannot be lost in this way. Phosphorus inputs are from rock mineralization and fertilizer/manure application. Phosphorus can then be taken up by plants or

transported with water through the watershed into rivers or other surface waters. The increase of agricultural land and fertilizer/manure application reveals the reason why the dissolved phosphorus in final year is around 4 times as the load in 2021.

Our results indicate that dissolved phosphorus has clear seasonal patterns, with quarter 2 and quarter 3 generally having the highest seasonal loads, which is consistent with fertilizer application time. This suggests that fertilizer application management practices can help reduce dissolved phosphorus loads. Local agencies could help farmers to choose fertilizer application days according to weather to reduce runoff.

In addition, the annual DP standard deviation analysis also clearly indicated LUCC was the dominant factor on DP load. However, climate had larger impacts in the proAg than BAU and proForest scenarios, suggesting that further climate changes have important impacts on DP load in agricultural lands. Thus, the interactions of LUCC and climate change should not be ignored.

5.5 Conclusion

This chapter developed a process-based RHESSys-P model by integrating the DayCent phosphorus module into RHESSys model. Our simulation results were promising. In both calibration and validation periods, simulated DP basically captured the observed DP. In the calibration period, the NSE was 0.41 and the RMSE was 0.00024 g/m^2. In the validation period, the NSE was 0.78, the RMSE was 0.00014 g/m^2 and the

R^2 of simulated vs overserved DP was 0.788. Because we only tested the model in Missisquoi River watershed with limited observed data, the model still needs verification in more study areas with observed data. Regardless, our results suggest that this model provides an alternative tool for phosphorus research and management at the watershed level.

We used RHESSys-P to study the climate change and LUCC impacts on dissolved phosphorus load in Missisquoi River watershed for the period of 2021 – 2050. Major findings from this research are: (i) LUCC was the dominant factor for dissolved phosphorus loading, however, climate change impacts on dissolved phosphorus shouldn't be ignored, especially in agricultural lands. (ii) In the simulation period of 2021 – 2050, annual loads were stable under proForest for all climate scenarios; Annual loads under BAU increased slightly for all climate scenarios; And annual loads under proAg dramatically increased, so that the load in final simulation year was 4 times that in the beginning year. (iii) Dissolved phosphorus loads in all scenarios generally showed a clear seasonal pattern, with higher loads in quarter 2 and quarter 3, when fertilizers are typically applied, than in quarter 1 and quarter 4. Our results indicated that BAU or proForest in Missisquoi watershed were acceptable for Lake Chaplain water quality, while proAg would export too much phosphorus and lead to water quality deterioration.

CHAPTER 6: CONCLUSION

This dissertation studied Missisquoi River watershed responses to climate change and Land Use/Cover Change (LUCC) with RHESSys model. Studied responses included watershed streamflow and streamflow NO_3-N, NH_4-N and Dissolved Phosphorus (DP). The dissertation contributions fall in to three categories: RHESSys model verification, model development and model applications.

6.1 Model verification

Although RHESSys has been used in several study areas, it is still used by a relatively small community model compared with the Soil and Water Assessment Tool (SWAT) model. Most of the published RHESSys papers studied streamflow at watershed outlet. Very few papers used RHESSys to study aquatic nitrogen and DOC even though RHESSys simulates NO_3-N, NH_4-N, DOC. Chapter 3 and chapter 4 systematically evaluated the ability of the RHESSys model to accurately simulate streamflow, NO_3-N, and NH_4-N.

Streamflow simulation performance was generally satisfactory. The NSE was 0.59 for daily streamflow during the calibration period of 1992.1.1 – 1994.12.31, and 0.52 during the validation period of 1995.1.1 – 1998.12. 31. However, we noticed that performance was dependent on individual year. For example, NSE was 0.41 for the calendar years of 1993 and 1998, but was 0.77 for the calendar year of 1994. The exact reason why RHESSys has such variable performance is not clear, but the results indicate multiple calibration years are necessary for RHESSys. Using a single year for calibration

could lead to lower NSE values in the following validation and application periods. Furthermore, the mismatch between the input data temporal scale and simulation time step. In this study, precipitation is daily, but RHESSys runs hourly processes internally. When lacking hourly time step data, RHESSys assumes the precipitation is evenly distributed throughout the day. This assumption will underestimate rain intensity, especially for storms, and likely reduces the ability of the model to capture observed high streamflow. In addition, due to the lack of in-stream processes, once the water reaches streams, the water and the nutrient in it are automatically exited at the outlet.

Streamflow NO_3-N and NH_4-N simulations were also conducted in this dissertation. Generally, simulated results captured observed patterns but with some errors. In the validation period, the R^2 was low for NO_3-N. NH_4-N had a higher R^2 value of 0.494. These results suggest that model improvement and verification work need to be done for accurate nitrogen simulation work. Potential areas for improvement include improved nutrient distribution in the soil from the current exponential decay with soil depth to avoid inappropriate nutrient vertical movement, adding a sediment module to incorporate the particulate nutrient transport, and incorporating in-stream routing processes and biogeochemical transformations. One additional improvement I want to emphasize is the calibration procedure. RHESSys only provides a standard calibration procedure for streamflow, but no such procedures are available for nutrient calibration. In this dissertation, we followed the streamflow calibration procedure to select the best parameter set by multiple goals – streamflow, NO_3-N and NH_4-N. In contrast, the SWAT model gives a step by step procedure for calibration with one goal in each step, in this

way, researchers can calibrate the model with one goal in each step for better calibration performance for multiple goals. A multiple-goal calibration procedure for RHESSys would be a good tool for improving model performance. To achieve this goal, nutrient-related parameter sensitivity analysis needs to be performed; Another useful addition would be a procedure detailing how to set up the initial conditions for different nutrient pools.

6.2 Model development – RHESSys-P

We developed a model RHESSys-P, which integrated the DayCent phosphorus module into RHESSys. The RHESSys-P model can simulate Dissolved Organic Phosphorus (DOP) and Dissolved Inorganic Phosphorus (DIP) in a watershed and output daily streamflow. To better represent the significant phosphorus source – agricultural land, we also developed a method that allowed the model to take in a spatially explicit time series of land management practices, such as fertilizer application date and amount, harvest date. This method can also be applied for nitrogen fertilizer application.

We tested the phosphorus simulation performance of RHESSys-P in the Missisquoi River watershed. Due to a lack of observed data, we combined the DIP and DOP pools as Dissolved Phosphorus (DP) to evaluate the model performance. DP was calibrated with the data of year 2002 – 2004 and validated with the data of year 2009 - 2010. In both calibration and validation periods, simulated DP basically captured the observed DP. In the validation period, the R^2 of simulated vs observed DP was 0.788.

As noted in the previous section, RHESSys-P has similar future improvement needs as RHESSys, such as improving the distribution of soil phosphorus, including a sediment module, incorporating in-stream routing and biogeochemical process, and developing a calibration procedure.

6.3 Model applications

The primary scientific questions for this dissertation were how climate change and LUCC affect watershed hydrology and nutrient dynamics. I used RHESSys and RHESSys-P to evaluate climate change and LUCC impacts. I used three GCM models to provide climate change projections: ccsm4, mri-cgcm3, and gfdl-esm2m. Each GCM had 4 projected climate datasets from 2021 – 2050 under four Representative Concentration Pathways (RCPs). The ILUTABM model (Y. S. Tsai et al., 2015) was used to generate three different land use scenarios maps: Business As Usual (BAU), Prefer Forest (proForest) and Prefer Agriculture (proAg). The strength of this framework was that it incorporated dynamic LUCC change into climate change model simulations.

The major conclusions are: climate had larger impacts than LUCC on streamflow, although there were no consistent impacts of the different RCPs by 2050; Fertilizer application was a major source for nitrogen export, therefore, LUCC scenarios with more agricultural land had higher nitrogen loads. Thus, LUCC scenarios had larger impacts on nitrogen loads than climate change; LUCC was the dominant driver of dissolved phosphorus loading, however, climate impacts on dissolved phosphorus shouldn't be ignored.

REFERENCES

Al-Mukhtar, M., Dunger, V., & Merkel, B. (2014). Assessing the Impacts of Climate Change on Hydrology of the Upper Reach of the Spree River: Germany. *Water Resources Management, 28*(10), 2731-2749. doi:10.1007/s11269-014-0675-2

Alaoui, A., Willimann, E., Jasper, K., Felder, G., Herger, F., Magnusson, J., & Weingartner, R. (2014). Modelling the effects of land use and climate changes on hydrology in the Ursern Valley, Switzerland. *Hydrological Processes, 28*(10), 3602-3614. doi:10.1002/hyp.9895

Alderman, K., Turner, L. R., & Tong, S. (2012). Floods and human health: A systematic review. *Environment International, 47*, 37-47. doi:10.1016/j.envint.2012.06.003

Alvarez-Cobelas, M., Angeler, D. G., Sanchez-Carrillo, S., & Almendros, G. (2012). A worldwide view of organic carbon export from catchments. *Biogeochemistry, 107*(1-3), 275-293. doi:10.1007/s10533-010-9553-z

Andersen, H. E., Kronvang, B., Larsen, S. E., Hoffmann, C. C., Jensen, T. S., & Rasmussen, E. K. (2006). Climate-change impacts on hydrology and nutrients in a Danish lowland river basin. *Science of the Total Environment, 365*(1-3), 223-237. doi:10.1016/j.scitotenv.2006.02.036

Arnold, J. G., Srinivasan, R., Muttiah, R. S., & Williams, J. R. (1998). LARGE AREA HYDROLOGIC MODELING AND ASSESSMENT PART I: MODEL DEVELOPMENT1. *JAWRA Journal of the American Water Resources Association, 34*(1), 73-89. doi:10.1111/j.1752-1688.1998.tb05961.x

Ban, Y., Gong, P., & Gini, C. (2015). Global land cover mapping using Earth observation satellite data: Recent progresses and challenges. *Isprs Journal of Photogrammetry and Remote Sensing, 103*, 1-6. doi:10.1016/j.isprsjprs.2015.01.001

Band, L. E., Mackay, D. S., Creed, I. F., Semkin, R., & Jeffries, D. (1996). Ecosystem processes at the watershed scale: Sensitivity to potential climate change. *Limnology and Oceanography, 41*(5), 928-938.

Band, L. E., Patterson, P., Nemani, R., & Running, S. W. (1993). Forest ecosystem processes at the watershed scale: incorporating hillslope hydrology. *Agricultural and Forest Meteorology, 63*(1–2), 93-126. doi:http://dx.doi.org/10.1016/0168-1923(93)90024-C

Band, L. E., Tague, C. L., Brun, S. E., Tenenbaum, D. E., & Fernandes, R. A. (2000). Modelling Watersheds as Spatial Object Hierarchies: Structure and Dynamics. *Transactions in GIS, 4*(3), 181-196. doi:10.1111/1467-9671.00048

Band, L. E., Tague, C. L., Groffman, P., & Belt, K. (2001). Forest ecosystem processes at the watershed scale: hydrological and ecological controls of nitrogen export. *Hydrological Processes, 15*(10), 2013-2028. doi:10.1002/hyp.253

Beven, K., & Kirkby, M. (1979). A physically based, variable contributing area model of basin hydrology/Un modèle à base physique de zone d'appel variable de l'hydrologie du bassin versant. *Hydrological Sciences Journal, 24*(1), 43-69.

Bouwman, L., Goldewijk, K. K., Van Der Hoek, K. W., Beusen, A. H. W., Van Vuuren, D. P., Willems, J., . . . Stehfest, E. (2013). Exploring global changes in nitrogen and phosphorus cycles in agriculture induced by livestock production over the

1900-2050 period. *Proceedings of the National Academy of Sciences of the United States of America, 110*(52), 20882-20887. doi:10.1073/pnas.1012878108
Cai, Q., Chen, Y., & King, L. (2001). Why Watershed Ecology? A new approach for research and protection of aquatic ecosystems.
Christensen, N. S., & Lettenmaier, D. P. (2007). A multimodel ensemble approach to assessment of climate change impacts on the hydrology and water resources of the Colorado River Basin. *Hydrology and Earth System Sciences, 11*(4), 1417-1434.
Christensen, N. S., Wood, A. W., Voisin, N., Lettenmaier, D. P., & Palmer, R. N. (2004). The effects of climate change on the hydrology and water resources of the Colorado River basin. *Climatic Change, 62*(1-3), 337-363. doi:10.1023/B:CLIM.0000013684.13621.1f
Christiansen, D. E., Markstrom, S. L., & Hay, L. E. (2011). Impacts of Climate Change on the Growing Season in the United States. *Earth Interactions, 15*. doi:10.1175/2011ei376.1
Cole, J. J., Prairie, Y. T., Caraco, N. F., McDowell, W. H., Tranvik, L. J., Striegl, R. G., . . . Melack, J. (2007). Plumbing the global carbon cycle: Integrating inland waters into the terrestrial carbon budget. *Ecosystems, 10*(1), 171-184. doi:10.1007/s10021-006-9013-8
Conley, D. J., Paerl, H. W., Howarth, R. W., Boesch, D. F., Seitzinger, S. P., Havens, K. E., . . . Likens, G. E. (2009). ECOLOGY Controlling Eutrophication: Nitrogen and Phosphorus. *Science, 323*(5917), 1014-1015. doi:10.1126/science.1167755
Coppin, P., Jonckheere, I., Nackaerts, K., Muys, B., & Lambin, E. (2004). Digital change detection methods in ecosystem monitoring: a review. *International Journal of Remote Sensing, 25*(9), 1565-1596. doi:10.1080/0143116031000101675
Correll, D. L. (1998). The role of phosphorus in the eutrophication of receiving waters: A review. *Journal of Environmental Quality, 27*(2), 261-266.
Crawford, N. H., & Linsley, R. K. (1966). Digital Simulation in Hydrology'Stanford Watershed Model 4.
D'Agostino, D. R., Trisorio, L. G., Lamaddalena, N., & Ragab, R. (2010). Assessing the results of scenarios of climate and land use changes on the hydrology of an Italian catchment: modelling study. *Hydrological Processes, 24*(19), 2693-2704. doi:10.1002/hyp.7765
Dayyani, S., Prasher, S. O., Madani, A., & Madramootoo, C. A. (2012). IMPACT OF CLIMATE CHANGE ON THE HYDROLOGY AND NITROGEN POLLUTION IN A TILE-DRAINED AGRICULTURAL WATERSHED IN EASTERN CANADA. *Transactions of the Asabe, 55*(2), 389-401.
Dinsmore, K. J., Billett, M. F., Skiba, U. M., Rees, R. M., Drewer, J., & Helfter, C. (2010). Role of the aquatic pathway in the carbon and greenhouse gas budgets of a peatland catchment. *Global Change Biology, 16*(10), 2750-2762. doi:10.1111/j.1365-2486.2009.02119.x
Dong, L., Xiong, L., Lall, U., & Wang, J. (2015). The effects of land use change and precipitation change on direct runoff in Wei River watershed, China. *Water Science and Technology, 71*(2), 289-295. doi:10.2166/wst.2014.510
Dunn, S. M., Sample, J., Potts, J., Abel, C., Cook, Y., Taylor, C., & Vinten, A. J. A. (2014). Recent trends in water quality in an agricultural catchment in Eastern

Scotland: elucidating the roles of hydrology and land use. *Environmental Science-Processes & Impacts, 16*(7), 1659-1675. doi:10.1039/c3em00698k

Ekholm, P., Kallio, K., Turtola, E., Rekolainen, S., & Puustinen, M. (1999). Simulation of dissolved phosphorus from cropped and grassed clayey soils in southern Finland. *Agriculture Ecosystems & Environment, 72*(3), 271-283. doi:10.1016/s0167-8809(99)00003-1

El-Khoury, A., Seidou, O., Lapen, D. R., Que, Z., Mohammadian, M., Sunohara, M., & Bahram, D. (2015). Combined impacts of future climate and land use changes on discharge, nitrogen and phosphorus loads for a Canadian river basin. *Journal of Environmental Management, 151*, 76-86. doi:10.1016/j.jenvman.2014.12.012

Elsner, M. M., Cuo, L., Voisin, N., Deems, J. S., Hamlet, A. F., Vano, J. A., . . . Lettenmaier, D. P. (2010). Implications of 21st century climate change for the hydrology of Washington State. *Climatic Change, 102*(1-2), 225-260. doi:10.1007/s10584-010-9855-0

Fan, M., & Shibata, H. (2015). Simulation of watershed hydrology and stream water quality under land use and climate change scenarios in Teshio River watershed, northern Japan. *Ecological Indicators, 50*, 79-89. doi:10.1016/j.ecolind.2014.11.003

Fan, M., & Shibata, H. (2016). Water yield, nitrogen and sediment retentions in Northern Japan (Teshio river watershed): land use change scenario analysis. *Mitigation and Adaptation Strategies for Global Change, 21*(1), 119-133. doi:10.1007/s11027-014-9574-3

Fang, N.-F., Shi, Z.-H., Yue, B.-J., & Wang, L. (2013). The Characteristics of Extreme Erosion Events in a Small Mountainous Watershed. *Plos One, 8*(10). doi:10.1371/journal.pone.0076610

Farquhar, G. D., & von Caemmerer, S. (1982). Modelling of Photosynthetic Response to Environmental Conditions. In O. L. Lange, P. S. Nobel, C. B. Osmond, & H. Ziegler (Eds.), *Physiological Plant Ecology II* (Vol. 12 / B, pp. 549-587): Springer Berlin Heidelberg.

Ficklin, D. L., Luo, Y., & Zhang, M. (2013). Watershed modelling of hydrology and water quality in the Sacramento River watershed, California. *Hydrological Processes, 27*(2), 236-250. doi:10.1002/hyp.9222

Foley, J. A., DeFries, R., Asner, G. P., Barford, C., Bonan, G., Carpenter, S. R., . . . Snyder, P. K. (2005). Global consequences of land use. *Science, 309*(5734), 570-574. doi:10.1126/science.1111772

Galloway, J. N., Winiwarter, W., Leip, A., Leach, A. M., Bleeker, A., & Erisman, J. W. (2014). Nitrogen footprints: past, present and future. *Environmental Research Letters, 9*(11). doi:10.1088/1748-9326/9/11/115003

Gao, M., Qiu, J., Li, C., Wang, L., Li, H., & Gao, C. (2014). Modeling nitrogen loading from a watershed consisting of cropland and livestock farms in China using Manure-DNDC. *Agriculture Ecosystems & Environment, 185*, 88-98. doi:10.1016/j.agee.2013.10.023

Gao, Y., Zhu, B., Yu, G., Chen, W., He, N., Wang, T., & Miao, C. (2014). Coupled effects of biogeochemical and hydrological processes on C, N, and P export during extreme rainfall events in a purple soil watershed in southwestern China. *Journal of Hydrology, 511*, 692-702. doi:10.1016/j.jhydrol.2014.02.005

Garcia-Ruiz, J. M., Begueria, S., Nadal-Romero, E., Gonzalez-Hidalgo, J. C., Lana-Renault, N., & Sanjuan, Y. (2015). A meta-analysis of soil erosion rates across the world. *Geomorphology, 239*, 160-173. doi:10.1016/j.geomorph.2015.03.008

Gessesse, B., Bewket, W., & Braeuning, A. (2015). Model-Based Characterization and Monitoring of Runoff and Soil Erosion in Response to Land Use/land Cover Changes in the Modjo Watershed, Ethiopia. *Land Degradation & Development, 26*(7), 711-724. doi:10.1002/ldr.2276

Godsey, S. E., Kirchner, J. W., & Tague, C. L. (2014). Effects of changes in winter snowpacks on summer low flows: case studies in the Sierra Nevada, California, USA. *Hydrological Processes, 28*(19), 5048-5064. doi:10.1002/hyp.9943

Gombault, C., Sottile, M.-F., Ngwa, F. F., Madramootoo, C. A., Michaud, A. R., Beaudin, I., & Chikhaoui, M. (2015). Modelling climate change impacts on the hydrology of an agricultural watershed in southern Quebec. *Canadian Water Resources Journal, 40*(1), 71-86. doi:10.1080/07011784.2014.985509

Guilbert, J. (2016). The Impacts Of Climate Change On Precipitation And Hydrology In The Northeastern United States. *Graduate College Dissertations and Theses*, 646.

Han, H., Bosch, N., & Allan, J. D. (2011). Spatial and temporal variation in phosphorus budgets for 24 watersheds in the Lake Erie and Lake Michigan basins. *Biogeochemistry, 102*(1-3), 45-58. doi:10.1007/s10533-010-9420-y

Hanan, E. J., Tague, C., & Schimel, J. P. (2017). Nitrogen cycling and export in California chaparral: the role of climate in shaping ecosystem responses to fire. *Ecological Monographs, 87*(1), 76-90. doi:10.1002/ecm.1234

Haygarth, P. M., & Sharpley, A. N. (2000). Terminology for phosphorus transfer. *Journal of Environmental Quality, 29*(1), 10-15.

Heber Green, W., & Ampt, G. A. (1911). Studies on Soil Phyics. *The Journal of Agricultural Science, 4*(01), 1-24. doi:doi:10.1017/S0021859600001441

Horton, R. E. (1939). Analysis of runoff-plat experiments with varying infiltration-capacity. *Eos, Transactions American Geophysical Union, 20*(4), 693-711. doi:10.1029/TR020i004p00693

Huang, J., & Hong, H. (2010). Comparative study of two models to simulate diffuse nitrogen and phosphorus pollution in a medium-sized watershed, southeast China. *Estuarine Coastal and Shelf Science, 86*(3), 387-394. doi:10.1016/j.ecss.2009.04.003

Hunter, N. M., Bates, P. D., Horritt, M. S., & Wilson, M. D. (2007). Simple spatially-distributed models for predicting flood inundation: A review. *Geomorphology, 90*(3-4), 208-225. doi:10.1016/j.geomorph.2006.10.021

Hwang, T., Kangw, S., Kim, J., Kim, Y., Lee, D., & Band, L. (2008). Evaluating drought effect on MODIS Gross Primary Production (GPP) with an eco-hydrological model in the mountainous forest, East Asia. *Global Change Biology, 14*(5), 1037-1056. doi:10.1111/j.1365-2486.2008.01556.x

Isles, P. D. F., Giles, C. D., Gearhart, T. A., Xu, Y., Druschel, G. K., & Schroth, A. W. (2015). Dynamic internal drivers of a historically severe cyanobacteria bloom in Lake Champlain revealed through comprehensive monitoring. *Journal of Great Lakes Research, 41*(3), 818-829. doi:10.1016/j.jglr.2015.06.006

Jacobson, L. M., David, M. B., & Drinkwater, L. E. (2011). A Spatial Analysis of Phosphorus in the Mississippi River Basin. *Journal of Environmental Quality, 40*(3), 931-941. doi:10.2134/jeq2010.0386

Jennings, E., Jarvinen, M., Allott, N., Arvola, L., Moore, K., Naden, P., . . . Weyhenmeyer, G. A. (2010). Impacts of Climate on the Flux of Dissolved Organic Carbon from Catchments. In G. George (Ed.), *Impact of Climate Change on European Lakes* (pp. 199-220).

Jeong, S.-J., Ho, C.-H., Gim, H.-J., & Brown, M. E. (2011). Phenology shifts at start vs. end of growing season in temperate vegetation over the Northern Hemisphere for the period 1982-2008. *Global Change Biology, 17*(7), 2385-2399. doi:10.1111/j.1365-2486.2011.02397.x

Jeppesen, E., Kronvang, B., Olesen, J. E., Audet, J., Sondergaard, M., Hoffmann, C. C., . . . Ozkan, K. (2011). Climate change effects on nitrogen loading from cultivated catchments in Europe: implications for nitrogen retention, ecological state of lakes and adaptation. *Hydrobiologia, 663*(1), 1-21. doi:10.1007/s10750-010-0547-6

Jiang, R., Hatano, R., Zhao, Y., Kuramochi, K., Hayakawa, A., Woli, K. P., & Shimizu, M. (2014). Factors controlling nitrogen and dissolved organic carbon exports across timescales in two watersheds with different land uses. *Hydrological Processes, 28*(19), 5105-5121. doi:10.1002/hyp.9996

Jonsson, A., Algesten, G., Bergstrom, A. K., Bishop, K., Sobek, S., Tranvik, L. J., & Jansson, M. (2007). Integrating aquatic carbon fluxes in a boreal catchment carbon budget. *Journal of Hydrology, 334*(1-2), 141-150. doi:10.1016/j.jhydrol.2006.10.003

Juutinen, S., Valiranta, M., Kuutti, V., Laine, A. M., Virtanen, T., Seppa, H., . . . Tuittila, E. S. (2013). Short-term and long-term carbon dynamics in a northern peatland-stream-lake continuum: A catchment approach. *Journal of Geophysical Research-Biogeosciences, 118*(1), 171-183. doi:10.1002/jgrg.20028

Kemanian, A. R., Julich, S., Manoranjan, V. S., & Arnold, J. R. (2011). Integrating soil carbon cycling with that of nitrogen and phosphorus in the watershed model SWAT: Theory and model testing. *Ecological Modelling, 222*(12), 1913-1921. doi:10.1016/j.ecolmodel.2011.03.017

Kim, D.-K., Kaluskar, S., Mugalingam, S., Blukacz-Richards, A., Long, T., Morley, A., & Arhonditsis, G. B. (2017). A Bayesian approach for estimating phosphorus export and delivery rates with the SPAtially Referenced Regression On Watershed attributes (SPARROW) model. *Ecological Informatics, 37*, 77-91. doi:10.1016/j.ecoinf.2016.12.003

Kolarova, E., Nekovar, J., & Adamik, P. (2014). Long-term temporal changes in central European tree phenology (1946-2010) confirm the recent extension of growing seasons. *International Journal of Biometeorology, 58*(8), 1739-1748. doi:10.1007/s00484-013-0779-z

Laboratory, C. a. I. S. (2017). Cheyenne: HPE/SGI ICE XA System (Climate Simulation Laboratory). Boulder, CO: National Center for Atmospheric Research. doi:10.5065/D6RX99HX

Li, S., Zhang, L., Liu, H., Loaiciga, H. A., Zhai, L., Zhuang, Y., . . . Du, Y. (2017). Evaluating the risk of phosphorus loss with a distributed watershed model

featuring zero-order mobilization and first-order delivery. *Science of the Total Environment, 609*, 563-576. doi:10.1016/j.scitotenv.2017.07.173

Li, Z., Liu, W.-z., Zhang, X.-c., & Zheng, F.-l. (2009). Impacts of land use change and climate variability on hydrology in an agricultural catchment on the Loess Plateau of China. *Journal of Hydrology, 377*(1-2), 35-42. doi:10.1016/j.jhydrol.2009.08.007

Li, Z., Zhang, G., Yu, X., Liu, Q., & Zhang, X. C. (2015). Phosphorus loss and its estimation in a small watershed of the Yimeng mountainous area, China. *Environmental Earth Sciences, 73*(3), 1205-1216. doi:10.1007/s12665-014-3475-3

Ling, Z., Zhuotong, N., Wenjun, Y., & Yingchun, G. (2015). Modeling Land-Use and Land-Cover Change and Hydrological Responses under Consistent Climate Change Scenarios in the Heihe River Basin, China. *Water Resources Management, 29*(13), 4701-4717. doi:10.1007/s11269-015-1085-9

Lopez-Moreno, J. I., Zabalza, J., Vicente-Serrano, S. M., Revuelto, J., Gilaberte, M., Azorin-Molina, C., . . . Tague, C. (2014). Impact of climate and land use change on water availability and reservoir management: Scenarios in the Upper Aragon River, Spanish Pyrenees. *Science of the Total Environment, 493*, 1222-1231. doi:10.1016/j.scitotenv.2013.09.031

Luo, Y., Ficklin, D. L., Liu, X., & Zhang, M. (2013). Assessment of climate change impacts on hydrology and water quality with a watershed modeling approach. *Science of the Total Environment, 450*, 72-82. doi:10.1016/j.scitotenv.2013.02.004

Malve, O., Tattari, S., Riihimaki, J., Jaakkola, E., Voss, A., Williams, R., & Barlund, I. (2012). Estimation of diffuse pollution loads in Europe for continental scale modelling of loads and in-stream river water quality. *Hydrological Processes, 26*(16), 2385-2394. doi:10.1002/hyp.9344

Martin, K. L., Hwang, T., Vose, J. M., Coulston, J. W., Wear, D. N., Miles, B., & Band, L. E. (2017). Watershed impacts of climate and land use changes depend on magnitude and land use context. *Ecohydrology, 10*(7), 17. doi:10.1002/eco.1870

Masood, M., Yeh, P. J. F., Hanasaki, N., & Takeuchi, K. (2015). Model study of the impacts of future climate change on the hydrology of Ganges-Brahmaputra-Meghna basin. *Hydrology and Earth System Sciences, 19*(2), 747-770. doi:10.5194/hess-19-747-2015

Mehdi, B., Ludwig, R., & Lehner, B. (2015). Evaluating the impacts of climate change and crop land use change on streamflow, nitrates and phosphorus: A modeling study in Bavaria. *Journal of Hydrology-Regional Studies, 4*, 60-90. doi:10.1016/j.ejrh.2015.04.009

Meiyappan, P., & Jain, A. K. (2012). Three distinct global estimates of historical land-cover change and land-use conversions for over 200 years. *Frontiers of Earth Science, 6*(2), 122-139. doi:10.1007/s11707-012-0314-2

Menzel, A., & Fabian, P. (1999). Growing season extended in Europe. *Nature, 397*(6721), 659-659. doi:10.1038/17709

Meyers, E. M., Dobrowski, B., & Tague, C. L. (2010). Climate Change Impacts on Flood Frequency, Intensity, and Timing May Affect Trout Species in Sagehen Creek,

California. *Transactions of the American Fisheries Society, 139*(6), 1657-1664. doi:10.1577/t09-192.1
Monteith, J. (1965). *Evaporation and environment.* Paper presented at the Symp. Soc. Exp. Biol.
Ockenden, M. C., Hollaway, M. J., Beven, K. J., Collins, A. L., Evans, R., Falloon, P. D., . . . Haygarth, P. M. (2017). Major agricultural changes required to mitigate phosphorus losses under climate change. *Nature Communications, 8*, 9. doi:10.1038/s41467-017-00232-0
Ongley, E. D., Zhang, X., & Yu, T. (2010). Current status of agricultural and rural non-point source Pollution assessment in China. *Environmental Pollution, 158*(5), 1159-1168. doi:10.1016/j.envpol.2009.10.047
Pachauri, R. K., Allen, M., Barros, V., Broome, J., Cramer, W., Christ, R., . . . Dasgupta, P. (2014). Climate Change 2014: Synthesis Report. Contribution of Working Groups I, II and III to the Fifth Assessment Report of the Intergovernmental Panel on Climate Change.
Park, J.-Y., Yu, Y.-S., Hwang, S.-J., Kim, C., & Kim, S.-J. (2014). SWAT modeling of best management practices for Chungju dam watershed in South Korea under future climate change scenarios. *Paddy and Water Environment, 12*, S65-S75. doi:10.1007/s10333-014-0424-4
Parton, W. J., Hartman, M., Ojima, D., & Schimel, D. (1998). DAYCENT and its land surface submodel: description and testing. *Global and Planetary Change, 19*(1-4), 35-48. doi:10.1016/s0921-8181(98)00040-x
Parton, W. J., Mosier, A. R., Ojima, D. S., Valentine, D. W., Schimel, D. S., Weier, K., & Kulmala, A. E. (1996). Generalized model for N-2 and N2O production from nitrification and denitrification. *Global Biogeochemical Cycles, 10*(3), 401-412. doi:10.1029/96gb01455
Patil, R. J., Sharma, S. K., & Tignath, S. (2015). Remote Sensing and GIS based soil erosion assessment from an agricultural watershed. *Arabian Journal of Geosciences, 8*(9), 6967-6984. doi:10.1007/s12517-014-1718-y
Penman, H. L. (1948). Natural Evaporation from Open Water, Bare Soil and Grass. *Proceedings of the Royal Society of London A: Mathematical, Physical and Engineering Sciences, 193*(1032), 120-145. doi:10.1098/rspa.1948.0037
Piao, S., Friedlingstein, P., Ciais, P., Viovy, N., & Demarty, J. (2007). Growing season extension and its impact on terrestrial carbon cycle in the Northern Hemisphere over the past 2 decades. *Global Biogeochemical Cycles, 21*(3), GB3018.
Poelmans, L., Van Rompaey, A., Ntegeka, V., & Willems, P. (2011). The relative impact of climate change and urban expansion on peak flows: a case study in central Belgium. *Hydrological Processes, 25*(18), 2846-2858. doi:10.1002/hyp.8047
Quinton, J. N., Govers, G., Van Oost, K., & Bardgett, R. D. (2010). The impact of agricultural soil erosion on biogeochemical cycling. *Nature Geoscience, 3*(5), 311-314. doi:10.1038/ngeo838
Ramankutty, N., Evan, A. T., Monfreda, C., & Foley, J. A. (2008). Farming the planet: 1. Geographic distribution of global agricultural lands in the year 2000. *Global Biogeochemical Cycles, 22*(1). doi:10.1029/2007gb002952
Running, S. W., & Coughlan, J. C. (1988). A GENERAL-MODEL OF FOREST ECOSYSTEM PROCESSES FOR REGIONAL APPLICATIONS .1.

HYDROLOGIC BALANCE, CANOPY GAS-EXCHANGE AND PRIMARY PRODUCTION PROCESSES. *Ecological Modelling, 42*(2), 125-154. doi:10.1016/0304-3800(88)90112-3

Running, S. W., & Hunt, E. R. (1993). Generalization of a forest ecosystem process model for other biomes, BIOME-BGC, and an application for global-scale models. *Scaling physiological processes: Leaf to globe*, 141-158.

Running, S. W., Nemani, R. R., & Hungerford, R. D. (1987). EXTRAPOLATION OF SYNOPTIC METEOROLOGICAL DATA IN MOUNTAINOUS TERRAIN AND ITS USE FOR SIMULATING FOREST EVAPOTRANSPIRATION AND PHOTOSYNTHESIS. *Canadian Journal of Forest Research-Revue Canadienne De Recherche Forestiere, 17*(6), 472-483. doi:10.1139/x87-081

Sajikumar, N., & Remya, R. S. (2015). Impact of land cover and land use change on runoff characteristics. *Journal of Environmental Management, 161*, 460-468. doi:10.1016/j.jenvman.2014.12.041

Saksa, P. C., Conklin, M. H., Battles, J. J., Tague, C. L., & Bales, R. C. (2017). Forest thinning impacts on the water balance of Sierra Nevada mixed-conifer headwater basins. *Water Resources Research, 53*(7), 5364-5381. doi:10.1002/2016wr019240

Sauer, T. J., Alexander, R. B., Brahana, J. V., & Smith, R. A. (2008). *The Importance and Role of Watersheds in the Transport of Nitrogen*.

Schroth, A. W., Giles, C. D., Isles, P. D. F., Xu, Y., Perzan, Z., & Druschel, G. K. (2015). Dynamic Coupling of Iron, Manganese, and Phosphorus Behavior in Water and Sediment of Shallow Ice-Covered Eutrophic Lakes. *Environmental Science & Technology, 49*(16), 9758-9767. doi:10.1021/acs.est.5b02057

Seitzinger, S. (2008). Nitrogen cycle: Out of reach. *Nature, 452*(7184), 162-163.

Seitzinger, S. P., Harrison, J. A., Dumont, E., Beusen, A. H. W., & Bouwman, A. F. (2005). Sources and delivery of carbon, nitrogen, and phosphorus to the coastal zone: An overview of Global Nutrient Export from Watersheds (NEWS) models and their application. *Global Biogeochemical Cycles, 19*(4). doi:10.1029/2005gb002606

Sen, S., Srivastava, P., Vadas, P. A., & Kalin, L. (2012). Watershed-level Comparison of Predictability and Sensitivity of Two Phosphorus Models. *Journal of Environmental Quality, 41*(5), 1642-1652. doi:10.2134/jeq2011.0242

Sha, J., Wang, Z. L., Lu, R., Zhao, Y., Li, X., & Shang, Y. T. (2018). Estimation of the Source Apportionment of Phosphorus and Its Responses to Future Climate Changes Using Multi-Model Applications. *Water, 10*(4), 17. doi:10.3390/w10040468

Shibata, H., Hiura, T., Tanaka, Y., Takagi, K., & Koike, T. (2005). Carbon cycling and budget in a forested basin of southwestern Hokkaido, northern Japan. *Ecological Research, 20*(3), 325-331. doi:10.1007/s11284-005-0048-7

Singh, V. P., & Woolhiser, D. A. (2002). Mathematical modeling of watershed hydrology. *Journal of Hydrologic Engineering, 7*(4), 270-292. doi:10.1061/(asce)1084-0699(2002)7;4(270)

Smeltzer, E., Shambaugh, A. D., & Stangel, P. (2012). Environmental change in Lake Champlain revealed by long-term monitoring. *Journal of Great Lakes Research, 38*, 6-18. doi:10.1016/j.jglr.2012.01.002

Smith, D. R., Francesconi, W., Livingston, S. J., & Huang, C.-h. (2015). Phosphorus losses from monitored fields with conservation practices in the Lake Erie Basin, USA. *Ambio, 44*, S319-S331. doi:10.1007/s13280-014-0624-6

Srinivasan, R., Ramanarayanan, T. S., Arnold, J. G., & Bednarz, S. T. (1998). LARGE AREA HYDROLOGIC MODELING AND ASSESSMENT PART II: MODEL APPLICATION1. *JAWRA Journal of the American Water Resources Association, 34*(1), 91-101. doi:10.1111/j.1752-1688.1998.tb05962.x

Strohmeier, S., Knorr, K. H., Reichert, M., Frei, S., Fleckenstein, J. H., Peiffer, S., & Matzner, E. (2013). Concentrations and fluxes of dissolved organic carbon in runoff from a forested catchment: insights from high frequency measurements. *Biogeosciences, 10*(2), 905-916. doi:10.5194/bg-10-905-2013

Sun, Y., Peng, S. S., Goll, D. S., Ciais, P., Guenet, B., Guimberteau, M., . . . Zeng, H. (2017). Diagnosing phosphorus limitations in natural terrestrial ecosystems in carbon cycle models. *Earths Future, 5*(7), 730-749. doi:10.1002/2016ef000472

Tague, C., McMichael, C., Hope, A., Choate, J., & Clark, R. (2004). Application of the RHESSys model to a California semiarid shrubland watershed. *Journal of the American Water Resources Association, 40*(3), 575-589. doi:10.1111/j.1752-1688.2004.tb04444.x

Tague, C., Seaby, L., & Hope, A. (2009). Modeling the eco-hydrologic response of a Mediterranean type ecosystem to the combined impacts of projected climate change and altered fire frequencies. *Climatic Change, 93*(1-2), 137-155. doi:10.1007/s10584-008-9497-7

Tague, C. L., & Band, L. E. (2001). Evaluating explicit and implicit routing for watershed hydro-ecological models of forest hydrology at the small catchment scale. *Hydrological Processes, 15*(8), 1415-1439. doi:10.1002/hyp.171

Tague, C. L., & Band, L. E. (2004). RHESSys: Regional Hydro-Ecologic Simulation System-An Object-Oriented Approach to Spatially Distributed Modeling of Carbon, Water, and Nutrient Cycling. *Earth Interactions, 8*.

Tavakoli, M., De Smedt, F., Vansteenkiste, T., & Willems, P. (2014). Impact of climate change and urban development on extreme flows in the Grote Nete watershed, Belgium. *Natural Hazards, 71*(3), 2127-2142. doi:10.1007/s11069-013-1001-7

Theis, C. V. (1935). *The relation between the lowering of the piezometric surface and the rate and duration of discharge of a well using ground water storage*: US Department of the Interior, Geological Survey, Water Resources Division, Ground Water Branch Washington, DC.

Thibeault, J. M., & Seth, A. (2015). Toward the credibility of Northeast United States summer precipitation projections in CMIP5 and NARCCAP simulations. *Journal of Geophysical Research-Atmospheres, 120*(19), 10050-10073. doi:10.1002/2015jd023177

Thornton, P. E., Thornton, M. M., & Vose, R. S. (2017). Daymet: Annual Tile Summary Cross-Validation Statistics for North America, Version 3: ORNL Distributed Active Archive Center.

Tong, S. T. Y., Sun, Y., Ranatunga, T., He, J., & Yang, Y. J. (2012). Predicting plausible impacts of sets of climate and land use change scenarios on water resources. *Applied Geography, 32*(2), 477-489. doi:10.1016/j.apgeog.2011.06.014

Tsai, Y., Zia, A., Koliba, C., Bucini, G., Guilbert, J., & Beckage, B. (2015). An interactive land use transition agent-based model (ILUTABM): Endogenizing human-environment interactions in the Western Missisquoi Watershed. *Land Use Policy, 49*, 161-176. doi:10.1016/j.landusepol.2015.07.008

Tsai, Y. S., Zia, A., Koliba, C., Bucini, G., Guilbert, J., & Beckage, B. (2015). An interactive land use transition agent-based model (ILUTABM): Endogenizing human-environment interactions in the Western Missisquoi Watershed. *Land Use Policy, 49*, 161-176. doi:10.1016/j.landusepol.2015.07.008

Ulen, B., Bechmann, M., Folster, J., Jarvie, H. P., & Tunney, H. (2007). Agriculture as a phosphorus source for eutrophication in the north-west European countries, Norway, Sweden, United Kingdom and Ireland: a review. *Soil Use and Management, 23*, 5-15. doi:10.1111/j.1475-2743.2007.00115.x

van Roosmalen, L., Sonnenborg, T. O., & Jensen, K. H. (2009). Impact of climate and land use change on the hydrology of a large-scale agricultural catchment. *Water Resources Research, 45*. doi:10.1029/2007wr006760

Veum, K. S., Goyne, K. W., Motavalli, P. P., & Udawatta, R. P. (2009). Runoff and dissolved organic carbon loss from a paired-watershed study of three adjacent agricultural Watersheds. *Agriculture Ecosystems & Environment, 130*(3-4), 115-122. doi:10.1016/j.agee.2008.12.006

Vicente-Serrano, S. M., Camarero, J. J., Zabalza, J., Sanguesa-Barreda, G., Lopez-Moreno, J. I., & Tague, C. L. (2015). Evapotranspiration deficit controls net primary production and growth of silver fir: Implications for Circum-Mediterranean forests under forecasted warmer and drier conditions. *Agricultural and Forest Meteorology, 206*, 45-54. doi:10.1016/j.agrformet.2015.02.017

Viola, M. R., de Mello, C. R., Chou, S. C., Yanagi, S. N., & Gomes, J. L. (2015). Assessing climate change impacts on Upper Grande River Basin hydrology, Southeast Brazil. *International Journal of Climatology, 35*(6), 1054-1068. doi:10.1002/joc.4038

Viola, M. R., Mello, C. R., Beskow, S., & Norton, L. D. (2014). Impacts of Land-use Changes on the Hydrology of the Grande River Basin Headwaters, Southeastern Brazil. *Water Resources Management, 28*(13), 4537-4550. doi:10.1007/s11269-014-0749-1

Vitousek, P. M., Naylor, R., Crews, T., David, M. B., Drinkwater, L. E., Holland, E., . . . Zhang, F. S. (2009). Nutrient Imbalances in Agricultural Development. *Science, 324*(5934), 1519-1520. doi:10.1126/science.1170261

Wigmosta, M. S., Vail, L. W., & Lettenmaier, D. P. (1994). A distributed hydrology-vegetation model for complex terrain. *Water Resources Research, 30*(6), 1665-1679. doi:10.1029/94WR00436

Winchell, M. F., Folle, S., Meals, D., Moore, J., Srinivasan, R., & Howe, E. A. (2015). Using SWAT for sub-field identification of phosphorus critical source areas in a saturation excess runoff region. *Hydrological Sciences Journal-Journal Des Sciences Hydrologiques, 60*(5), 844-862. doi:10.1080/02626667.2014.980262

Winter, J. M., Beckage, B., Bucini, G., Horton, R. M., & Clemins, P. J. (2016). Development and Evaluation of High-Resolution Climate Simulations over the Mountainous Northeastern United States. *Journal of Hydrometeorology, 17*(3), 881-896. doi:10.1175/jhm-d-15-0052.1

Wu, F., Zhan, J., Su, H., Yan, H., & Ma, E. (2015). Scenario-Based Impact Assessment of Land Use/Cover and Climate Changes on Watershed Hydrology in Heihe River Basin of Northwest China. *Advances in Meteorology*. doi:10.1155/2015/410198

Yadav, V., Malanson, G. P., Bekele, E., & Lant, C. (2009). Modeling watershed-scale sequestration of soil organic carbon for carbon credit programs. *Applied Geography, 29*(4), 488-500. doi:10.1016/j.apgeog.2009.04.001

Yang, X., Ren, L., Singh, V. P., Liu, X., Yuan, F., Jiang, S., & Yong, B. (2012). Impacts of land use and land cover changes on evapotranspiration and runoff at Shalamulun River watershed, China. *Hydrology Research, 43*(1-2), 23-37. doi:10.2166/nh.2011.120

Young, R. A., Onstad, C. A., Bosch, D. D., & Anderson, W. P. (1989). AGNPS - A NONPOINT-SOURCE POLLUTION MODEL FOR EVALUATING AGRICULTURAL WATERSHEDS. *Journal of Soil and Water Conservation, 44*(2), 168-173.

Yuan, Z., Chu, Y., & Shen, Y. (2015). Simulation of surface runoff and sediment yield under different land-use in a Taihang Mountains watershed, North China. *Soil & Tillage Research, 153*, 7-19. doi:10.1016/j.still.2015.04.006

Zhang, Y., Su, F., Hao, Z., Xu, C., Yu, Z., Wang, L., & Tong, K. (2015). Impact of projected climate change on the hydrology in the headwaters of the Yellow River basin. *Hydrological Processes, 29*(20), 4379-4397. doi:10.1002/hyp.10497

Zia, A., Bomblies, A., Schroth, A. W., Koliba, C., Isles, P. D. F., Tsai, Y., . . . Van Houten, J. (2016). Coupled impacts of climate and land use change across a river-lake continuum: insights from an integrated assessment model of Lake Champlain's Missisquoi Basin, 2000-2040. *Environmental Research Letters, 11*(11), 13. doi:10.1088/1748-9326/11/11/114026

Zierl, B., Bugmann, H., & Tague, C. L. (2007). Water and carbon fluxes of European ecosystems: An evaluation of the ecohydrological model RHESSys. *Hydrological Processes, 21*(24), 3328-3339. doi:10.1002/hyp.6540

APPENDIX (RHESSys-P variable list)

Variable	Description	Units
γ_i	The proportion of flow the ith neighbor can receive from the central patch	DIM
$Q_{c,n}$	The saturated flow quantity from the central patch to a neighbor patch	m^3 day^{-1}
$T_{c,n}$	The transmissivity between the central patch and the neighbor patch	m^2 day^{-1}
$\tan\beta_{c,n}$	The slope between the two patches	DIM
$w_{c,n}$	The flow width between the central patch and neighbor patch	m
Z_{sat}	The water table depth	m
z	The soil depth	m
$K_{sats}(z)$	The saturated hydrologic conductivity at the depth z	m day^{-1}
K_{sats0}	The saturated hydrologic conductivity at the soil surface	m day^{-1}
m	The decay coefficient of hydraulic conductivity with depth	DIM
$soil_P(z)$	The soil phosphorus amount at the depth z	kgP m^{-2}
$P_{surface}$	The soil phosphorus amount at the surface	kgP m^{-2}
P_{decay}	The soil phosphorus decay coefficient	DIM
$soil_P$	The total soil phosphorus amount	kgP m^{-2}
$soil_{P\_z_1-z_2}$	The total phosphorus amount from soil depth z_1 to z_2	kgP m^{-2}
$P_{absorbed\_z_1-z_2}$	The absorbed phosphorus amount for the soil layer from depth z_1 to z_2	kgP m^{-2}
$P_{absorbRate}$	The soil-specific coefficient describing how much phosphorus can be absorbed by unit weight soil	DIM
ρ_b	The soil bulk density	kg m^{-3}
$P_{avail\_z_1-z_2}$	The solution state phosphorus of the layer from soil depth z_1 to z_2	kgP m^{-2}
$P_{c,n}$	The phosphorus amount moving from central patch to its neighbor patch through subsurface flow	kgP
$Q_{c,n}$	The saturated flow quantity from central patch to a neighbor patch	m^3

Variable	Description	Units
Q_{sat}	The saturated layer water quantity in the central patch	m^3
S_{patch}	The central patch area	m^2
Q_{return}	The return flow quantity	m
Q_{unsat}	The unsaturated soil layer water	m
$Q_{rootzone}$	The rootzone layer water for vegetation land use	m
W_{sat}	The patch water saturation deficit	m
$n(z)$	The soil porosity at soil depth z	%
n_0	The soil surface porosity	%
p	The soil porosity decay coefficient	DIM
$Tn_{z_1-z_2}$	The total porosity from depth z_1 to z_2	%
z_{return}	The bottom depth of return flow layer	m
Q'_{det}	The new detention store water quantity after return flow moves to the surface	m
Q_{det}	The old detention store water quantity before return flow moves to the surface	m
P'_{surf}	The new patch surface phosphorus amount after return flow moves to the surface	kgP m^{-2}
P_{surf}	The old patch surface phosphorus amount before return flow moves to the surface	kgP m^{-2}
Q_{det_excess}	The water quantity exceeding the detention store size	m
S_{det}	The patch detention store size	m
$pmpf\_p1p2$	The potential mineral phosphorus flux from pool 1 to pool 2 without soil DIP limit	kgP m^{-2}
$p1\_closs$	The carbon loss in pool 1	kgC m^{-2}
rf_p1p2	The respiration fraction on the decomposition pathway from pool 1 to pool 2	%
cp_p2	The ratio of carbon and phosphorus in pool 2	DIM
cp_p1	The ratio of carbon and phosphorus in pool 1	DIM